https://doi.org/10.1070/RCR4909

Sensory effects of fluorescent organic dyes

Valerii F. Traven,* Dmitrii A. Cheptsov

D.Mendeleev University of Chemical Technology of Russia,
Miusskaya pl. 9, 125047 Moscow, Russian Federation

Organic dyes are very promising substrates for modern sensing technologies. Their utility is based on the 'push-pull' polarization of a π-electron system, as well as their polyfunctionality. These properties make organic dyes capable of fluorescent sensory response to many analytes and provide different mechanisms of both fluorescence increase and fluorescence quenching. Specific organic reactions and structural transformations of fluorescent organic dyes are under consideration in this review. The data confirming the structures of the products of the related analytical reactions are discussed in more detail. Knowledge of the transformations that fluorescent organic dyes undergo in sensory effects can contribute to successful design of specific probes for novel sensory technologies.
The bibliography includes 365 references.

Contents

1. Introduction 713
2. Scope of analytes and sensory reactions of fluorescent organic dyes 714
   2.1. Electrophiles as analytes 714
   2.2. Nucleophiles as analytes 715
   2.3. Conformation-effected analytes 715
   2.4. Fluorescent organic dyes as probes and their sensory reactions 715
3. Photophysical mechanisms of sensory effects of fluorescent organic dyes 717
   3.1. Photoinduced electron transfer effect 717
   3.2. Intramolecular charge transfer effect 718
   3.3. Excited-state intramolecular charge- and proton transfer effects 718
4. Probes with induced fluorescence 719
   4.1. Acids and metal ions as analytes 719
   4.2. Nucleophiles as analytes 723
5. Probes activated from their latent forms 725
   5.1. Acid activation of latent forms 725
   5.2. Activation of latent forms of organic dyes by metal ions 727
   5.3. Activation of latent forms by other analytes 729
6. Probes with quenched fluorescence 733
   6.1. Quenching of fluorescence by metal ions 733
   6.2. Fluorescence quenching by other analytes 734
7. Ratiometric probes 735
8. Probes for multiple analytes 739
9. Probes sensitive to conformational effects 742
10. Conclusion 744

V.F.Traven. Doctor of Chemical Sciences, Professor, Head of the Skoltech Chair (Organic and hybrid materials for energy conversion and storage) of D.Mendeleev University of Chemical Technology of Russia.
E-mail: valerii.traven@gmail.com.
Current research interests: photochemistry of heterocyclic compounds, synthesis and study of photophysical properties of organic dyes, synthesis and study of fluorescent chemosensors.
D.A.Cheptsov. PhD, Assistant at the Department of Organic Chemistry of D.Mendeleev University of Chemical Technology of Russia.
E-mail: dchepcov@yandex.ru
Current research interests: synthesis of organic dyes (including their latent forms), synthesis of photoacid generators, synthesis of fluorescent chemosensors, chemistry of coumarin compounds.

1. Introduction

Fluorescence is a very sensitive and selective characteristic. Even a single molecule can be detected by its fluorescence. The fluorescence can be controlled in various ways — by varying the solvents and concentrations, ions, polymer matrix, pressure, chemical transformations, irradiation, *etc*. Therefore, the use of fluorescence in sensing technologies has several advantages, such as high sensitivity, high resolution, convenient operation and low cost. On closer examination, the following features of organic dyes as promising substrates for sensor technologies can be noted:

Received 11 July 2019

© 2020 Uspekhi Khimii, ZIOC RAS, Russian Academy of Sciences and IOP Publishing Limited

— electronic states of organic dyes are available for excitation by light in a wide range of energies up to the IR region;

— the majority of organic dyes have rigid planar molecules; planarity reduces the non-radiative decay of excited states of a dye and increases its fluorescence;

— organic dyes possess functional groups that are capable of protonation, binding to metal ions and other reactions with analytes;

— the well-developed π-electronic structure of organic dyes enables efficient charge transfer interactions with π-acceptors as analytes.

The efficiency of each sensor is determined by a series of factors. In this situation, unambiguous characterization and ranking of sensors are very subjective. We do not intend to solve such a task and just want to define the mechanisms of sensory effects of the related organic dyes to be useful both for understanding of their application and for creating novel sensory systems and technologies.

Fluorescent organic dyes that provide sensory effects to the certain analytes are called 'probes' in this review. The applications of fluorescent organic dyes as 'probes' have been intensively studied and summarized in a great number of recent reviews. Some of them are listed here.[1–30] Thus, metal ions and pH chemosensors, fluorescent dyes for oxygen analytes, fluorogenic probes for biologically active substrates and many other applications of fluorescent dyes have been discussed there in much detail. In this review, we focus on chemical reactions of organic dyes with analytes that are responsible for the corresponding sensory effects.

Before analyzing sensory effects, some definitions should be given. A chemosensor means a molecular probe in which the interaction with an analyte is dynamic, reversible and thus labile. Conversely, a chemodosimeter operates under kinetic control in an irreversible fashion. Over the years, these two definitions, as well as the term 'fluorescent probe', have been used interchangeably and ambiguously. In our review we differentiate organic dyes between the 'chemosensor' (or fluorescent probe) and 'chemodosimeter' definitions.

The review adopts the following abbreviations:

AIE — aggregation-induced emission,
ACQ — aggregation-caused quenching,
Boc — *tert*-butoxycarbonyl,
BODIPY — boron-dipyrromethene,
CFG — conformational functional group,
CHEF — chelation-enhanced fluorescence,
Cys — cysteine,
DCMB — dicyanomethylene-benzopyran,
DFT — density functional theory,
DLS — dynamic light scattering,
DP — dye precursor,
ESI-MS — electrospray ionization mass spectrometry,
ESICT — excited-state intramolecular charge transfer,
ESIPT — excited-state intramolecular proton transfer,
FE — fluorescence enhancement,
FRET — Förster resonance energy transfer,
FT-IR spectroscopy — Fourier transform infrared spectroscopy,
GR — glutathione reductase,
GSH — glutathione,
Hcy — homocysteine,
HeLa — cervical cancer cells,
HOMO — highest occupied molecular orbital,
HR-MS — high resolution mass spectrometry,
ICT — intramolecular charge transfer,
LMOG — low molecular mass organic conjugate,
LUMO — lowest unoccupied molecular orbital,
MALDI TOF MS — matrix-assisted laser desorption time-of-flight mass spectrometry,
MF — mechanofluorescence,
MO — molecular orbital,
NBO — nonbonding orbital,
NIR — near-infrared,
PAG — photoacid generator,
PAH — polycyclic aromatic hydrocarbons,
PBS — phosphate-buffered saline,
PDE — polymorphism-dependent emission,
PET — photoinduced electron transfer effect,
PMMA — poly(methyl methacrylate),
ppb — parts per billion,
ppm — parts per million,
Py — pyridyl,
RIR — restriction of intramolecular rotation,
SDBS — sodium dodecylbenzenesulfonate,
Tf — trifluoromethanesulfonate (triflate),
TNT — trinitrotoluene,
U.S. EPA — U.S. Environmental Protection Agency,
WHO — World Health Organization,
Φ — quantum yield of the reaction.

2. Scope of analytes and sensory reactions of fluorescent organic dyes

2.1. Electrophiles as analytes

The number of analytes that have been detected with the use of organic dyes is growing. First of all, precise pH measurements attract considerable attention of researchers due to the potential applications in live systems and environmental monitoring. Metal ions, oxidants, hazard gases, organic pollutants, bioorganic substrates have been found to provide responses of the related fluorescent organic dyes. A brief description of the analytes is given below in order to better understand the importance of finding new sensors for their analysis.

Mercury(II) ion. Heavy metal ions are highly toxic to the environment, since they are not biodegradable and can be accumulated in some body organs. Among these ions, mercury is of great danger due to its extremely high toxicity in living systems. It is potent inhibitor of certain enzymes, *e.g.*, thioredoxin reductase in vitamin biosynthesis.[31] Thus it would be of great interest to detect and quantify mercury at nano level in order to control and prevent environmental and biological contamination by this metal. There are several reports on detection of Hg^{2+} ions involving fluorescence sensing.[32–43] The naked-eye chemosensors for detection of Hg^{2+} have drawn special attention offering fast and easy result. However, most of such chemosensors use organic or inorganic molecules with sulfur atoms as donor detecting centres.[44–46] But these sensors have selectivity problems because of disturbance of thiophilic metal ions such as Ag^{+}, Cu^{2+} and Cd^{2+}. Therefore, they are not really useful in selective detection.

Lead(II) ion. Pb^{2+} is another highly poisonous metal ion. The presence of lead causes many severe health problems such as mental retardation, memory loss, anemia, muscle paralysis, kidney damage and disorder of the blood.[47–50]

Zinc(II) ion. Zinc is the second most abundant and essential transition element in the human body after iron.

It is indispensable to living organisms in minor quantities.[51–54] However, zinc is regarded as a metal pollutant of environment, significant concentrations of which may reduce the soil microbial activity causing phytotoxic effects. It is a common contaminant in agricultural and food wastes. As a result, the detection of zinc is important for environmental safety.[55]

Iron(III) ion. Ferric ion is one of the most essential metal ions in biological systems. It plays a significant role in physiological processes such as oxygen metabolism and enzyme catalysis.[56–58] Both excess and deficiency of Fe^{3+} ion from normal level can trigger serious problems. An excess of Fe^{3+} in the body is associated with the development of cancers, hepatitis, heart and liver diseases.[59–61] The cellular toxicity of iron ions leads to Parkinson's, Alzheimer's and Huntington's diseases.[62,63] On the other hand, a deficiency of Fe^{3+} ion hinders oxygen delivery to cells, resulting in fatigue and poor work performance.[64]

Copper(II) ion. Cupric ions play a critical role in many physiological processes in the human body. They act as active sites of metalloenzymes and proteins, being involved in oxygen transportation and redox processes.[65] Copper(II) compounds in the brain are involved in inter- and intracellular communication.[66,67] The disorder of copper level leads to neurodegenerative diseases such as Menkes, Parkinson's and Alzheimer's diseases.[68–70] Besides, Cu^{2+} is identified as an environmental contaminant damaging microorganisms and the human body.[71–73]

Nickel(II) ion. Nickel is an essential trace element for supporting life.[74–77] It is involved in biochemical processes, such as metabolism, respiration and biosynthesis.[78] However, it is also extensively used in many industrial processes: electroplating, pigment and ceramic production, magnetic tapes of computers and nickel cadmium batteries.[79] Therefore, possible excess of Ni^{2+} ions in human body can be highly toxic. Its toxicity includes effects on gastrointestinal system, blood and kidneys.[80]

Silver(I) ion. Ag^{+} ions are very important bioactive cations. These ions exhibit different levels of activity in living organisms, depending on their content. At low concentration they provide strong inhibitory and bactericidal effects, as well as a broad spectrum of antimicrobial activities.[81] These ions are effective for disinfection and conservation of drinking water. However, a high level of Ag^{+} ions has been found to be highly toxic to humans, since these ions form harmful complexes with amino acids, nucleic acids and other bioorganic compounds in the body. Silver ions exhibit a high affinity towards sulfhydryl and amino functions.[82,83]

Gold(III) ion. Au^{3+} ions are bioactive cations. They are considered to be highly toxic in biological systems. These ions can cause damage to DNA strands and to the liver and kidneys.[84–87]

2.2. Nucleophiles as analytes

Biological thiols. Thiol function is found in biologically relevant species such as cysteine, homocysteine and glutathione. These biothiols are vital for the support of cellular redox status. Alterations in their level can cause severe diseases such as AIDS, cancer and Alzheimer's disease. Therefore, sensing and signalling of biological thiols is an important analytical task.[88–93]

Cyanide ion. Cyanide ion is a wide-spread highly toxic anion.[94] A small amount of CN^{-} can result in lethal poisoning. It inhibits cellular respiration in cells *via* its binding to a heme unit in the active site of cytochrome a_3, leading to vomiting, convulsion and eventual death.[95] The World Health Organization (WHO) restricts the maximum acceptable level of cyanide in drinking water to be not more than 1.9 μmol L^{-1}.[96] However, the use of cyanides cannot be avoided due to their extensive use in many industrial processes, such as electroplating, gold mining and plastics manufacture.[97]

Phosphate ions. Phosphate ions are of particular interest among other anions, playing an important role in many chemical, biological and industrial processes.[98–103] These ions are key substrates in some biochemical reactions and components of biomolecules.[104,105] Even though phosphates have great contributions to the industrial production and life of human beings, the over-use of phosphates in agriculture causes serious environmental problems, including damage of aquatic ecosystems.[106–110]

Hypochlorite ion. Hypochlorite is the main component of cleaning agents and is extensively used in industry. Therefore, it exists widely in biological environment.[111,112] There is a certain amount of hypochlorite in the immune system, which is essential for human health. Nevertheless, the excess of this anion can cause some diseases such as cardiovascular and kidney diseases, neuron degeneration and cancer.[113–115]

Nitrite ion. NO_2^{-} ion is a hazardous inorganic contaminant that exists widely in ground and surface water systems.[116,117] It is also often used as a colour fixer and food preserver. NO_2^{-} ion has proved to be of a great threat to human health. Nitrite reacts with amines, resulting in the formation of nitrosamine, which is known to be highly carcinogenic.[118–120] In blood, nitrite can oxidize iron(II) of haemoglobin, thus hindering oxygen transfer.[121,122] The U.S. Environmental Protection Agency (U.S. EPA) restricts the maximum acceptable level of nitrite in drinking water to 1 ppm (21.7 μmol L^{-1}).

Hydrazine. Hydrazine (N_2H_4) is widely used in chemical industry, agriculture, pharmacy. It is also used in missile systems and aerospace. Meanwhile, hydrazine exerts deleterious effects on human health. It can be absorbed by skin and lungs, providing serious damage to the kidneys, liver and central nervous system.[123–125] Moreover, hydrazine has been found to be carcinogenic and mutagenic.[126,127]

2.3. Conformation-effected analytes

As a special group of analytes, the present review considers a number of examples wherein fluorescent properties of organic dyes depend on the effects caused by changes in temperature, pressure and aggregation. These effects are often extremely high, since those changes are usually accompanied by significant responses in the molecular structure of the fluorophore, which, in turn, directly affect the energy of its electronic states and transitions between them. A number of examples of the 'work' of this group of analytes, conventionally named by the authors of the present review as conformation-effected analytes, are considered in Section 6.

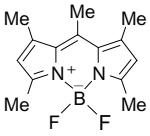
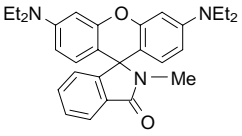
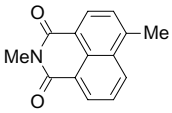
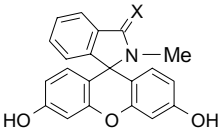
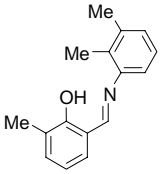
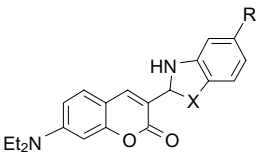
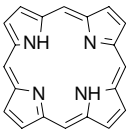
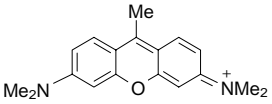
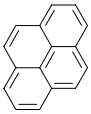
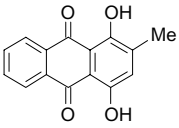
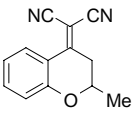
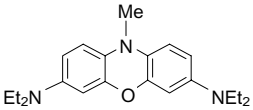
2.4. Fluorescent organic dyes as probes and their sensory reactions

A fluorescent organic dye capable of acting as a 'probe' must comprise at least two fragments: a receptor that is responsible for binding to the analyte and a fluorophore that provides a spectral response during the sensory reaction.

In some probes, receptor and fluorophore fragments are separated by a spacer. In other probes, the role of the receptor may be performed by the corresponding functional group of the fluorophore. Binding to electrophilic analytes is provided by heteroatoms having lone electron pairs, for example, in amino- or hydroxy functions of the related probes. Binding to nucleophilic analytes is provided by receptors that have electron-withdrawing properties. Organic dyes and their analogues, acting as fluorophore fragments in sensory probes, are very diverse in their structures. For convenience, we have summarized the structures of fluorophores and their application in sensory technologies in Table 1. Besides, the designations of the corresponding probes are indicated. The detected analytes and references are also given.

As one can see, a molecule of each organic fluorophore contains a certain number of functional groups that can potentially provide a response to a particular analyte. This response is based on the corresponding organic reaction

Table 1. Fluorophores and analytes duscussed in this review.

Fluorophore, probe designations	Analytes	Ref.	Fluorophore, probe designations	Analytes	Ref.
 Boron-dipyrromethenes (BODIPY) (**1**, **17**, **34**, **43**, **44**, **49**, **61**, **64**)	H^+, biological thiols, Cu^{2+}, ClO^-	29, 128 – 140	 Rhodamine derivatives (**22** – **27**, **29** – **31**)	H^+, Hg^{2+}, Zn^{2+}, Fe^{3+}	222 – 246
 Naphthalimide derivatives (**2**, **3**, **36**, **37**, **45**, **67**)	Cu^{2+}, Au^{3+}, $H_2PO_4^-$, Hg^{2+}, Ag^+, CN^-, F^-	141 – 158	 Fluorescein derivatives (**28**)	Hg^{2+}	247 – 250
 Schiff bases and their analogues (**4** – **7**, **21**, **35**, **53**, **59**, **65**)	Cu^{2+}, Cr^{3+}, Al^{3+}, Zn^{2+}, F^-, Ni^{2+}, CN^-, HClO, SO_3^{2-}	159 – 203	 Coumarin derivatives (**32**, **33**, **42**, **48**)	Cu^{2+}, As^{3+}, irradiation, H_2O	251 – 256
 Porphyrins, related macrocycles and derivatives (**14**, **15**, **55**, **56**)	Mg^{2+}, Zn^{2+}, CN^-, F^-	204 – 206	 Pyronin derivatives (**38**)	Phosgene	257
 Pyrene, related PAH, their derivatives (**16**)	Ni^{2+}	207 – 212	 Quinizarin derivative (**40**)	H^+	237
 Dicyanomethylene-benzopyran (DCMB) derivates (**18**)	SO_3^{2-}	213	 Oxazine derivatives (**41**, **70**, **71**)	Irradiation, aggregation effects	258, 259
Cyanine dyes and their analogues (**19**, **20**, **50**, **51**, **52**, **54**, **57**, **58**)	CN^-, hydrazine, HSO_3^-, SO_2^{2-}, Hg^{2+}	214 – 221	Hetarene conjugates (**46**, **47**, **63**, **66**, **68**, **69**, **72**, **73**)	TNT, aniline, H^+, Zn^{2+}, S^2, aggregation effects	260 – 295

Note. PAH are polycyclic aromatic hydrocarbons, TNT is trinitrotoluene.

that occurs when the fluorophore molecules contact the analyte.

Depending on the structure of the fluorescent organic dye and the analyte, different sensing reactions can be observed. Almost every organic dye contains heteroatoms that can be protonated. The protonation changes significantly the electronic structure of the organic dye molecule and therefore its potential fluorescence. Acid – base interactions often underlie the sensory effects of organic dyes. Binding to a metal ion has often a similar effect on the electronic structure of the dye molecule and thus on its spectral response.

Organic dyes are multifunctional organic compounds with a significant reactivity. Electron-withdrawing functional groups (such as carbonyl, carbalkoxy or imino functions) can react with highly nucleophilic analyte molecules *via* Ad_N-reactions, thus providing serious violation of the push-pull electron distribution specific to fluorescent organic dyes. Addition of a nucleophilic analyte to a polarized carbon – carbon double bond of a fluorescent organic dye can occur, for example, during the Michael-type reaction. Nucleophilic substitution reactions can perturb the push-pull electronic structure of a fluorescent probe as well. A good leaving group in the fluorescent dye is often able to provide an effective sensory response even in the presence of a low-nucleophilic analyte.

Particular attention should be given to reactions of the so-called latent (hidden) forms of organic fluorophores. Lactone and lactam forms of rhodamine dyes, N-acyl derivatives of oxazines and coumarin dyes can be mentioned as examples. Such latent forms have generally no fluorescence. Latent forms of the fluorescent dyes often readily transform into their active forms, thus providing the corresponding sensory effects during hydrolysis, oxidation or complexation under mild conditions.

3. Photophysical mechanisms of sensory effects of fluorescent organic dyes

There is a certain number of photophysical mechanisms that should be mentioned for better understanding of the sensory effects of fluorescent organic dyes when they interact with analytes.[29,296] Many photophysical processes (*e.g.*, quenching *via* collision, photoinduced electron transfer, exciplex formation, photoinduced proton transfer, energy transfer, *etc.*) may be responsible for the fuorescence change upon binding of the analyte by the receptor. The most frequently met mechanisms in the design of probes are discussed briefy in this section.

3.1. Photoinduced electron transfer effect

Many fluorescent probes are specified by the photoinduced electron transfer effect, which can be responsible for the emission changes. There are two types of PET effects that can control the probe fluorescence.

In the reductive PET mechanism, the fluorophore moiety of the probe and the receptor are connected by a linker. In this mechanism, fluorophore as the electron acceptor is reduced, whereas the receptor as the electron donor is oxidized. In terms of molecular orbitals, the highest occupied molecular orbital (HOMO) of the fluorophore is lower than the HOMO of the receptor. Thus, an electron from receptor can transfer to the excited fluorophore and fills its singly occupied HOMO. Figure 1 *a* shows an analyte-free fluorophore with an electron-rich receptor. In this case the probe will be in the fluorescence 'off'-state due to the reductive PET effect.

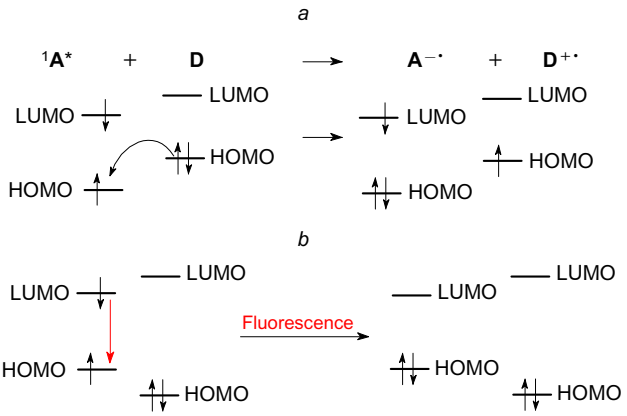
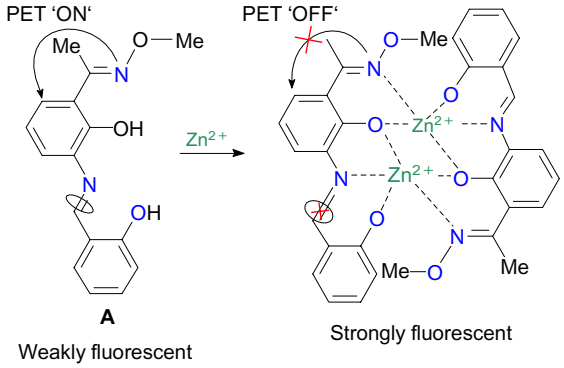


Figure 1. (*a*) Scheme of the reductive PET fluorescence inhibition; (*b*) the PET effect is 'off' due to the probe – analyte interaction. The fluorescence is 'on'.
A is an electron acceptor, **D** is an electron donor. PET is photoinduced electron transfer

Interaction of the receptor with an analyte will 'switch off' the PET effect and restore fluorescence. Thus, the fluorescence turns to the 'on'-state (Fig. 1 *b*).

As example of the reductive PET mechanism, the control of the emission of the probe **A** by its interaction with the Zn^{2+} ion is shown in Scheme 1. The fluorescence of this probe is quenched by the PET interaction of the benzene ring with the nitrogen atom in the absence of a metal ion.

Scheme 1



When bound to a metal ion, the nitrogen lone pair of electrons is no longer available for the PET process. As a result, photoinduced electron transfer is terminated and the probe becomes highly fluorescent. The UV/Vis spectra of the **A**-Zn^{2+} complex exhibit four clear isosbestic points, which may be assigned to the **A** moieties bound to Zn^{2+} ion (see Scheme 1).[297] The probe **A** operates *via* the chelation-enhanced fluorescence (CHEF) and PET mechanisms (see Fig. 1 *a*). Fluorescence measurements show that **A** has an excellent fluorescent selectivity for Zn^{2+} ions over many other metal ions due to the intramolecular charge transfer (ICT) mechanism. The results demonstrate that the binding between probe **A** and Zn^{2+} is chemically reversible. The structure of the **A**-Zn^{2+} complex has been confirmed by the X-ray diffraction analysis.

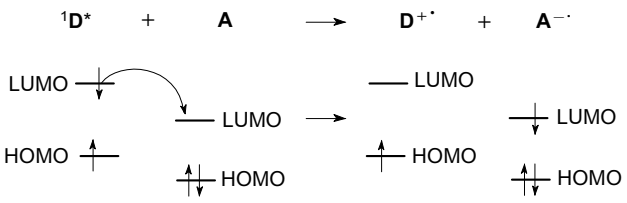


Figure 2. Scheme of the oxidative PET fluorescence inhibition.

The oxidative PET mechanism of fluorescence inhibition is illustrated in Fig. 2. The energy levels of molecular orbitals (MO) provide the electron transfer where the singlet excited state (LUMO) of fluorophore can donate electrons to the analyte's LUMO. In this case, the fluorophore (an electron donor) is oxidized, while the analyte (an electron acceptor) is reduced.

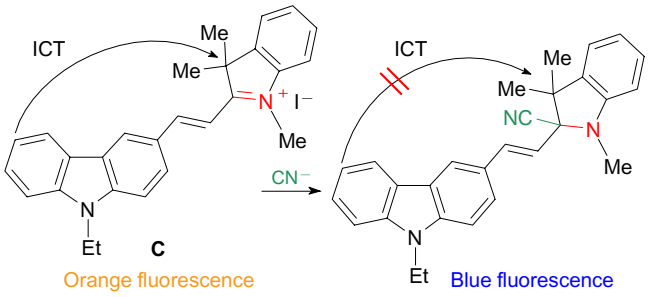
The probe **B** exhibits an absorbance increase at 506 nm and distinct emission at 635 nm. The addition of Cu^{2+} ions causes quenching of fluorescence due to the formation of cuprous complex according to the oxidative PET mechanism (Scheme 2).[137]

3.2. Intramolecular charge transfer effect

Fluorophore possessing an electron-donating (*e.g.*, amino, methoxy) group conjugated to an electron-withdrawing group undergoes ICT from a donor to an acceptor upon photo-excitation and hence, the increase in the dipole moment can be considerable. The fluorescence emission spectra of probes with an ICT state strongly depend on the solvent polarity. Increase in the latter results in the red shift of the emission bands. The most obvious difference between PET and ICT effects lies in different fluorescence responses of the probe in the analyte recognition. PET probes display fluorescence enhancement or quenching without pronounced spectral shifts, so that the terms 'off-on' and 'on-off' for fluorescent sensors are often used. The absence of shift in the spectra rules out ratiometric measurements at two wavelengths. In contrast, the ICT-based indicators show clear fluorescence band shifts upon analyte binding, making ratiometric measurements possible.

The ICT effect, which is responsible for the high emission of a fluorophore molecule, is hindered by the analyte molecule interaction with the π-conjugated system, thus blue-shifting the emission process. The probe **C** is shown below as an example (Scheme 3).[217] It turned to be a novel ratiometric fluorescent chemodosimeter for cyanide detection. In the presence of cyanide ions, this dye shows a significant fluorescent response, with the emission having a large Stokes shift (≈210 nm). The sensory effect of the probe **C** is discussed in more detail in Section 7.

Scheme 3



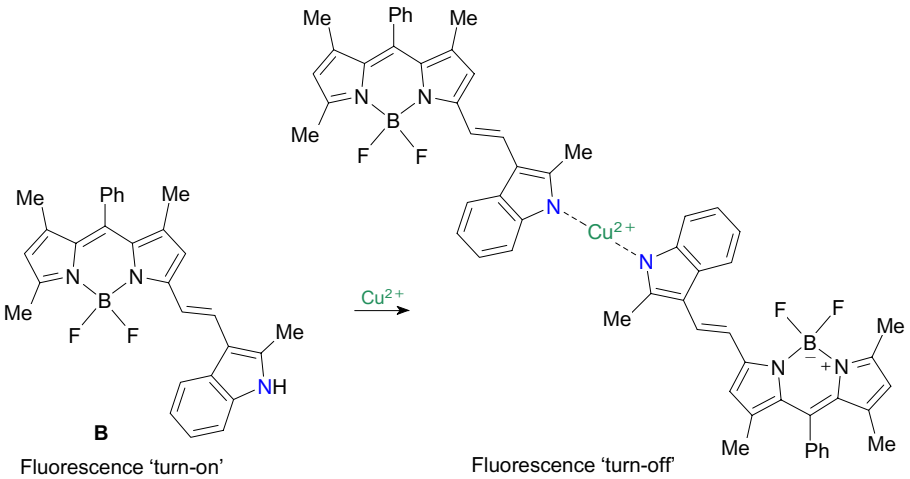
3.3. Excited-state intramolecular charge- and proton transfer effects

The excited-state intramolecular proton transfer reactions of salicylideneaniline derivatives and their analogues have been often discussed in the sensory reactions of the related probes. The ESIPT effect implies the transfer of a hydroxy proton to the imine nitrogen atom through a pre-existing intramolecular hydrogen bonding configuration, and has also been extensively described in the literature.[298 – 304] As illustrated in Fig. 3, the resulting proton-transfer tautomer (keto-form) significantly differs in structure and electronic configuration from its corresponding ground state, *i.e.*, it shows a large Stokes shifted fluorescence. Upon Franck – Condon excitation, excited-state intramolecular charge transfer (ESICT) can follow the ESIPT process thus providing definite emission changes.[201, 305, 306]

A novel dipole-functionalized Schiff base **D**, as well as related compounds **E** – **G**, can illustrate the role of ESIPT/ESICT processes in sensory reactions of salicylideneaniline derivatives and their analogues.[307]

In solid state and in aprotic solvents Schiff bases **D** – **G** exist mainly as *E*-conformers possessing a strong intramolecular hydrogen bond. Compounds **E** – **G** exhibit solely a long-wavelength proton-transfer tautomer emission, while dipole-functionalized salicylideneaniline **D** shows remarkable dual emission originating from the ESICT and ESIPT

Scheme 2



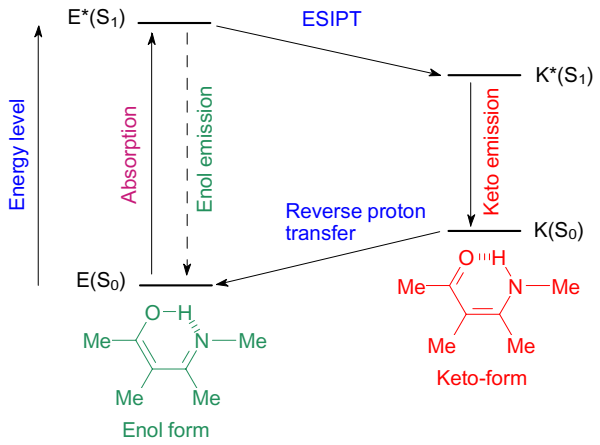
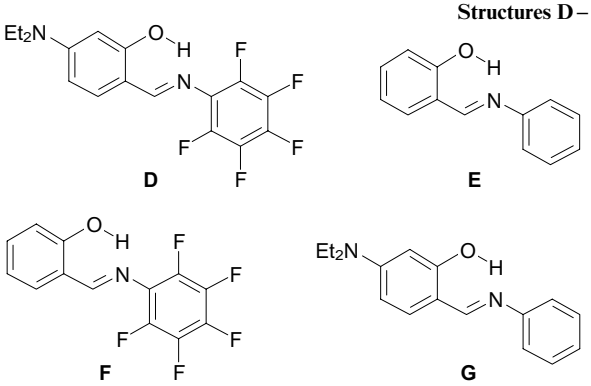


Figure 3. Energy levels of a Schiff base in the excited-state intramolecular proton transfer process (E is the energy level of enol form in the ground state, E* is the energy level of enol form in the excited state, K is the energy level of keto-form in the ground state, K* is the energy level of keto-form in the excited state).

Structures D – G



states. Analysis of the geometric structures clearly demonstrates that the intramolecular hydrogen bond is shortened upon photoexcitation, which is regarded as a crucial factor for ESIPT. The results make further rational design of the ESICT/ESIPT coupled systems feasible by modifying the ESIPT molecules.

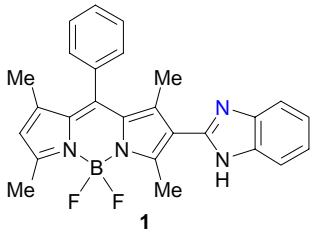
Depending on the probe structure and the nature of the analyte, other mechanisms can operate in the corresponding fluorescent probes. These sensory effects are discussed in the relevant sections of this review.

4. Probes with induced fluorescence

4.1. Acids and metal ions as analytes

Boron dipyrromethene fluorophores possess outstanding photophysical properties, including high molar absorption coefficients and fluorescence quantum yields, narrow emission bandwidths and high stability in physiological conditions.[29,128] Moreover, their spectroscopic characteristics can be fine-tuned by introducing appropriate substituents at various positions of the BODIPY backbone. These unique advantages facilitate the design of various BODIPY-derived fluorescent probes in analyte detection, bio-imaging and labelling.[129–133]

Structure 1



An optical and fluorometric pH probe **1** has been prepared by combining a pH sensitive benzimidazole (as a receptor) and the boron-dipyrromethene fluorophore.[308]

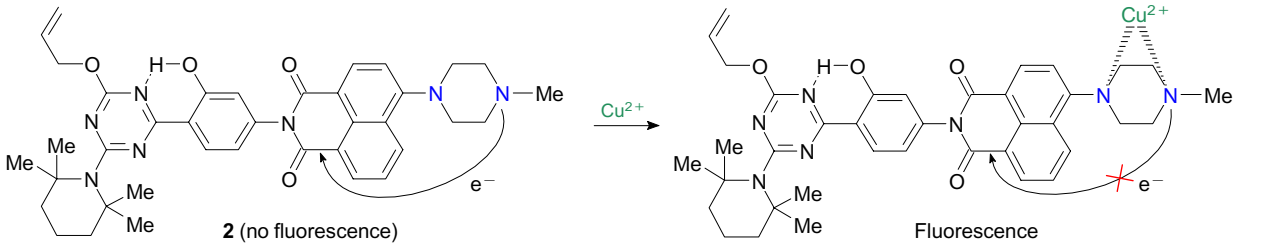
Benzimidazole group has two acid-base equilibrium states with pK_a values of 5.7 (protonated-neutral) and 12.6 (neutral-anionic), the former of which is ideally located within the physiological pH-range of acidic organelles such as lysosome (pH 4.5 – 5.5) and endosome (pH 4.5 – 6.8). Therefore, benzimidazole derivatives are usually employed to modify the fluorophore so as to develop intracellular pH sensors.[309,310] Due to the electron-donating effect, the benzimidazole group causes an obvious red shift in the absorption and fluorescence spectra. Upon protonation, the probe **1** exhibits definite blue-shifted absorption and enhanced red-shifted fluorescence. Thus the probe **1** operates *via* the PET-inhibition mechanism.

The sensory effect was substantiated by quantum chemical calculations. The structures of the neutral and protonated forms of the probe **1** were optimized at the B3LYP/6-31 + G(d) level, followed by analysis on the frontier orbitals. As one can see from the calculation results, the HOMO of the neutral **1** was found to be localized on the BODIPY core and benzimidazole, while the LUMO is mainly composed of the BODIPY unit. However, both HOMO and LUMO of the protonated **1** are localized in the BODIPY core. Thus, the PET between BODIPY and benzimidazole moiety exists in the neutral form. It is inhibited in the protonated form, since the imine N-atom is protonated. The energy band-gap was estimated to be 2.84 eV for the neutral and 3.12 eV for the protonated form, reflecting an increased transition energy in good accordance with the blue-shift of the batochromic band in the electronic absorption spectra. Therefore, the benzimidazole-BODIPY dye **1** can be effectively used as an optical switch and the fluorescent pH-indicator. Internalization of both 1.0 nM and 10.0 nM antibody concentrations was detected. Cell experiments were carried out to verify that the probe **1** can be selectively used in the acidic lysosome.

Naphthalimide derivatives are a useful class of pH- and metal ion-sensitive fluorophores.[141–143] Due to their high fluorescence and good photostability, 4-amino-1,8-naphthalimide derivatives have found wide application in a number of fields including laser active media,[144,145] potential photosensitive biological units,[146] fluorescent markers,[147] fluorescence sensors and switches in electroluminescent materials,[148–150] liquid crystal displays[151] and ion probes.[152]

A highly photostable yellow-green emitting 1,8-naphthalimide-based dye **2** containing active fragments of a hindered amine radical scavenger, *s*-triazine UV-absorber and a polymerizable allyl function was designed as a PET fluorescence chemosensor for metal ions and protons, as well as an additive capable of chemical fluorescence dyeing of polymers (Scheme 4).[153]

Scheme 4

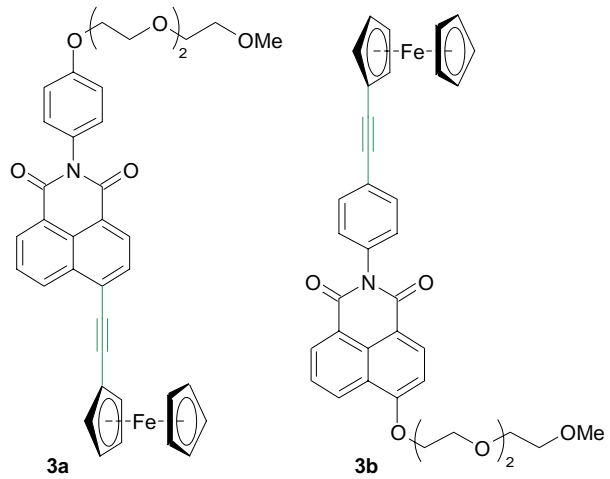


The photophysical properties of the 'turn-on' probe **2** were studied in DMF and water – DMF solutions. Thus, the presence of metal ions (Cu^{2+}, Pb^{2+}, Zn^{2+}, Co^{2+} and Ni^{2+}) and protons markedly changed the fluorescence intensity of the molecule. These changes can be attributed to the coordination of the piperazine amine receptor with the analyte as illustrated in Scheme 4. The probe **2** itself shows a low fluorescence quantum yield due to the PET from *N*-methylpiperazine donor moiety to 1,8-naphthalimide acceptor. Thus, the fluorescence of **2** is quenched. The highest fluorescence enhancement (FE) of the dye **2** was observed in the presence of Cu^{2+} ions (FE = 30.94). Fluorescence intensity was noticeably increased at Cu^{2+} concentration of 6.67×10^{-6} mol L^{-1}. Titration plot of the probe **2** shows a 1 : 1 metal – probe complex formation. According to this, a blue shift ($\approx$11 nm) of the fluorescence maxima in the presence of Cu^{2+} is observed. However, the recognition of the Cu^{2+} ion *via* complex formation eliminates the donor ability of the piperazine moiety, allowing the emission to be 'switched on'. The discussed mechanism of the fluorescence enhancement is similar to that of protonation. For example, after protonation of the alkylated amine receptors in the probe **2** in an acidic medium, the fluorescence increased more than 40-times (FE = 40.64 – 46.37).

Two novel 'turn-on' probes **3a**,**b** containing a ferrocene unit and a strongly fluorescent naphthalimide moiety were synthesized and tested for the gold ion detection.[154]

The incorporation of a hydrophilic triethylene glycol unit improves the water solubility and facilitates the dispersion of compounds **3a**,**b** in aqueous media. The presence of the ferrocene unit in both compounds decreases their emission due to the PET. However, the probe **3b** exhibits a selective fluorescent 'turn-on' upon addition of the Au^{III} ion. The selectivity towards gold ions is explained by their special affinity to the triple bond. Two acetylenic carbons resonate at 90.3 and 85.8 ppm in the ^{13}C NMR spectrum of **3b** in CD_3CN. Upon addition of Au^{III} ions to the sample, these signals disappear, thus providing a strong evidence for the presumed coordination of Au^{III} to the triple bond. The calculations using the DFT method (B3LYP/LANL2DZ) indicate that the HOMO energy level of the ferrocenyl(imidophenyl)acetylene moiety in **3b** is at -5.54 eV, which is higher than those of the naphthalimide moiety in the same molecule (-6.47 eV). Coordination of the gold ion to the triple bond disturbs the conjugation and inhibits the PET effect, thus enhancing the fluorescence signal. A low to negligible interference by a 100-fold concentration of other metal ions in acetonitrile – water solution is also noted. Under the conditions used, the detection limit for Au^{III} ions was found to be 95 ppb.

Structures 3



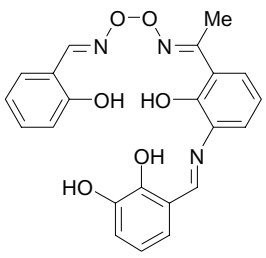
3a **3b**

Schiff bases are much of interest due to their wide application in many fields, *e.g.*, as liquid crystals,[159 – 162] organic dyes[163 – 170] and catalysts.[171 – 173] The spectral response of salicylideneaniline derivatives is based on the ESIPT effect, which includes transfer of a hydroxy proton to the imine nitrogen through a preexisting intramolecular hydrogen bonding configuration. This phenomenon has been extensively investigated in sensory reactions.[174 – 186, 298 – 304] This unusual optical property has found many important applications, *e.g.*, in photochromic materials,[187] chemosensors[188 – 192] and organic light-emitting diodes.[193 – 195]

A new Salamo-type bisoxime (probe **4**) has been synthesized.[196]

Bisoxime **4** shows 'turn-on' sensing properties towards several metal ions such as Pb^{2+}, Zn^{2+} and Cu^{2+}. An obvious colour change in sensing Pb^{2+} ions from yellow **4** to pale pink **4**-Pb^{2+} can be observed by the naked eye in visible light. Probe **4** can also act as a fluorescent sensor for recognition of Zn^{2+} ions with high selectivity and sensitivity. The binding constant K of the probe **4**-Zn^{2+} complex was estimated to be 4.04×10^9 mol L^{-1} by the Benesi – Hildebrand equation. The detection limit of the Zn^{2+} ion was 4.07×10^{-7} mol L^{-1}. The mechanism of sensory effect of

Structure 4



4

the probe **4** towards metal ions has been evaluated from the crystallographic data for the isolated probe **4**-Cu^{2+} complex. According to the X-ray diffraction data, complex [Cu(**4**)(μ-OAc)Cu] contains two Cu^{2+} atoms, one molecule of **4** and one μ-acetato group. The cupric ion is located in the N_2O_2 coordination environment of **4** moiety while the Cu^{+} ion is located in the NO_3 site. Two oxygen atoms [O(3) and O(6)] of the donor NOON moiety of compound **4** bridge the Cu^{+} and Cu^{2+} ions. Upon binding to a metal ion, the nitrogen lone pair is no longer available for the PET process.

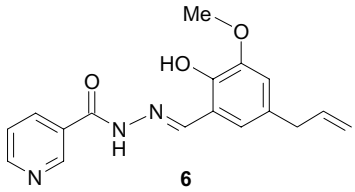
The 4-(benzo[*d*]thiazol-2-yl)-2,5-dihydroxybenzaldehyde derivative has been synthesized to develop a novel multifunctional fluorescent probe **5**.[197]

The probe provides emission *via* the ESIPT mechanism under excitation. Fluorescent analysis showed the probe **5** to exhibit excellent recognition properties towards Cr^{3+}, Al^{3+}, Zn^{2+} and F^{-} ions with large Stokes shifts. Moreover, under optimal conditions, the detection limits of probe **5** for these ions were lower than 10^{-8} mol L^{-1}. However, fluorescent and ^{1}H NMR titration experiments show the recognition mechanisms of probe **5** towards the mentioned ions to be somewhat different. Upon increasing the concentration of Cr^{3+} ion, a significant upfield chemical shift of the OH proton has been observed. Meanwhile, the singlet signal of the imine functions converted to triplets, which were slightly shifted downfield. It indicates that *orto*-OH functions and the imine N atoms are responsible for the recognition of Cr^{3+} ions. Thus, in the presence of Cr^{3+} and Al^{3+} ions, recognition mechanism shown in Scheme 5 operates. The presence of Zn^{2+} ions provides a definite deprotonation of the phenolic OH and induces an ESIPT red-shifted (60 nm) emission wavelength. The recognition mechanism is illustrated in Scheme 5.

The presence of F^{-} ion results in the complete deprotonation of the free phenolic OH groups. Therefore, a remarkable ESIPT emission is observed. As a result, it was shown that the ESIPT mechanism can be controlled by the four mentioned ions. The discussed mechanisms were further supported by a computational study. The application of probe **5** as a biosensor in living cells (PC3 cells) towards Cr^{3+}, Al^{3+} and Zn^{2+} ions has also been demonstrated.

Receptor **6** with a cavity table to accommodate Zn^{2+} ions was synthesized.[198]

Structure 6



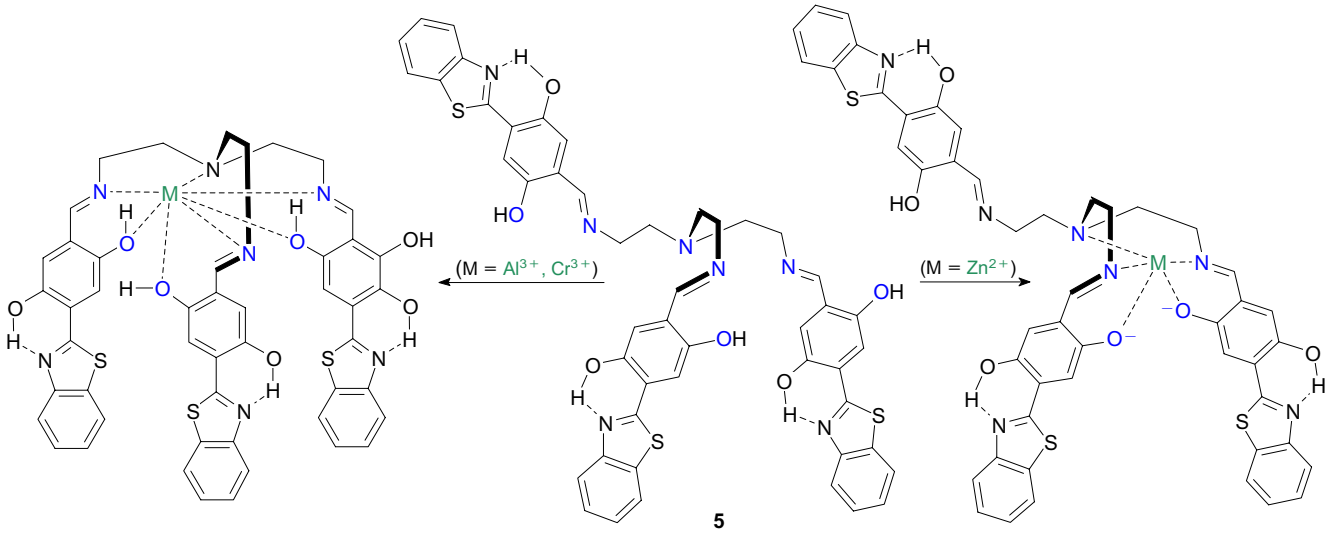
6

The absorption and fluorescence titrations with this selectively detected analyte showed satisfactory linear relationship between the added concentrations and the band intensities. The emission peak maximum was located at 517 nm. Considering the 1 : 1 binding stoichiometry between the probe **6** and the Zn^{2+} ions, the possible 3D-structure was calculated by applying the DFT method. All calculations were performed in Gaussian 09W by applying the exchange-correlation functional B3LYP and the 6-31G(d,p) basis set for the C, H, N and O atoms, and LANL2DZ for the Zn atom. The optimized structure of the probe **6** showed an intramolecular hydrogen bonding with the length of 1.814 Å, which agrees well with the position of the phenolic OH signal (12.18 ppm) in the downfield region of ^{1}H NMR spectrum. The fluorescence enhancement of receptor **6** in the presence of Zn^{2+} at 517 nm can be explained by the inhibition of the C=N isomerization in the excited state, which caused a large CHEF effect.[311 – 313] The competitive experiment was performed by recording the fluorescence spectra of receptor **6** in the presence of 1 equiv. of Zn^{2+} ion mixed with 1 equiv. of other potent cations mentioned above. No significant variation in the fluorescence spectra of receptor **6** was found in comparison with those with the same amounts of Zn^{2+} solution in the presence and in the absence of other cations. The estimated detection limit was found down to 10.75 nm.

Sensor **7** based on a Schiff base derivative has been suggested for selective detection of Ni^{2+} ion (Scheme 6).[199] The probe exhibits the remarkable fluorescent response to Ni^{2+} ion with a 1 : 1 stoichiometric ratio and detection limit equal to 8.62×10^{-7} mol L^{-1}.

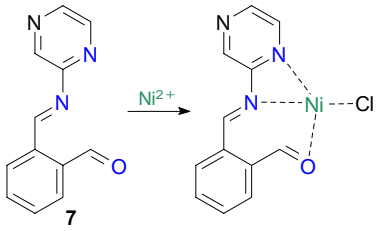
The 1 : 1 binding was supported by using electrospray ionization (ESI) mass spectrometry and FT-IR spectra. The probe **7** reveals the stretching vibration peaks of N=CH and C(H)=O functions appearing at 1641 and 2764 cm^{-1},

Scheme 5



5

Scheme 6

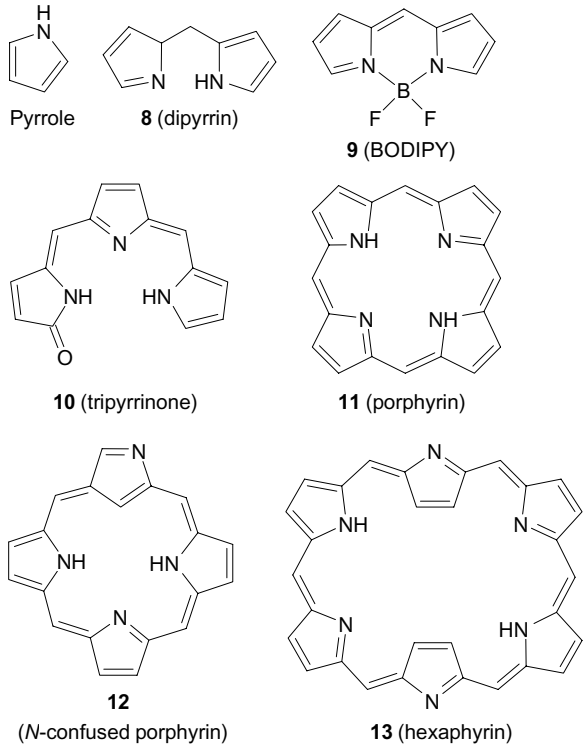


respectively. After addition of Ni^{2+} ion, both N=CH and C(H)=O bands shift to lower frequencies, with the intensity of the latter peak decreasing. Two characteristic peaks were also observed at 457 and 543 cm^{-1}, showing Ni^{2+} ion coordination with the binding site of the probe. The sensor **7** alone exhibits a weak fluorescence at 393 nm due to the C=N isomerization process in its excited state. In the presence of Ni^{2+} ion, the sensor displays a new strong emission band at 630 nm. The significant enhancement of fluorescence intensity is explained by inhibition of the C=N isomerization and promotion of the CHEF effect upon Ni^{2+} ion binding at the N=CH, C(H)=O site.

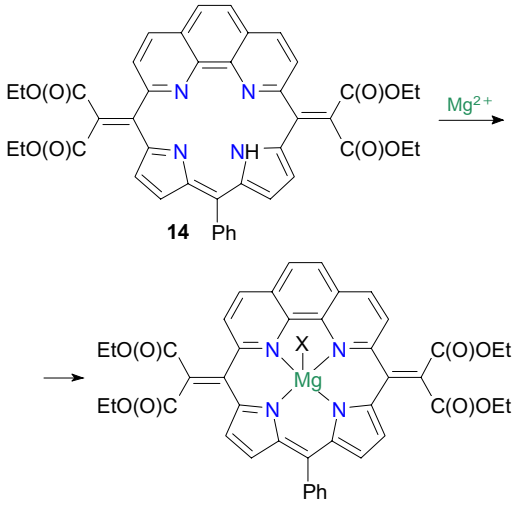
Porphyrinoids **8**–**13** represent optimal structures of fluorescent probes in which both the analyte binding part (receptor) and the fluorescent fragment define the same structural element. From this point of view, pyrrole is considered as a promising building block. It can be easily incorporated into linear and macrocyclic conjugated structures.

Simple oligopyrrins have flexible conformations. Therefore, metal coordination improves their rigidity, which results in a definite fluorescence enhancement. Compared to normal porphyrins, these compounds are supposed to be more suitable to provide fluorescence 'turn-on' probes for metal ions with large signal-to-noise ratios and high sensitivity.[204] As an example, the probe **14** is considered to be effective chemosensor for Mg^{2+} ions (Scheme 7). It has a suitable central cavity size selective to Mg^{2+} over Na^+, K^+ and Ca^{2+} ions, showing complexing constant of 37.3 mol^{-1} in the presence of water. The probe **14** shows a very weak fluorescence at 572 nm with a quantum yield of 0.3%. NMR and MS spectral measurements show that the addition of Mg^{2+} ions to the solution of compound **14** in acetonitrile generates 1 : 1 complex leading to 16-fold fluorescence enhancement with an emission wavelength at 639 nm and quantum yield of 1.5%. The binding constant of the **14**-Mg^{2+} ion complex was estimated as being equal to 7.3 mol^{-1}.

Structures 8–13



Scheme 7



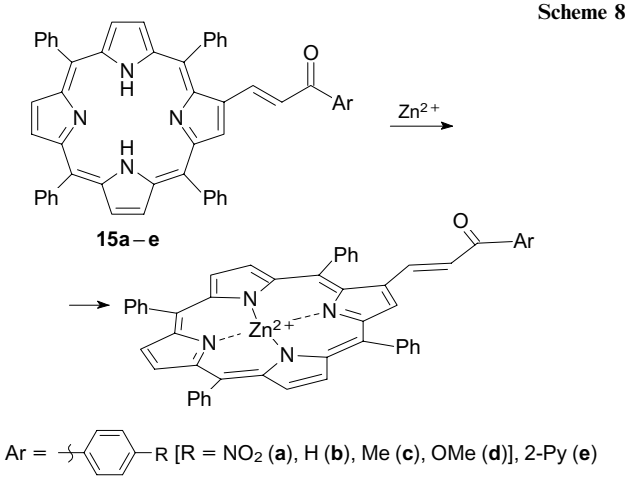
Porphyrin–chalcone type probes with efficient red fluorescence have been prepared.[205]

For some of them (compounds **15a**–**e**), their ion recognition ability towards Ag^+, Cu^{2+}, Zn^{2+}, Cd^{2+} and Hg^{2+} ions in organic solvents, in solid state as well as in polymers [*e.g.*, poly(methyl-methacrylate) (PMMA)] has been determined using absorption and emission spectroscopy techniques. The best ion sensing was observed for the Zn^{2+} ion using the probe **15a** with the detection limit equal to 60 ppb (Scheme 8).

A decrease in intensity of two bands centred at *ca.* 671 and 728 nm in the emission spectra of probes **15a**–**e** was accompanied by the appearance of a new band at 633 nm after addition of the Zn^{2+} ion. This new emission band was assigned to the metal-to-ligand charge transfer. It shows the generation of a new fluorophore due to the metal–porphyrin association. In order to study various reaction pathways of probes **15a**,**c** and Zn^{2+}, the effect of addition of this ion was monitored by ^1H NMR spectroscopy technique. The interaction of the probe **15a** with Zn^{2+} ion leads to the loss of symmetry of the porphyrinic macrocycle and to nonequivalence of its NH protons, which appear as a singlet at −2.5 ppm in the probe **15a**, but are observed as two pairs of separate singlets after Zn^{2+} ion addition.

Among various types of known fluorophores, pyrene shows unique photophysical properties and is useful in the environmentally benign sensor systems.[207,208] Pyrene derivatives are used for constructing various types of probes due to their advantageous properties such as polarity sensitive vibronic emission, long fluorescence lifetime, high charge carrier mobility, π–π staking behaviour and chemical

Scheme 8



stability.[209 – 211] A novel pyrene-based fluorescent probe, 4-phenyl-2-(pyren-1-yl)-1,8-naphthyridine **16**, has been synthesized.[212]

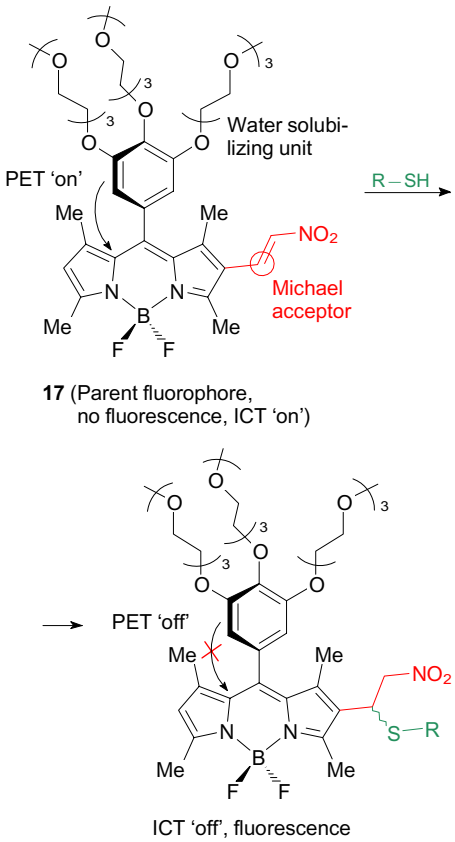
The probe **16** was used as a selective sensor for Ni^{2+} ion over other cations. The solvent polarity-dependent photoluminescence characteristics strongly confirm the presence of photoinduced electron transfer from pyrene to 1,8-naphthyridine unit in the probe. Upon Ni^{2+} addition, the fluorescence wavelength was shifted to 450 nm due to the formation of a square planar 2 : 1 complex of the probe with Ni^{2+} ion (Scheme 9). The resultant excimer formation and PET from pyrene moiety to the 1,8-naphthyridine part was supported by DFT calculations. The HOMO of the probe **16** is localized on pyrenyl unit, while the LUMO is located on the 1,8-naphthyridine unit. The PET takes place from pyrenyl unit to the 1,8-naphthyridine unit resulting in a weaker emission. When Ni^{2+} binds to the nitrogen atoms in the complex, the PET process is inhibited through the CHEF effect and excimer formation. The remarkable fluorescence enhancement with a 20 nm red shift is observed. The detection limit was 2.5×10^{-1} mol L^{-1}. The probe **16** also exhibits very low cytotoxicity and strong fluorescence emission in living cells.

4.2. Nucleophiles as analytes

The BODIPY dye **17** containing nitroethenyl substituents connected with the BODIPY core is shown to be a sensitive ICT-probe to biological thiols particularly, to cysteine (Cys) (Scheme 10).[134]

Both absorbance and emission spectral changes have been registered. Fluorescence intensity increased up to

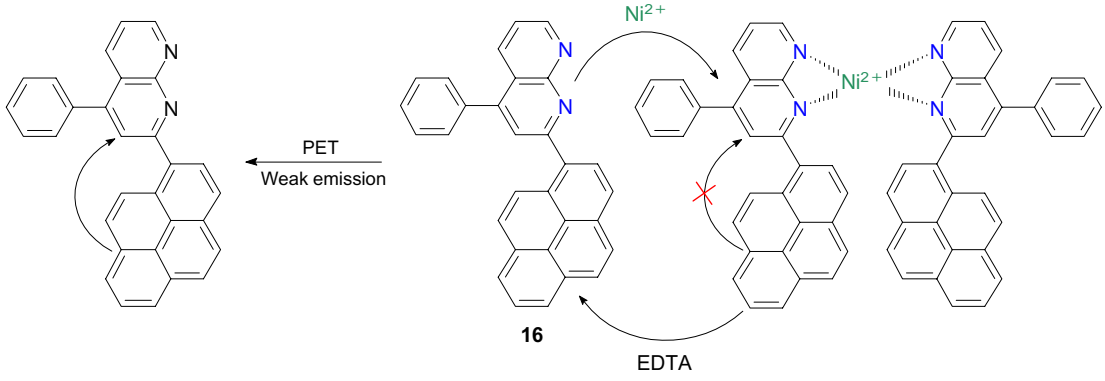
Scheme 10



20-fold upon increasing the cysteine concentrations (0 – 400 equiv.) with an emission band centred at 515 nm (λ_{ex} = 500 nm). Significant change was observed neither in absorption nor in emission spectra when natural amino acids other than cysteine were treated with the probe **17**. Nitroalkene unit represents a strong Michael acceptor, which turns to be highly sensitive to the sulfhydryl nucleophile. The Michael reaction of probe **17** has been studied by ^{1}H NMR spectroscopy. The addition of the analyte to sensor **17** results in the disappearance of the vinylic protons at 8.07 and 7.44 ppm with immediate appearance of protons of the formed nitroalkane moiety at 4.80 ppm. A nucleophilic attack of the sulfhydryl nucleophile to the β-position of nitroethene disrupts the π-conjugation and hinders the ICT. As a result, combination of two mechanisms (PET and ICT) provides fluorescence response of the probe **17**.

Dicyanomethylene-benzopyran (DCMB)-based fluorescent probes have been developed for the detection of

Scheme 9



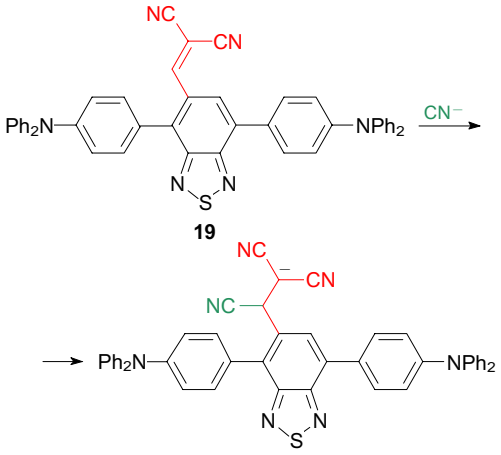
harmful small molecules of food additives, such as benzoyl peroxide,[314, 315] formaldehyde,[316] sodium sulfite[317, 318] and sodium nitrite.[319] Some probes for these analytes show hypochromic effect and emission in the visible region and suffer from the interference from background. The DCMB-based probes are characterized by significant hyperchromic effect and near-infrared (NIR) fluorescence 'turn-on' response towards analytes. This effect can minimize the interference from background, such as flavonoids with yellowish green fluorescence, and provide a possibility to detect analytes in food with the naked eye. Dicyanomethylene-benzopyran is known as a photostable and easy-to-prepare precursor of fluorophores that exhibit emission in the NIR region.[320–323]

A NIR 'turn-on' fluorescent chemodosimeter **18** for the detection of SO_3^{2-} ions in food has been synthesized (Scheme 11).[213] The strong electron-withdrawing quinolinyl was chosen as a building block to prepare DCMB due to its ability to quench the fluorescence of DCMB and increase the solubility in water. Sensor **18** shows a significant colorimetric and NIR fluorescent response to the SO_3^{2-} ion. Compared to non-fluorescent compound **18**, a great fluorescence enhancement at 675 nm was observed in the presence of SO_3^{2-} [quantum yield (Φ) = 0.38]. The detection limit of the probe **18** for SO_3^{2-} is calculated to be 31.6 nmol L^{-1}. The detection is specified by the high contrast ratio based on the 1,4-nucleophilic addition reaction. Thus, the conjugated Michael addition turns to be a sensing mechanism of the sensor **18**, which was confirmed by the ^1H NMR and high-resolution mass spectrometry (HR-MS) spectra. After treatment with 10 equivalents of SO_3^{2-}, the chemical shifts at 9.97 ppm and 4.67 ppm changed to 4.97 ppm and 3.36 ppm, respectively, suggesting that the quinolinium skeleton is broken by the 1,4-Michael addition of the nucleophilic SO_3^{2-}.

The probe **19** containing triphenylamine as a donor and benzothiadiazole as an acceptor has been synthesized (Scheme 12).[214] Several chemosensor systems for CN^- detection had been earlier developed. These systems are based on nucleophilic addition reactions[324–326] and hydrogen bonding interaction.[327, 328] The probe **19** differs by 'red-shifted' emission as a sensing effect. The calculated detection limit by the fluorescence changes is equal to 0.014 mmol L^{-1}, being comparable with those of other dicyanovinyl-based probes.

The mechanism of probe **19** for CN^- sensing was analyzed using ^1H NMR spectroscopy. The cyanide ion adds to the dicyanovinyl fragment by the Michael addition

Scheme 12

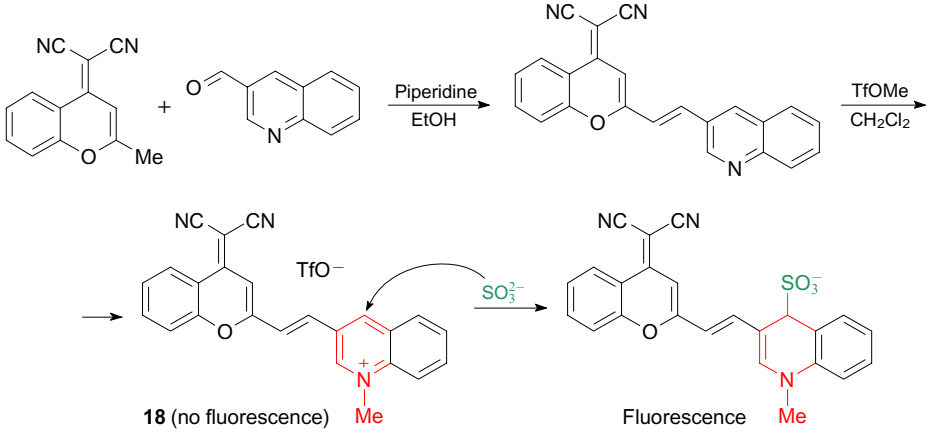


mechanism resulting in a definite reduction of the vinylic proton signal at 8.38 ppm, which finally disappears upon addition of 1.0 equiv. of CN^- ion. A new signal corresponding to the β-proton of dicyanovinyl is observed at 4.70 ppm. Interaction of the cyanide ion with the sensor molecule inhibits the ICT and results in the disappearance of the absorption peak at 521 nm, and the appearance of a new one at 450 nm. Besides, nucleophilic addition of the CN^- ion to the dicyanovinyl moiety provides a large change in the emission spectra. The band centred at 627 nm increases prominently. It has a large Stokes shift and the fluorescence wavelength is close to the infrared region.

The ICT effect is often responsible for low emission of fluorophore molecule, which is enhanced upon addition of the analyte molecule to the π-conjugated system of the probe. The probe **20** has also been synthesized for the cyanide ion detection. It is characterized by the absence of fluorescence due to the ICT effect. The ICT is blocked in **20**-CN because of breakdown of the conjugation between coumarin and indole groups. Thus, the fluorescence enhancement for **20**-CN becomes possible.[215]

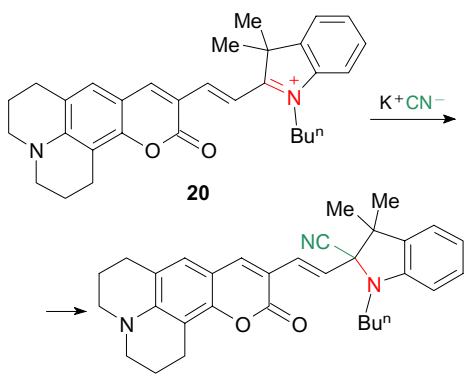
It should be noted that no significant fluorescence changes were noticed for other potassium salt anions. The molecular orbitals relevant to the excitations and electron transitions in the structures **20**–**38** and **20**-CN (Scheme 13) are described below. The HOMO–LUMO transition solely contributes to the excitation in probe **20**, while the contribution of the HOMO–LUMO is only 9.4% and that of HOMO-1–LUMO is 90.6% in **20**-CN. As expected, the

Scheme 11



Tf is triflate

Scheme 13



electron density of the LUMO of compound **20**-CN is only distributed over the coumarin moiety, while that of the LUMO in **20** is distributed over the entire coumarin through the indole moieties. In cyanide detection, sensors utilizing affinity of CN^- to Cu^{2+} ions to form stable $[Cu(CN)_x]$ species are of special attention.[329] In many fluorescent probes, the fluorescence was reported to be quenched upon addition of Cu^{2+} ions because of the PCT or heavy metal ion effect of the Cu^{2+} ion.[330–333] Upon the addition of the cyanide anion, the quenched fluorescence is immediately recovered because of the formation of stable $Cu(CN)_2$ complex.

Compound **21** represents one more probe for the cyanide ion detection. This probe containing hydroxy-function at the π-conjugated system can display the ESICT effect (Scheme 14).[164]

As a result, the probe **21** alone shows a weak, single fluorescence emission band at 468 nm when excited at 356 nm. The addition of CN^- ion to an aqueous solution (pH 7.26, 80% DMSO) of probe **21** leads to a significant fluorescence enhancement. The fluorescence intensity increased by more than 200 times as the concentration of CN^- reached 20.0 mmol L^{-1} in the solution of **21**. The detection limit calculated from this titration data showed to be 14 pmol L^{-1} in aqueous solution. Due to the exceptional nucleophilicity of the cyanide anion, nucleophilic substitution by CN^- is a very sensitive method for probing its presence, and addition of CN^- to activated double bonds is one of the important strategies that are selective to cyanide only.[334–337]

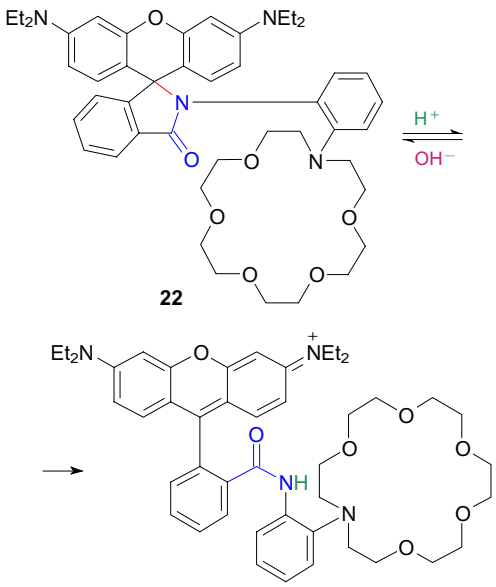
5. Probes activated from their latent forms

5.1. Acid activation of latent forms

Rhodamine, a classical fluorescent dye, has been widely used as a fluorophore moiety because of its excellent photophysical and chemical properties.[222–229] Moreover, nonfluorescent and colourless rhodamine spirolactam (or spirolactone) ring undergoes fast opening in the presence of H^+ or a metal ion. This results in a strong fluorescence and bright pink colour. Therefore, several fluorescent probes for lysosomal pH based on rhodamine dyes have been reported. These probes selectively detect acidic pH and can be also used in living cells to monitor pH changes in acidic organelles.

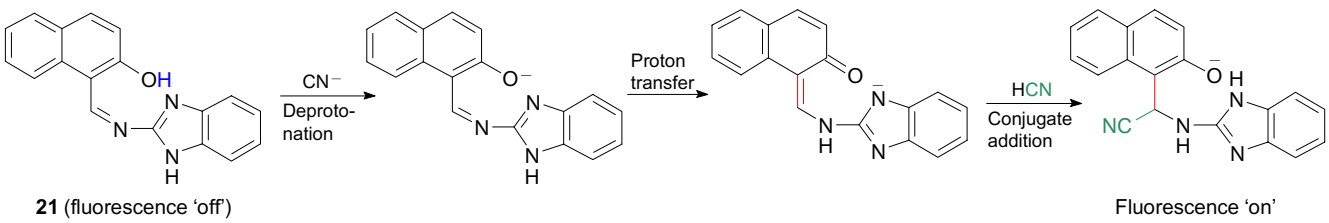
Rhodamine B lactam dye (18-aza-6-crown ether conjugate **22**) has been developed for monitoring changes in lysosomal pH in living cells (Scheme 15).[230]

Scheme 15



This probe is worth of much attention, since abnormal fluctuation of intracellular pH can cause serious diseases, such as indiscriminate cell apoptosis, necrosis and generation of free radicals. Moreover, it is associated with serious conditions like Alzheimer's disease and cancer. The lysosome acts also as a cell's recycling center because it is involved in a variety of important events, including energy metabolism, cell membrane repair and secretion. Nonfluorescent and colourless rhodamine spirolactam ring of **22** undergoes opening in the presence of H^+ ions. Acid hydrolysis of the cyclic amide affords Rhodamine B laser dye. The sensing effect results in a strong fluorescence and appearance of the bright pink colour. The emission of probe **22** at 588 nm increased with a pH value decreasing from pH 7 to 4.0. The probe **22** exhibited good water solubility, high quantum yield (Φ = 0.45 at pH 4.0), as well as fast response to the pH changes. Besides, chemosensor **22** can stain lysosomes in living cells while manifesting high photostability and low cytotoxicity. The necessity of presence of aza-18-crown-6 group in compound **22** for sensing effect is discussed. As a reference probe, Rhodamine B spirolactam dye without aza-18-crown-6 group has also been synthesized. However, its low water solubility and low p*K*a value

Scheme 14

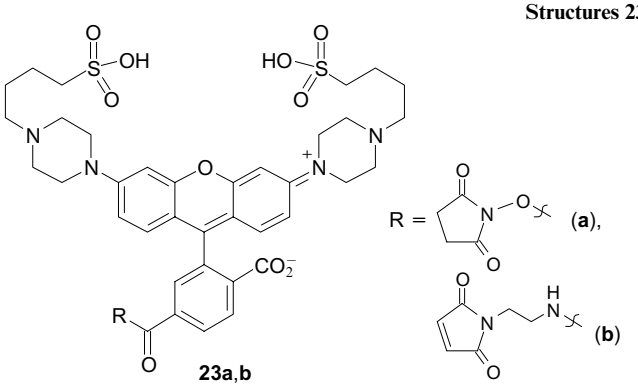


suggest this analogue to be inappropriate to detect pH changes in living cells. Therefore, the presence of the aza-18-crown-6 group seems to be vital for probe **22** to exhibit specific fluorescent responses to physiologically acidic environment along with having high water solubility.

Receptor-mediated antibody internalization plays a key role in the mechanism of action of a number of anticancer therapeutics. A new homogeneous approach for direct measurement of time- and concentration-dependent antibody internalization has been developed.[231] This method is based on novel hydrophilic and bright pH dyes **23a**,**b**, which do not exhibit any significant emission under neutral conditions (at pH $\geqslant$7.5), but turn highly fluorescent at acidic pH values. The probes have excitation and emission maxima of 532 nm and 560 nm, respectively, are photostable in solution and display no loss of signal during multiple cycles of acid/base titration.

The structures of the probes **23a**,**b** comprise a rhodamine dye moiety and two saturated 1,4-diazine groups. To be useful for antibody internalization, the dye was modified to have amino (probe **23a**) and thiol (probe **23b**) reactive groups for connection with the antibody at lysine amino acids presenting at the antibody surface. To solve the precipitation problem, the dyes were provided with two sulfonate groups. As a result, a high dye **23a**,**b** to antibody ratio has been achieved without precipitating antibody. Upon binding to the receptor, the dye conjugated to antibody is not fluorescent because of the neutral pH of the media. But after internalization the pH value decreases and the dye becomes fluorescent.

Structures 23

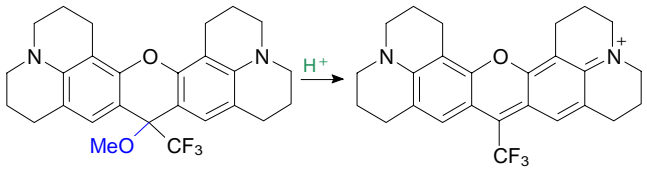


23a,**b**

Several laser dyes in latent forms sensitive to photogenerated acids should also be discussed. A novel non-fluorescent compound **24** as a latent form of the Rhodamine 700 dye sensitive to a photogenerated acid has been developed.[232] The probe **24** was synthesized by titration of Rhodamine 700 solution with potassium hydroxide in methanol. The obtained compound is colourless and stable in neutral media. However, in the presence of an acid it transforms to Rhodamine 700 dye, which is a coloured and highly fluorescing compound, known as a laser dye (Scheme 16). Here, ether hydrolysis takes place. Protonation of the methoxy function leads to methanol elimination and formation of the iminium ion, which is highly conjugated and stabilized. Thus, compound **24** can be considered as a probe for acidity.

It works also in polymer films and has been used as optical information recording media. Two major

Scheme 16



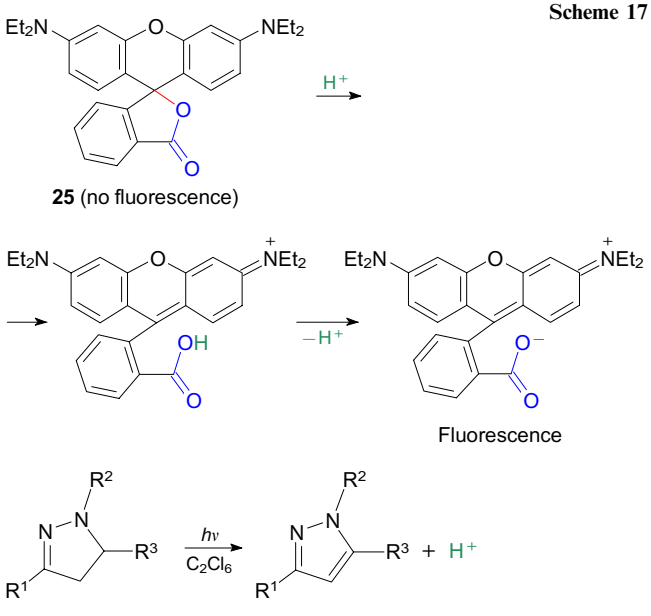
24 (no fluorescence) Fluorescence

components — latent form **24** and photoacid generator (PAG) — were uniformly dispersed in a PMMA film. Two-photon absorption at 532 nm generated by a picosecond neodymium-doped yttrium aluminium garnet (Nd:YAG) laser was used in the recording procedure. The photogenerated acid reacts with the probe **24** to form Rhodamine 700 coloured fluorescing molecules, which provide spots at the focus of the laser pulses (bits), inside the memory PMMA disk. The written information can be read by irradiation of the written bits using a low power continuous wave (CW) diode laser that emits at 650 nm absorption maximum of Rhodamine 700. The diode laser light provides a fluorescence of the stored bits. Measuring the emitted fluorescence allows one to read the stored information.

Rhodamine B lactone form **25** has been shown to act as a sensor to acidity photogenerated in organic solvents as well. It gives rise to intense absorption at 530 nm and emission at 560 nm due to the formation of the laser dye Rhodamine B during its irradiation in the presence of PAGs (Scheme 17). The ring opening is also promoted by the acid provided by photodehydrogenation of pyrazolines in the presence of perchloroalkanes.

Thus, dehydrogenation of pyrazolines generates highly fluorescent laser dye Rhodamine B from its lactone form during irradiation in polymer (PMMA) films. This acid sensitivity of the rhodamine latent forms has been successfully used for creation of new media in optical recording of information.[233 – 236]

Scheme 17



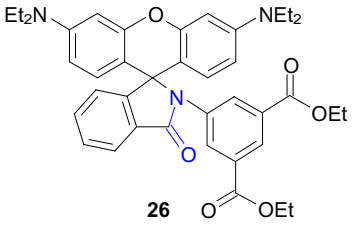
R^1 = Bu^t, Ar, HetAr; R^2 = R^3 = Ar

5.2. Activation of latent forms of organic dyes by metal ions

A Rhodamine B-based fluorescence probe **26**, which exhibits a sensitive and selective recognition towards mercury(II), has been synthesized.[237]

As expected, the probe **26** itself exhibits a very weak fluorescence. After the addition of mercury ions to a solution of **26** in acetonitrile, the emission band at 580 nm appears being assigned to the delocalized xanthene structure of the open form of rhodamine moiety. The fluorescence intensity of the solution shows *ca.* 65-fold increase compared to that of the free probe **26** and the solution turns from colourless to pink. The association constant for the Hg^{2+} ion complex formation is estimated as 1.73×10^9 mol^{-2} in acetonitrile with 1 : 2 stoichiometry. The ^{1}H NMR experiments confirm the ring opening mechanism. The addition of Hg^{2+} ion does not cause any obvious shifts in the ^{1}H NMR spectrum. It was suggested that there was not any direct binding between the molecule of **26** and Hg^{2+} ion. The addition of Hg^{2+} ions leads only to the simple opening of rhodamine spirolactam ring. The same conclusion has been made from the ESI-MS spectra. The probe **26** showed an intense peak with m/z = 662.32 in acetonitrile, which was assigned to $[\mathbf{26}+H]^+$ both with and without Hg^{2+} ion. The probe **26** was suggested to have certain steric hindrance for reliable complexing with Hg^{2+} ion. Nevertheless, the competition experiments revealed that the Hg^{II}-induced fluorescence rise was unaffected in the presence of relevant ions. The alkali-, alkaline-earth-, the first row transition metal ions did not interfere with the Hg^{II}-induced fluorescence enhancement (the concentration of Hg^{2+} is 10 μmol L^{-1}), confirming the remarkable selectivity of the probe **26** (1 μmol L^{-1}) for Hg^{2+} over other metal ions. Even the presence of 10 μmol L^{-1} of Zn^{II}, Cd^{II} as well as Pb^{II} and Ag^{I} could not bring any obvious fluorescence change.

Structure 26

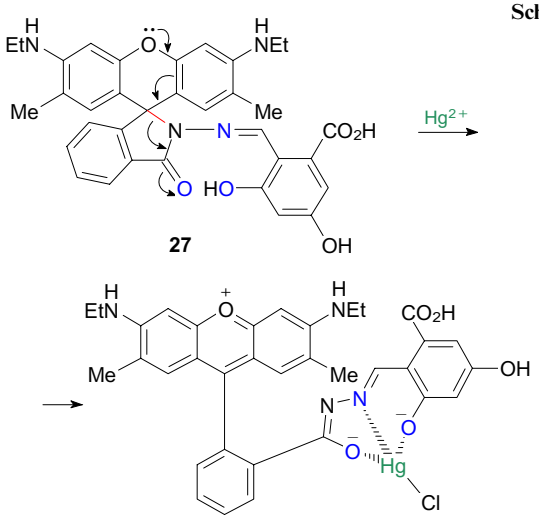


26

The rhodamine derivative **27** was synthesized and found to be highly selective to the mercury ion. In opposite to the probe **26**, compound **27** forms a well registered complex with Hg^{2+} ion and can be recommended as a 'turn-on' probe for facile mercury sensing (Scheme 18).[238]

The specificity of Hg^{2+}-**27** interaction provides definite selectivity for the Hg^{2+} detection. The visible naked-eye detection due to a drastic emission enhancement is reported. In the presence of the Hg^{2+} ion, the opening of the spirolactam ring takes place. In a fluorescence correlation spectroscopic study of probe **27**, detection of Hg^{2+} ion in solution was found at a level of 5 pmol L^{-1}. The binding constant equal to 2.4×10^7 mol^{-1} was estimated from Benesi – Hildebrand plot. The 1 : 1 binding stoichiometry was confirmed by the Job's plot and also by ESI-MS mass spectra. The peak at m/z 829.1700 corresponding to the **27**-Hg^{2+}Cl complex was observed, whereas the probe **27** without Hg^{2+} exhibited peak only at m/z 593.2406 corresponding to $[\mathbf{27}+H]^+$ ion. The probe **27** can be also applied

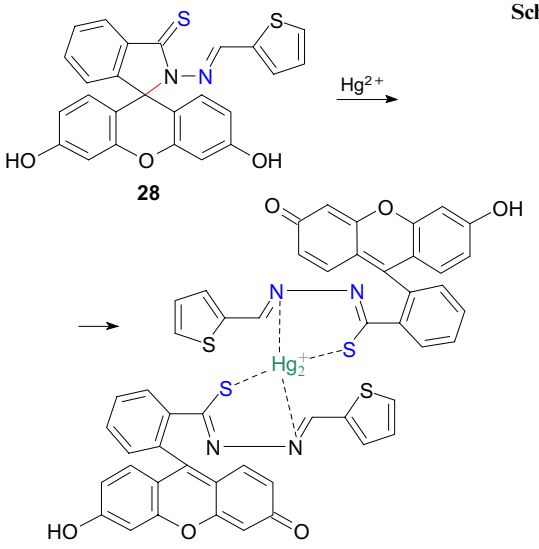
Scheme 18



to detect Hg^{2+} ions in living cells such as cervical cancer (HeLa) and macrophage cells. Lifetime of the compound **27** in HeLa cells increases from 0.21 to 2.01 ns after complexation with Hg^{2+}. These obvious changes indicate that **27** was cell membrane permeable and capable of imaging Hg^{2+} ions in living cells.

Lactam ring opening provides sensory effects of fluorescein dyes as well. Among various fluorophores, fluorescein is one of the most common fluorophores having some excellent spectroscopic properties: high fluorescence quantum yield, long absorption and emission wavelengths, easy operation and fast response, good biocompatibility and low toxicity.[247] Nevertheless, fluorescein-based probes have received comparatively little attention.[248,249] Thus, thioxofluorescein-based probe **28** has been reported for Hg^{2+} ion sensing (Scheme 19).[250]

Scheme 19



In the absence of Hg^{2+} ions, non-fluorescent signal in the range from 500 to 610 nm was observed, which was ascribed to the ring-closed spirolactam structure of **28**. Upon the addition of Hg^{2+} ions, a notable fluorescence enhancement emerged at 529 nm. With the concentration of Hg^{2+} ions being up to 2 equiv., the fluorescence intensity increased by ~37 times. The relative fluorescence intensity

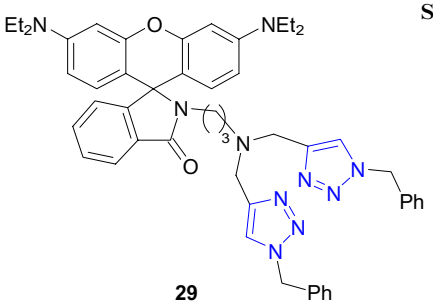
of **28** solution was linearly proportional to the concentration of Hg^{2+} ions in the range from 0.25 to 2.5 μmol L^{-1}. The detection limit was calculated to be 3.90×10^{-8} mol L^{-1} ($R^2 = 0.9933$). On the basis of the Job's plot, a possible model for binding of probe **28** with Hg^{2+} ions was proposed (Scheme 19), the molecules prefered their spirolactam ring-closed state and low fluorescence and absorbance signal could be recorded in the absence of Hg^{2+}. However, when the probe **28** encountered with Hg^{2+} ions, the imino N and the thioether S atoms of both ligands were involved in the binding with Hg^{2+} ions as confirmed by LC-MS analysis. In the absence of Hg^{2+}, a peak at *m*/*z* 457.0671 corresponding to **28** was observed. With 5 equiv. Hg^{2+}, a peak appeared at *m*/*z* 1108.2, which was assigned to the [2(**28**) + Hg^{2+} − 2 H^+]. To further explore the complexation behaviour of probe **28** towards Hg^{2+} ions, ^{1}H NMR titration experiment was also performed.

The substituent at the lactam nitrogen atom of rhodamine derivatives can be involved into the recognition process in a higher extent. Thus, compound **29** with two appended 1,2,3-triazole moieties *via* a diaminopropyl linker was found to be a highly selective fluorogenic chemosensor for Zn^{2+} ions.[239]

In the presence of Zn^{2+}, a colourless solution of probe **29** turns pink with maximum absorption at 555 nm and a large fluorescence enhancement (140-fold) at 579 nm ($\Phi = 0.12$). Such spectroscopic properties indicate that the 'turn-on' fluorescence emission of probe **29** is similar to that of other rhodamine-based fluorescent probes and is based on the opening of the spirolactam ring through the Zn^{2+} ion chelation with the nitrogen and the carbonyl oxygen atoms of the spirolactam moiety of the binding units. The probe **29** turned to be highly selective towards Zn^{2+} compared to other metal ions including Cd^{2+}, with a binding constant (K_a) of 7.4×10^3 mol^{-1} (by the Benesi–Hildebrand equation) and a detection limit of 1 μM (65 ppb). To further investigate the sensing mechanism of the probe **29**, rhodamine bis(triazole-ethylenediamine), an analogue of **29** with a shorter linker and mono-triazolyldiaminopropane rhodamine, an analogue of **29** with the only one 1,2,3-triazole group have been tested. In the presence of Zn^{2+} both analogues did not exhibit fluorescence, suggesting that both triazolyl units of **29** are responsible for Zn^{2+} binding and the length of the diamino linker is also important for the **29**–Zn^{2+} complexation. The application of **29** in the living cell imaging was also found. For this purpose, cultured HeLa cells were incubated with compound **29** for several hours. The fluorescence images demonstrated visual evidence that the probe **29** is cell-permeable and can be used to detect the intracellular presence of Zn^{2+}.

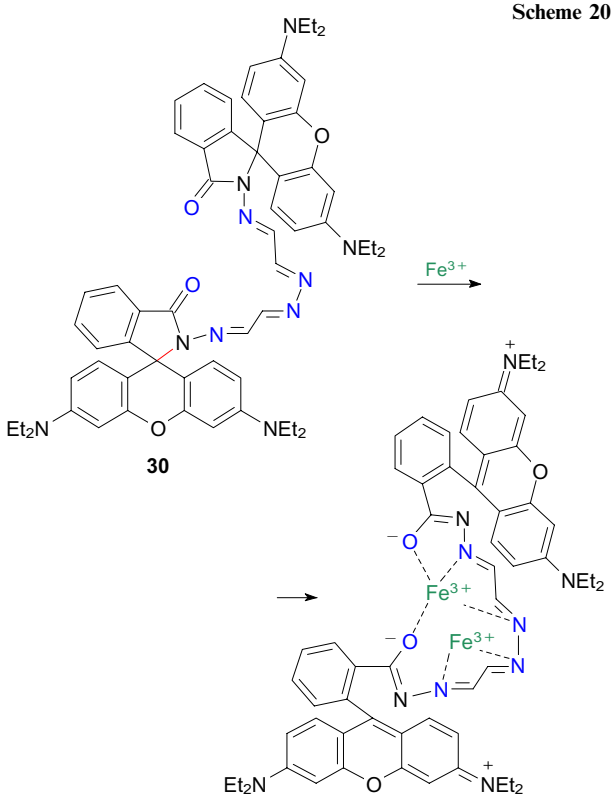
Several novel rhodamine-based fluorescent probes for Fe^{3+} ion (*e.g.*, compound **30**) were also designed.[240]

Structure 29



29

Scheme 20



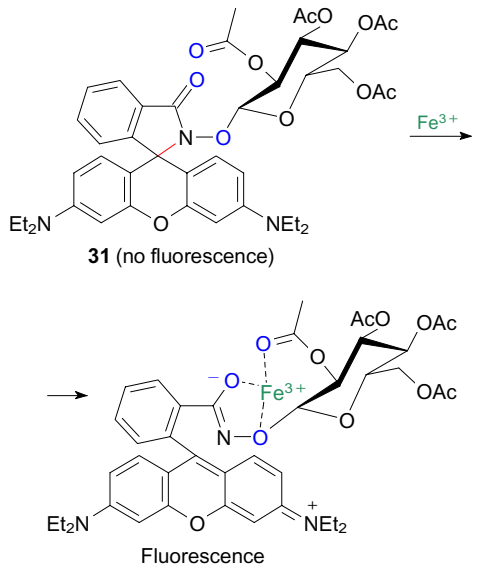
30

Lactam ring opening in the rhodamine moiety of probe **30** leads to the formation of two binding sites (Scheme 20). Highly selective and sensitive recognition toward Fe^{3+} over other metal ions is observed. The detection limit of probe **30** has been evaluated to be 0.2438 μmol L^{-1}. To better understand the nature of this probe and the 'turn-on' sensing mechanism, its energy optimized structure was determined using the DFT calculations with the Gaussian 09 program at the B3LYP/6-31G level. The spatial distributions and orbital energies of HOMO and LUMO of **30** were also obtained using DFT calculations. The HOMO of **30** turns to be spread out on the Rhodamine B xanthene ring while the LUMO is more localized and centred on the spirocycle. The DFT calculations based on the Fukui function $f^+(r)$ were also performed to elucidate the reaction mechanism of probe **30**. The results explain the reactivity of the latter towards nucleophilic attack, which has been earlier suggested for the Fe^{3+} detection. According to non-bonding orbital (NBO) analysis, the condensed Fukui function for **30** consists of O(1) 0.013, N(1)−0.001, N(2) 0.017, N(3) 0.007, N(4) 0.01, N(5) 0.008, N(6)−0.004, O(2) 0.021, indicating that **30** has two active sites for binding two Fe^{3+} ions, such as O(1), N(2), N(3) and O(2), N(5), N(6) atoms. The 1 : 2 complex formed by the probe **30** and Fe^{3+} ion is shown in Scheme 20. In a whole, the sensing response of the probe **30** meets the selective requirements for biomedical and environmental applications.

New sugar–rhodamine conjugate **31** and its deacetylated analogue have also been used as highly selective and very useful 'turn-on' probes for Fe^{3+} ion recognition (Scheme 21).[241]

Fluorescence and absorption responses of compound **31** to Fe^{3+} ion in comparison with other metal ions were investigated. The addition of 10 equivalents of Fe^{3+} ions to a solution of probe **31** in CH_3CN–water (20 : 1, v/v mix-

Scheme 21

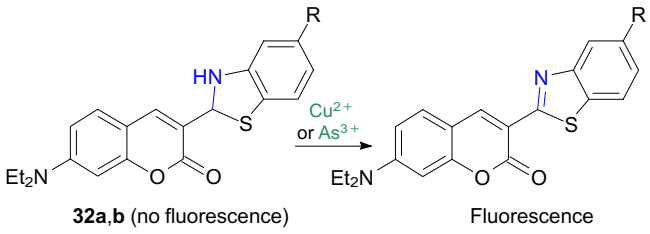


ture) led to a change in its colour from colourless to the pink one and remarkably enhanced fluorescence at 582 nm. The probe **31** shows a very good linear relationship between UV absorbance and Fe^{3+} concentration with the correlation coefficient equal to 0.997 and the detection limit of 3.46×10^{-6} mol L^{-1}. According to the Job's plot, 1 : 1 metal – ligand complex was formed. After addition of other metal ions (Hg^{2+}, Ca^{2+}, Mg^{2+}, Pb^{2+}, Ni^{2+}, Cu^{2+}, Ba^{2+}, Cd^{2+}, Zn^{2+}, Fe^{2+}, Ag^{+}, K^{+}, Na^{+}) the solutions did not show any colour and fluorescence. While discussing mechanism of Fe^{3+} ion detection, Chen and Fang [241] suggested the opening of the spirolactam ring of probe **31** and formation of a 1 : 1 metal – ligand complex (see Scheme 21). It should be noted that sugar-based probes showing better optical and biological responces had been earlier reported.[37, 242 – 244] With their use, Hg^{2+} ion [245, 246] and bovine serum albumin (BSA) were also successfully detected.[338, 339]

Benzothiazolines **32a**,**b** were described as chemodosimeters for oxidation reagents, including Cu^{2+} (Ref. 251) and As^{3+} ions [252] (Scheme 22). The oxidation reactions occur quantitatively and provide excellent sensing properties of these probes.

The fluorescence of **32a** in a water – acetonitrile mixture (1 : 1, v/v) is weak ('off' state). With 10 equiv. of Cu^{2+} ion added, a strong green fluorescence ('on' state) is observed.[251] It was shown that fluorescence spectra were similar both in the absence and in the presence of oxygen suggesting that benzothiazoline was oxidized by the Cu^{2+}

Scheme 22



R = H (**a**), CF_3 (**b**)

ion. The addition of a chelating reagent (*e.g.*, diethylenetriamine) to the solution did not change the fluorescence intensity, thus demonstrating that the oxidation process is irreversible. The sensing effect of the probe **32a** is highly selective. To explain why stronger oxidants (Fe^{3+} ion, H_2O_2, NaClO) show only little oxidative effect, the synergistic effect of coordination and oxidation during oxidation was proposed. The possible oxidative mechanism is shown in Scheme 23.

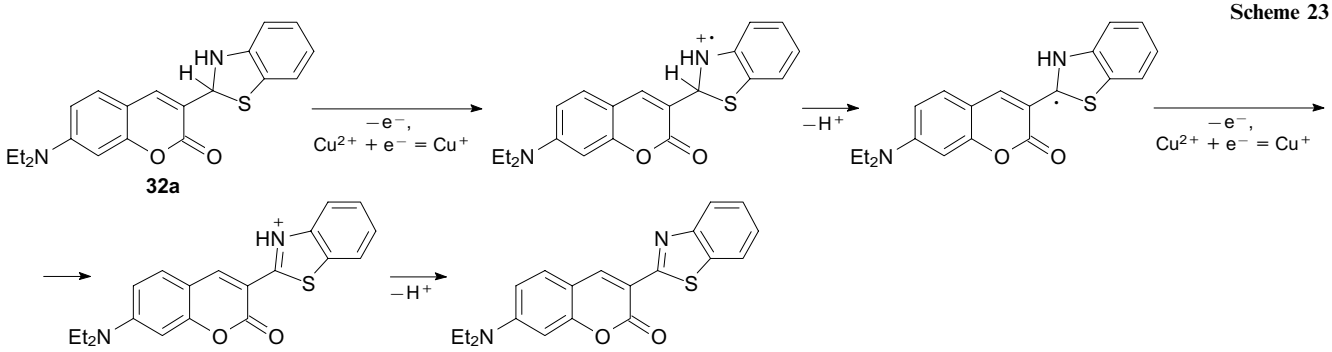
At the same time, other common metal ions such as Hg^{2+}, Ca^{2+}, Mg^{2+}, Pb^{2+}, Ni^{2+}, Cu^{2+}, Ba^{2+}, Cd^{2+}, Zn^{2+}, Ag^{+}, K^{+}, Na^{+} provide only little fluorescence intensity enhancement.

Benzothiazoline **32b** turned to provide excellent sensory effect towards As^{3+} ion.[252] This is a significant result, since arsenic contamination is a serious environmental problem. The currently accepted upper limit for arsenic in water is $\approx$10 ppb. Therefore, there is a need for highly sensitive and selective probes. The dye **32b** is the first chemosensor for As^{3+} ion detection in organic solvents. It shows a 25-fold fluorescence increase in the emission spectrum (λ_{em} = 496 nm), when As^{3+} ion is added to the solution of **32b** in THF. The recorded spectral changes are due to oxidation of benzothiazoline moiety to form benzothiazole one. It should be noted that the probe **32b** is thermally stable in both solid state and in solution when stored in the dark. It does not spontaneously oxidize to benzothiazole even after long exposure to pure oxygen or air. Interestingly, the probe **32b** is selective for As^{3+} ion over many competing ions (Na^{+}, Mg^{2+}, Ca^{2+}, Mn^{2+}, Fe^{2+}, Ni^{2+} and Zn^{2+}) in THF even at their 10-fold excess.

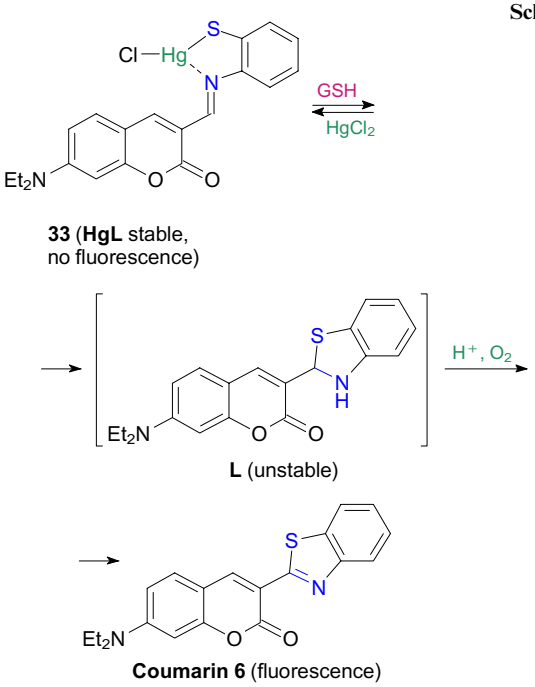
5.3. Activation of latent forms by other analytes

A new 'turn-on' fluorescent chemodosimeter **33** has been developed to identify glutathione reductase (GR) selectively among a series of other proteins or enzymes.[253] In the sensing step, free ligand **33** was released from the Hg^{2+}-**33**

Scheme 23



Scheme 24

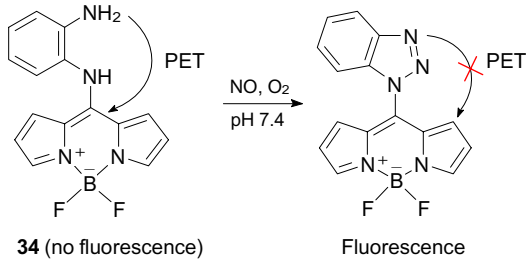


complex upon the reaction with a thiol compound such as glutathione (GSH) and then was immediately oxidized to the laser dye Coumarin 6, which was detected due to a strong fluorescence increase (Scheme 24). No colour change and fluorescence enhancement were observed within 5 min after glutathione oxidized form GSSG (50 μmol) was added to the Hg^{2+}-**33** complex solution. To illustrate the reaction between Hg^{2+}-**33** and GSH, their fluorescent product has been isolated and identified by ^{1}H NMR spectrum data as the Coumarin 6. In this study, Hg^{2+}-**33** complex was applied to quantify GSH and GR with excellent sensitivity and selectivity. This method opens a novel way for enzyme sensing.

An *o*-phenylenediamine–BODIPY hybrid **34** has been successfully designed and studied to be 'turn-on' low-background fluorescence chemodosimeter to detect both NO and nitrite ion.[135] The probe **34** was constructed through attachment of the BODIPY dye at the *meso*-position to the amino function of *o*-phenylenediamine (Scheme 25).

The probe **34** is nonfluorescent due to the PET effect. However, it easily turns into a fluorescent state with high selectivity and low detection limit upon treatment with NO under neutral conditions or with nitrite in an acidic medium. After addition of NO solution, fluorescence intensity at 532 nm rose with increasing concentrations of NO. A good linear correlation ($R^2 = 0.993$) between the intensity and NO concentration was found in the range of NO

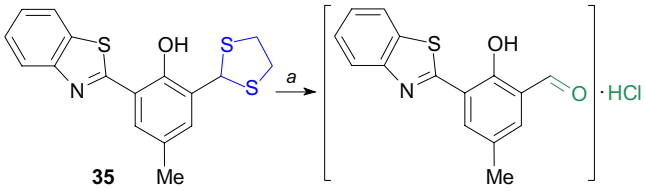
Scheme 25



concentration from 0 to 50 μmol L^{-1}. Thus, the detection limit was calculated to be 28 nmol L^{-1}. The cyclization of *o*-phenylenediamine with NO to form benzotriazole is a well-studied reaction.[340] Therefore, the resulting dye was prepared from the probe **34** by the reaction with $NaNO_2$ and characterized by ^{1}H and ^{13}C NMR spectra as well as electro-spray ionization high resolution mass spectrometry (ESI-HRMS). The resulting 8-benzotriazolyl BODIPY dye can detect bioorganic thiols such as Cys, homocysteine (Hcy) and GSH. In cell experiments, only blue fluorescence was observed with chemodosimeter **34** using a standard NO-source and with assistance by intracellular Cys and GSH. However, with an increase in GSH concentration, green fluorescence declined rapidly and blue fluorescence increased when a large excess of GSH was used. The observed blue fluorescence was explained by an increased intermolecular replacement of the amino function with a thiol moiety.

A fluorescent probe **35** for hypochlorite detection with high selectivity and sensitivity has also been developed.[200] Compound **35** easily turns into an oxidized state, which is accompanied by fluorescence yellow to blue shift upon addition of hypochlorite along with various reactive oxygen and nitrogen species (Scheme 26). The limit of detection was $\leqslant$8.9 nmol L^{-1} showing good sensitivity to hypochlorite.

Scheme 26



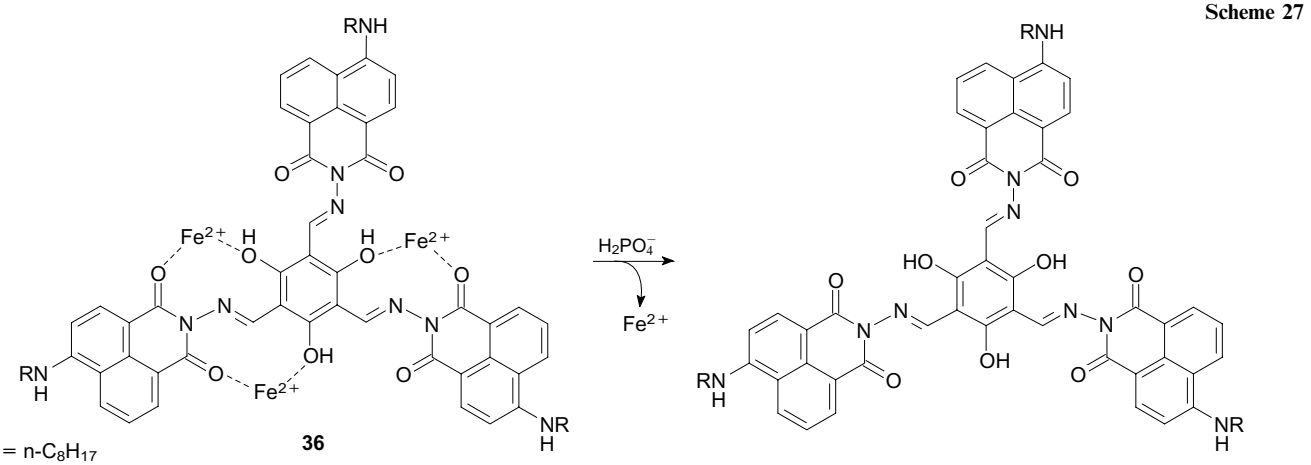
(*a*) HClO, PBS (pH 7.4); PBS is phosphate-buffered saline

A sensing mechanism for the fluorescence change in the presence of hypochlorite has been suggested. The benzothiazole-hydroxy hybrid shows an excellent excited ESIPT effect, which generally leads to emission at ~470 nm. However, the probe **35** itself provides an emission at a longer wavelength (*ca.* 546 nm), which can be assigned to the aggregation-induced emission (AIE) effect of the probe **35**. Upon addition of hypochlorite, compound **35** undergoes deprotection of the dithiolane fragment, to give an aldehyde function. In the ^{1}H NMR spectrum, the signal of the CHO proton appears at 10.43 ppm, supporting the formation of an aldehyde group. The latter forms a complex with hydrochloric acid, which emits blue fluorescence at 464 nm due to the ESIPT effect.

The $H_2PO_4^-$ ion is of significant interest in chemical, biological and environment aspects. A novel chemodosimeter **36**, being a complex of the naphthalimide moiety with Fe^{2+} ion, was synthesized for the detection of the $H_2PO_4^-$ ion with high sensitivity and selectivity (Scheme 27).[155]

The probe **36** consists of two parts: the fluorescent group (naphthalimide moiety) and the receptor group (Schiff base). The experimental results show that conjugate **36** has no fluorescence, thus representing the latent form of fluorophore. In the presence of $H_2PO_4^-$, the solution of probe **36** shows a bright yellow fluorescence. It should be mentioned that compound **36** detects $H_2PO_4^-$ ions sensitively and selectively, the detection limit being

Scheme 27



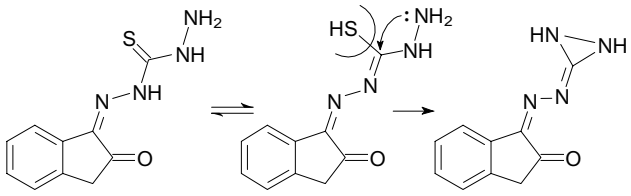
1.897×10^{-7} mol L^{-1}. Upon addition of other common anions (PO_4^{3-}, HPO_4^{2-}, $H_2PO_4^-$, F^-, Cl^-, Br^-, I^-, *etc.*) to the above solution, the probe **36** gave no response.

A quick responsive new 'turn-on' probe **37** also based on 1,8-naphthalimide and thiourea was reported (Scheme 28).[156] It can colorimetrically detect Fe^{3+} and Pb^{2+} ions in MeCN – H_2O solution. Moreover, the fluorescent signal of Hg^{2+} ion in such systems is accompanied by vivid colour changes observable with the naked eye.

The found detection is highly sensitive and selective and is almost not affected by the presence of fluoride anion and common coexisting metal ions such as Na^+, K^+, Ca^{2+}, Mg^{2+}, Fe^{2+}, Cu^{2+}, Zn^{2+}, Cr^{3+}, Ni^{2+}, Mn^{2+}, Co^{2+} and Cd^{2+} ions. The probe **37** chelates Fe^{3+} and Pb^{2+} ions reversibly at a 1 : 1 stoichiometry, while the Hg^{2+} ion forms first a 1 : 1 complex. The resulting complex releases HgS to produce a three-membered ring-containing structure (see Scheme 28). The ^{1}H NMR spectra supported the suggested mechanism. The signal at 10.13 ppm relating to the thiourea NH proton shifted to 10.21 ppm was markedly weakened. The signal at 9.88 ppm assigned to the NH function bound to the naphthalene ring disappeared and the signals in the range of 6.99 – 8.70 ppm became more complex. These phenomena define a structure with a three-membered ring. Similar mechanism was proposed earlier[341, 342] and is shown in Scheme 29.[343]

Chemosensor **37** was suggested for tracking the environmental and intracellular Hg^{2+} ion.[156] Linear concentration ranges for Fe^{3+}, Pb^{2+} and Hg^{2+} ions were 0 – 150, 0 – 80 and 0 – 90 μmol L^{-1} with the found detection limits of 6.86, 5.09 μmol L^{-1} and 82.1 nmol L^{-1}, respectively.

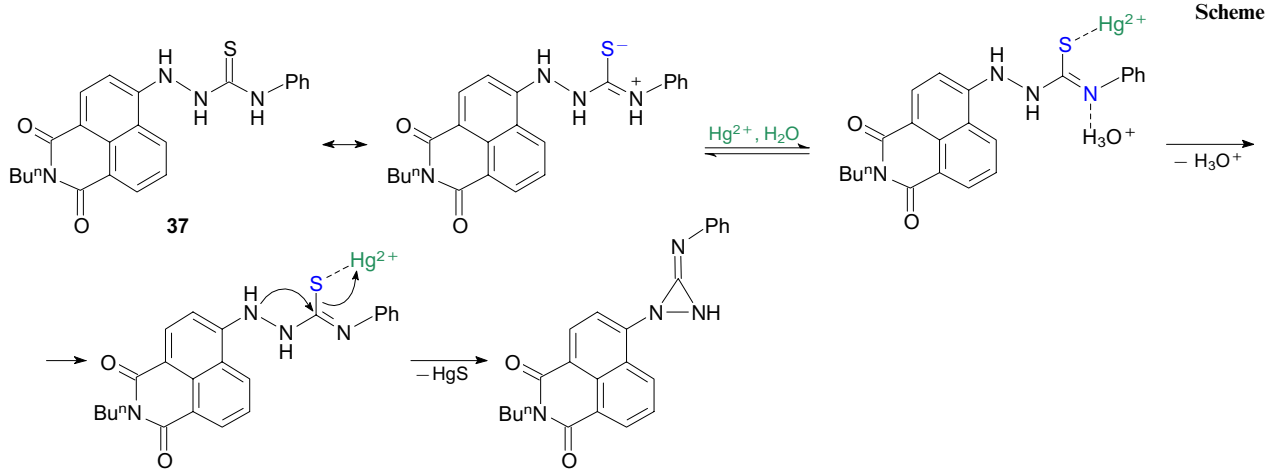
Scheme 29



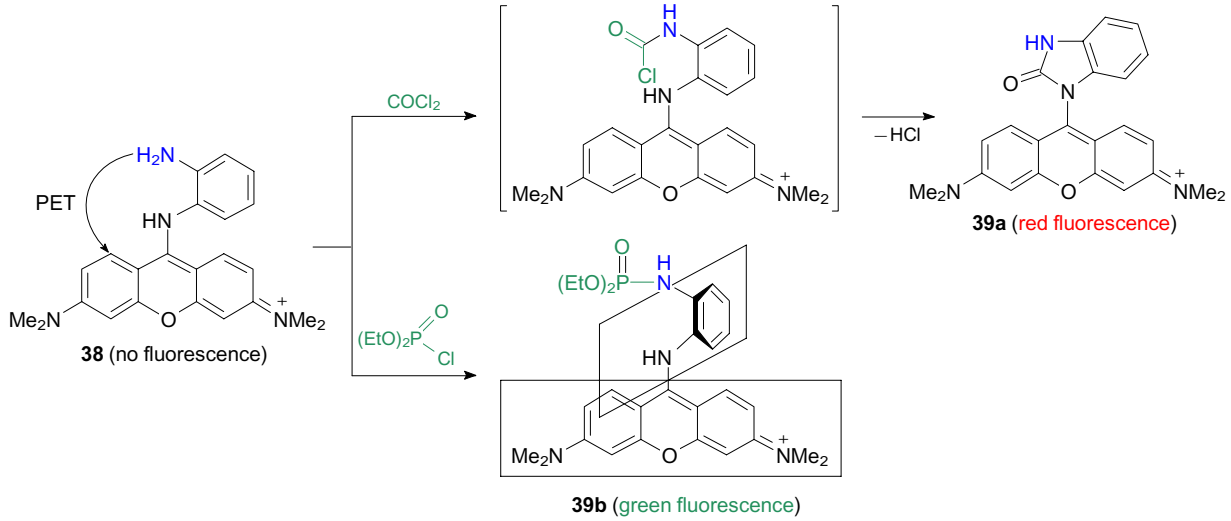
An *o*-phenylenediamine-pyronin-bound dye **38** was shown to provide 'turn-on' fluorescent sensing effect.[257] It is able to discriminate between phosgene and the prototypical nerve-agent mimic such as diethyl chlorophosphate in solution or gas phase as confirmed by both fluorescent and electron absorption spectra (Scheme 30).

The probe **38** is not fluorescent owing to the PET-promoted quenching of fluorescence but it shows red emission in the presence of phosgene (with formation of **39a**) and green emission with diethyl chlorophosphate (affording **39b**). To support the shown mechanisms, ESI-MS and NMR spectroscopy techniques were used to detect the product formed during mixing the dye **38** with phosgene. Mass spectrometric data showed that the peak at *m*/*z* 373.3 relating to the molecular ion of **38** disappeared after addition of phosgene and a new peak at *m*/*z* 399.2 appeared, corresponding to adduct **39a**. It should be noted that no

Scheme 28



Scheme 30

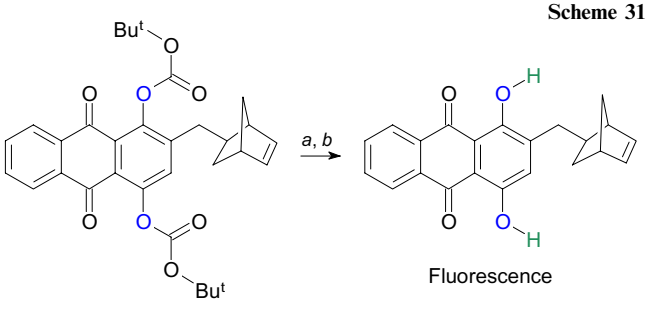


peaks other than those associated with compounds **38** and **39a** were found in the recorded spectra, thus indicating the quantitative formation of product **39a**. Furthermore, adduct **39a** was isolated from the reaction mixture and completely characterized by ^{1}H and ^{13}C NMR spectra. The probe **38** was used to prepare a portable kit for detection of phosgene. For this purpose, the probe **38** was immobilized on a polyethylene oxide membrane. The membrane, which contained only a small amount of the sensor, was initially transparent and colourless, emittting a weak blue fluorescence under 365 nm UV-irradiation. After exposure to various amounts of phosgene vapour (0 – 20 ppm) for several seconds, the colour of the membrane fluorescence became pink-red.

A norbornene-based Boc-protected quinizarin **40** as a dye precursor (DP) was prepared for fluorescence imaging by irradiation.[344] The unprotected quinizarin derivative absorbs at 486 nm due to the quasiaromatic nature induced by the intramolecular H-bonding. Protection of both hydroxy-functions removes the H-bonding and causes shift of the absorption maximum to 341 nm. The Boc protecting groups of the DP can be easily removed under irradiation in the presence of a PAG — triphenylsulfonium triflate (TPSOTf) — thus regenerating the highly fluorescing quinizarin derivative (Scheme 31).

These reactions can also proceed in polymer films. A thin PMMA film containing compound **40** and PAG was prepared by spin coating on a quartz plate.[345] When this light-yellow transparent film was irradiated at 250 nm wavelenght, a red film was formed in 1 min following the post-exposure bake treatment indicating the regeneration of the original quinizarin derivative by the above-mentioned mechanism.

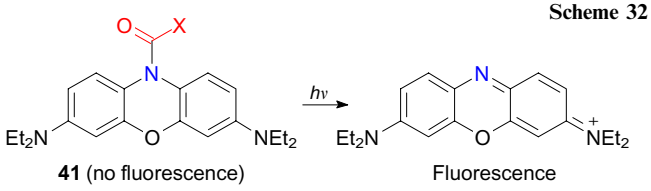
Scheme 31



(*a*) *hν*, TPSOTf; (*b*) 110 °C; TPSOTf = $[F_3'CSO_3]^-[Ph_3S]^+$

Some latent derivatives of organic laser dyes can be transformed into active fluorescent forms just by the irradiation. For example, *N*-acyloxazines **41** exhibited fluorescence activation during the irradiation, resulting in the generation of a novel cationic oxazine dye (Scheme 32).[258]

Scheme 32



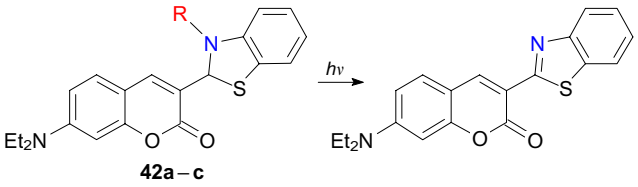
X = Me, Ph, C_6H_4Br-4, $C_6H_3Br_2$-3,5, CBr_3

The acetyl derivative **41** was found to be the more light-sensitive compared to the benzoyl one. The photochemical response was analyzed by several methods including UV, NMR and mass spectrometry. The mass spectral data strongly suggest the acyl radical formation *via* homolytic cleavage of the C – N bond. The observed signal at m/z = 324.5 supports the oxazine dye formation.

The dihydro form of the laser dye Coumarin 6 and its *N*-acylated derivatives **42a** – **c** represent another example of photoactivated latent forms of laser dyes.[254, 255] In general, transformation into fully conjugated heterocycles could be achieved for such systems upon the action of SET-based oxidants. However, the ease of the benzothiazole ring rearomatization on exposure to the UV light was used to prepare highly fluorescent dyes as novel materials for the effective storage of optical information (Scheme 33).

Compounds **42a** – **c** were highly sensitive to irradiation in organic solvent medium. Their photoaromatization with formation of Coumarin 6 was proved by comparison of the isolated product with the authentic sample. Of particular interest is that the similar changes in the absorption and emission spectra were also observed for thin PMMA films. There, an isosbestic point at 410 nm was detected in the

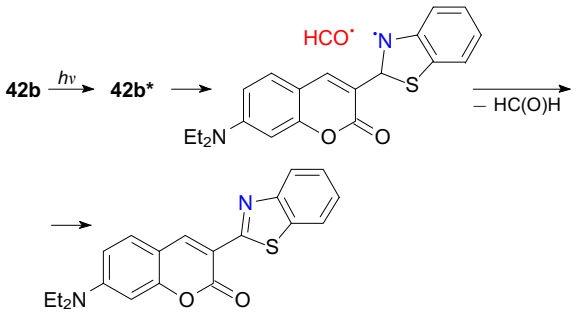
Scheme 33



R = H (**a**), CHO (**b**), Ac (**c**)

absorption spectra after UV irradiation of the PMMA film. The intensity of the absorption maximum at 394 nm decreased and absorption maxima at 450 and 520 nm appeared. Changes in the absorption spectra were accompanied by the appearance of fluorescence maxima at 475 and 550 nm. In was found that the photoaromatization did not depend on the oxygen presence and probably followed the mechanism as depicted in Scheme 34.

Scheme 34



Spectral characteristics of the irradiated polymer films show that *N*-acylated derivatives of the Coumarin 6 dihydro form in a polymer film are also converted to the aromatic species under irradiation, thus providing a polymer material for optical information recording based on precursors of fluorescent compounds.

6. Probes with quenched fluorescence

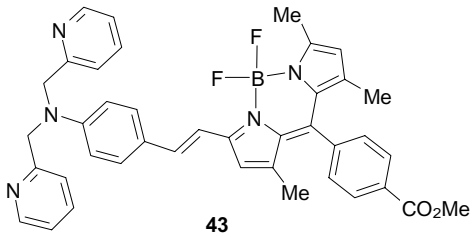
This part of the review discusses the fluorescent organic dyes whose fluorescence is quenched or blue-shifted during their reaction with an analyte. Disturbance of the π-conjugated electronic structure of the dye is often responsible for this sensing effect.

6.1. Quenching of fluorescence by metal ions

A near-infrared fluorescent 'turn-off' probe **43** characterized by a large Stokes shift, high photostability and high quantum yield has been developed to provide Cu^{2+} ion imaging in live mice.[136]

Addition of Cu^{2+} ion leads to a hypsochromic absorption shift from 600 to 563 nm. The titration shows a clear isosbestic point at 575 nm according to the transition from free probe **43** to Cu-complex. The Job's plot based on the 563 nm band shows 1 : 1 binding stoichiometry in the **43**-Cu^{2+} complex. The Cu^{2+} titration of **43** leads to an instantaneous decrease of emission. In the ESI-MS spectrum in the presence of Cu^{2+}, the main signal of m/z 765.83 for $[\mathbf{43} + Cu + Cl]^+$ was observed confirming the 1 : 1 complex stoichiometry. The complex formation prohibits the promoted ICT effect that takes place in the probe **43**. The decreased fluorescence of compound **43** can be recovered by EDTA addition. The 'off-on' transitions were observed at least five times, showing reversible sensing ability of the probe **43**. With such a result, this chemosensor is recommended to monitor the Cu^{2+} ion fluctuation during Cu^{2+} loading and unloading in living cells. The Cu^{2+} fluorescence detection limit of the probe **43** is ~0.15 mmol L^{-1}, which is much lower than the permissible Cu^{2+} level in drinking water (31 mmol L^{-1}). These results open way to the future development of NIR chemosensors for the *in vivo* detection of metal cations.

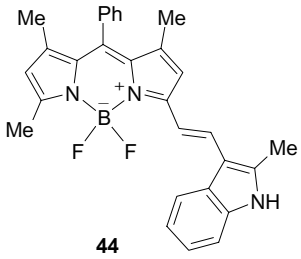
Structure 43



The BODIPY–indole 'turn-off' chemosensor **44** of similar structure was also synthesized by a condensation reaction.[137]

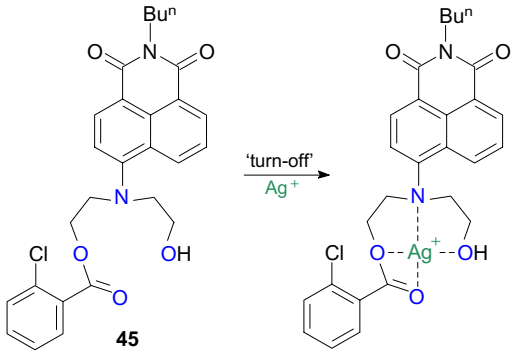
Compound **44** exhibits absorbance increase at 506 nm and distinct emission at 635 nm. The addition of Cu^{2+} ion causes quenching of fluorescence intensity due to the formation of cupric complex with the estimated detection limit of 0.124 μmol L^{-1}. The Job's plot was employed to analyze the binding stoichiometry (**44** : Cu^{2+} = 2 : 1) with a good linear relationship, the 2 : 1 ratio was further confirmed by the matrix-assisted laser desorption–ionization technique (MALDI-MS) data. The complex formation is believed to involve the indole ligand N(1)—Cu coordination (see probe **B** in Scheme 2 for more detail). Quenching of the intense fluorescence of probe **44** is assigned to oxidative PET from the excited-state fluorophore to the indole moiety coordinated to Cu^{2+} (oxidative PET mechanism). It shows high photostability, being quite resistant against a number of other main group and transition metal cations, as well as their mixtures and was successfully used in the living cell imaging for both mammalian and bacterial cells.

Structure 44



A novel quick responsive, colorimetric and 'turn-off' fluorescent chemosensor **45** for the Ag^+ ions has been synthesized.[157] Compound **45** turned to be essentially insensitive to protons over a wide pH range while showing high selectivity and sensitivity towards the Ag^+ ions in ethanol–water solution (Scheme 35).

Scheme 35



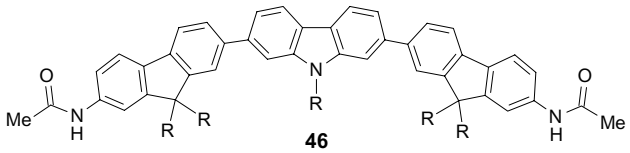
45

The strong emission band at 525 nm is typical of 4-amino-substituted 1,8-naphthalimide derivatives due to the induced intramolecular charge transfer. Its intensity is markedly reduced in the presence of Ag^+, whereas the presence of a variety of other metal ions, including K^+, Ba^{2+}, Cu^{2+}, Ni^{2+}, Sn^{4+}, Mg^{2+}, Ca^{2+}, Fe^{3+}, Pb^{2+}, Co^{2+}, Na^+, Hg^{2+}, Li^+ and Al^{3+} induces no visible changes in the emission spectra. These results show that the probe **45** coordinates with Ag^+ ion to form a highly stable complex. The binding constant calculated from the Stern–Volmer equation was found to be 6.498×10^4. The Job's plot revealed that the 2:1 complex is formed. The probable coordination path between compound **45** and Ag^+ was studied by the IR spectroscopy to determine the coordination mode. Upon addition of Ag^+ to a solution of probe **45**, a new peak appeared in the range of 3700–3100 cm^{-1} in the IR spectra suggesting that the aromatic amine and hydroxy functions are involved in the coordination.

6.2. Fluorescence quenching by other analytes

Detection of nitroaromatics, particularly trinitrotoluene, is of great interest due to its importance in security and environmental safety control.[260,261] A fluorescence-based technique is preferred for molecular sensing because of its high sensitivity and ease of implementation.[262,263] Therefore, a number of fluorescent materials derived from organic molecules having efficient excited state energy migration and strong interaction with a target analyte have been tested for such application.[264–266] Since the most common explosives possess poor emissive properties, formation of charge-transfer complexes of π-electron deficient molecules of explosives with fluorophores became an indirect approach to detect the traces of nitroaromatics in water and air. Thus a functionalized carbazole-based probe **46** proved to be an effective detector of TNT even at picomolar concentrations.[267] The probe **46** can be used for testing the contamination of water by TNT. The fluorescence intensity of the probe **46** nanoparticles in water was found to vary in the presence of TNT. Upon addition of 1×10^{-12}–1×10^{-6} mol L^{-1} of an aqueous TNT solution, a gradual quenching of the emission occurred, reaching the maximum value of 50% at 1×10^{-6} mol L^{-1} of TNT. The lowest detection limit of TNT was 10^{-12} mol L^{-1}.

Structure 46



46

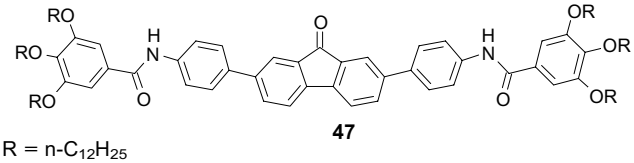
R = n-$C_{12}H_{25}$

As described earlier, carbazole-based assemblies are known as good donor materials and quenching of their fluorescence upon vapour exposure must be due to an electron transfer to TNT.[264–266,268,269] Detailed studies confirmed the supramolecular aggregation of probe **46** into rods and nanoparticles under certain conditions. Solvents were changed from methylcyclohexane to water, while poorer results were obtained using THF. In order to get more insight into the mechanism of TNT vapour detection by the probe **46** nanostructures, the quartz crystal microbalance experiments were performed. The frequency of the quartz crystal was shown to decrease over time, which is an indication of adsorption of TNT vapours. After 100 s, the self-assembled rods showed 2.58 ng of TNT adsorption registering a 38% fluorescence quenching and 2.12 ng of TNT adsorption by nanoparticles exhibiting a 35% fluorescence quenching. The former aggregates exhibited *ca.* 50% fluorescence quenching within several minutes on exposure to TNT and dinitrotoluene (DNT) vapours and sufficient selectivity over acceptor non-nitroaromatics, such as benzonitrile or benzoic acid.

Low molecular mass organic conjugates (LMOGs) have received extensive attention in various fields because of their fascinating properties and potential applications such as photovoltaics,[346] tissue engineering,[347] molecular detection,[271] controlled drug release and delivery,[348] oil or dye absorbing[349] and various stimuli-responsive materials.[350] In particular, LMOGs are of bright promise as a new type of sensing material due to their 3D-network structure, various optical properties, chemical stability and larger surface area, which can be applied in the selective and sensitive detection of humidity, explosives and small molecules.[351–353]

The probe **47** consisting of a fluorenone core and two polyalkoxybenzamide branches was prepared and tested for the 'turn-off' detection of aniline vapours.[270]

Structure 47



47

R = n-$C_{12}H_{25}$

This compound self-assembles into a three-dimensional system, which increases the diffusion of analytes and provides a fast response. The PET was postulated as the sensing mechanism, while no chemical reaction was observed between the decorated fluorenone and aniline. Quantum chemical calculations were used to analyze the HOMO/LUMO energy gap and provided additional information regarding the electron transfer process. In order to verify that the detection mechanism of compound **47** towards aniline is based on the PET rather than on a chemical reaction, a titration experiment of aniline with **47** in THF was carried out. Two new absorption peaks appeared in the IR spectra, the absorption increasing as the concentration of aniline rose. Comparing these data with the absorption of pure aniline, one can see that the above two absorption peaks relate to aniline. According to the concentration-

dependent emission spectra of the **47** – aniline mixture, the emission of **47** decreases obviously with the increase of aniline concentration. However, no red or blue shift of the emission band is observed suggesting that the probe **47** does not react with aniline to form a new compound. Therefore, the quenching mechanism is explained from the energy levels perspective in combination with the DFT level of theory. Density functional theory calculation for compound **47** and aniline demonstrated that after excitation the hole of **47** could be filled by an electron from the HOMO orbital of aniline. Thus, the PET occurred and the fluorescence quenching could be observed. The probe **47** is chemically resistant, can be easily recovered many times for reuse with $<5\%$ efficiency losses and the detection limit of ~ 10 μg L^{-1}.

7. Ratiometric probes

Compound **48** consisting of two coumarin molecules linked by a short enone bridge proved to be a sensor of H_2O impurities in common organic solvents, such as DMF, DMSO and acetone.[256]

In a whole, a solvent was found to have a dramatic effect on the emission spectra of probe **48** including the position of the emission band and quantum yield. As the solvents polarity increased when passing from toluene to acetonitrile, the decrease of fluorescence quantum yields and immediate increase of the Stokes shift were revealed. This is due to the interactions between the fluorophore and the surrounding solvent molecules, which affect the stabilization energy difference between the ground and excited states. Protic solvents increase the possibility for nonradiative relaxation of the excited dye, thus leading to a decrease of fluorescence quantum yield. Meanwhile, water influences the fluorescence quenching far more significantly. The probe **48** has a number of advantages over the known fluorescent probes for H_2O detection. The linear ratiometric fluorescence response to the water content with excitation at 380 nm is worth to be mentioned. The results were found to be in a good agreement with the standard Karl Fischer titration method. Twisted intramolecular charge transfer is the most convenient mechanistic explanation of the observed fluorescence quenching, similarly to the known push-pull dyes.

A fluorescent ratiometric probe **49** based on a chlorinated BODIPY dye for detection of glutathione has been synthesized.[138] The sensor is characterized by high selectivity to GSH over Cys/Hcy (Scheme 36).

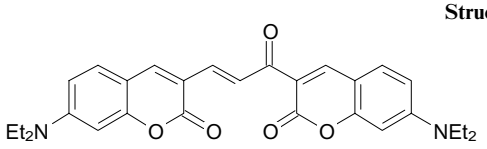
The chlorine atom in the dye **49** turned to be highly reactive to nucleophilic attack. It can be rapidly replaced by biothiols. The amino functions of Cys/Hcy (but not GSH) further replace the thiolate groups to form an amino-substituted BODIPY, which exhibits extremely different photophysical properties when compared to the sulfur-substituted BODIPY produced in the reaction with GSH. In the ^{1}H NMR spectrum, a broad signal at $\sim$6.86 ppm and a triplet at 1.75 ppm were assigned to the exchangeable protons of the aromatic amine and SH, respectively. These signals show that cysteine is attached to BODIPY moiety through the amino function. Thus, the probe **49** provides the unique example of discrimination of glutathione from Cys – Hcy pair.

Different mechanisms for the detection of CN^- ion have been already discussed. However, ratiometric probes are also worth of attention, since they provide additional sensory mechanisms based on ESICT,[219] ESIPT[164] and ESICT-ESIPT switching.[201] Moreover, some probes shown below differ advantageously from many reported CN^- ion sensors[354, 355] by the simplicity of synthetic procedures.

A simple 7-azaindole derivative **50** was synthesized.[216] 1-Methyl-7-azaindole moiety was substituted with a dicyanovinyl moiety acting as an electron-withdrawing group, which is responsible for a sensing function (Scheme 37).

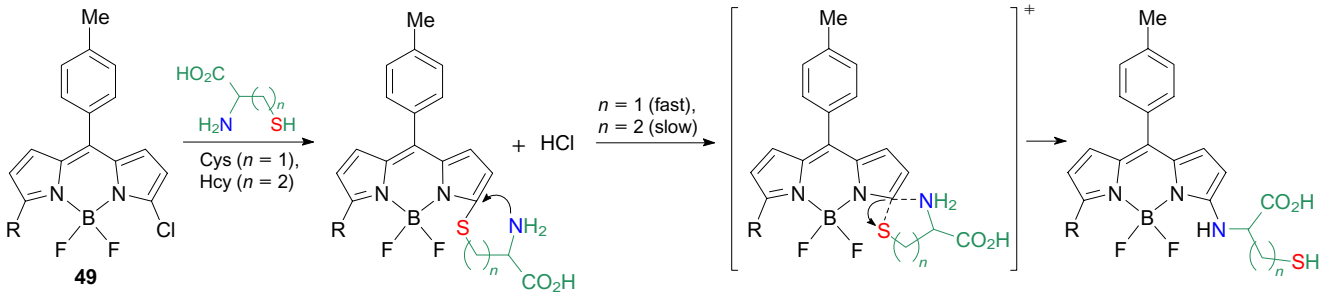
The probe **50** exhibits two absorption bands at $\sim$293 and 362 nm. The latter is due to the ICT transition. The emission spectra of compound **50** are significantly red-shifted with increase of the solvent polarity, which agrees with strong ICT character of the excited state of the probe. The blue shift induced by the addition of CN^- is large (144 nm) with an isoemissive point at 465 nm. After addition of CN^-, the peak at 532 nm is completely quenched, while the band at 388 nm appears. The ratios of fluorescence intensities at 388 and 532 nm (I_{388}/I_{532}) exhibit a dramatic change from 0.05 : 1 to 6.93 : 1, indicating a ratiometric fluorescent sensing ability of the probe **50** for cyanide detection in aqueous media. According to the ^{1}H NMR spectra, addition of cyanide ions to probe **50** results in decreasing vinylic proton signal at 8.23 ppm, while a new

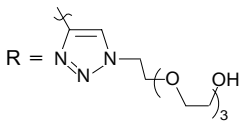
Structure 48



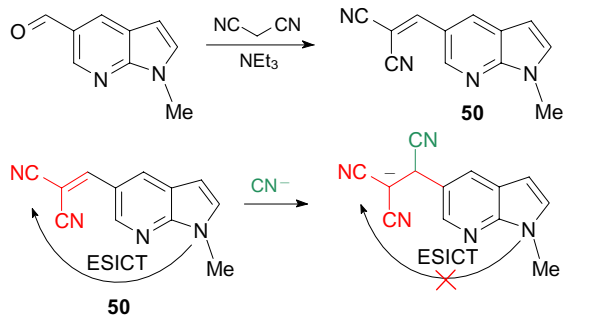
48

Scheme 36



R = , $CH(CO_2Et)_2$, $S(CH_2)_2CO_2H$, OMe, $C_6H_4CO_2H$-4, NHPh; Cys is cysteine, Hcy is homocysteine

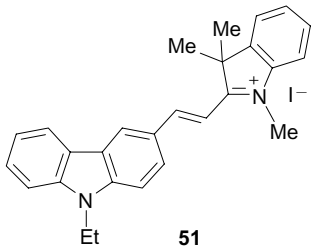
Scheme 37



signal corresponding to the proton of the dicyanovinyl group appears at 4.43 ppm. The interruption of the π-conjugation results in a substantial blue shift in the absorption spectrum and weakening of the ICT character.

The probe **51** represents one more example of how the ICT can be hindered by the analyte molecule interaction with the π-conjugated system, *i.e.*, blue-shifting (or quenching) of the emission process.[217]

Structure 51

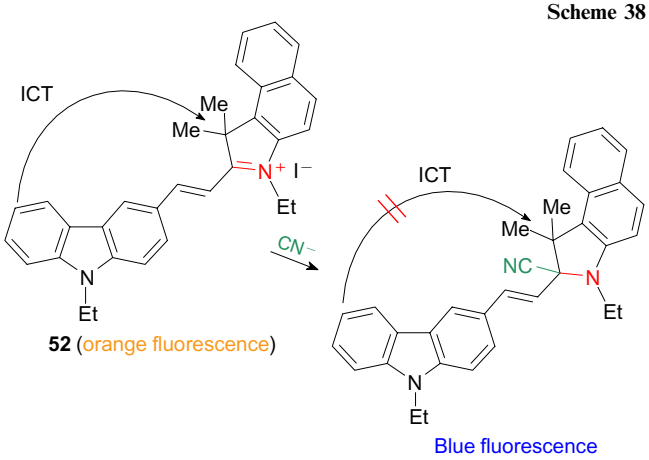


The probe **51** turned out to be a novel ratiometric fluorescent chemodosimeter for 'blue-shifted' cyanide detection (photophysical mechanism was illustrated in Scheme 3). In the presence of cyanide ions, dye **51** shows a significant fluorescent response, with emission having a large Stokes shift (~210 nm). The detection of cyanide ion is performed *via* its nucleophilic addition to the indolium group of the dye **51**. The addition product was separated and totally characterized by ^{1}H and ^{13}C NMR spectra. Competitive anions do not show any notable changes in either colour or emission. This indicates the high selectivity of the sensor **51** to CN^- ions.

The close analogue of the probe **51**, fluorescent chemodosimeter **52**, was synthesized *via* linking *N*-ethylcarbazole-3-formaldehyde and 1,1,2-trimethyl-3-ethyl-1*H*-benzo[*e*]indolium iodide with the ethylene bridge.[218] It turned to be a useful 'blue-shifted' probe for cyanide ion detection at very low concentrations (Scheme 38). The detection limit was evaluated as 0.23 μmol L^{-1} ($S/N = 3$), which is much lower than the WHO permissive level (1.9 μmol L^{-1}). It is also worth mentioning that the shift of two emission wavelengths is very large, up to 155 nm, which allowed the accurate measurement of their intensities, as well as resulted in a huge ratiometric value.

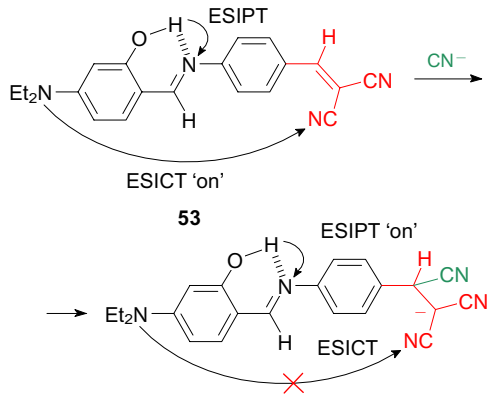
The visible colour and strong fluorescence of the probe **52** are due to its outstanding ICT effect from the electron-donating carbazole group to the electron-withdrawing benzoindole moiety. The detection effect is based on the nucleophilic addition of the cyanide anion to the polarized C=N bond of the benzo[*e*]indolium group. All ^{1}H NMR signals turn to be shifted upfield. Furthermore, the formation of the sensor **52**-CN adduct was also confirmed by mass spectrometry. As a result, π-conjugation between benzo[*e*]indolium moiety and carbazole group is blocked. This reaction provides a prominent fluorescence and colour changes. The hindrance of the π-conjugation in fluorophore **52** results in a blue shift both in absorption (218 nm) and emission spectra (155 nm).

Scheme 38



Recently, several potential ESICT–ESIPT coupled systems were synthesized and investigated. The ESICT–ESIPT-based fluorescent probe **53** for the detection of cyanide is shown below (Scheme 39).[201]

Scheme 39



The structure of the probe **53** is composed of a well-known ESIPT molecule, salicylideneaniline, in which diethylamino and dicyanovinyl groups are attached so as to act as electron-donating and electron-withdrawing groups, respectively. The electrophilic nature of the dicyanovinyl group provides its receptor properties to the cyanide ion. Compound **53** shows two absorption bands at ~330 and 470 nm; the former is attributed to the π–π* transition and the latter is due to the ICT transition. Unlike the small shift in absorption spectra, the emission spectra of probe **53** are noticeably red-shifted with increase in the solvent polarity, indicating the strong ICT character for the excited state of the compound. Upon the addition of F^-, Cl^-, Br^-, I^-, SCN^-, AcO^-, NO_3^-, BzO^-, $H_2PO_4^-$, $HP_2O_7^-$ and HSO_4^- anions, no substantial change was observed in the emission spectra of compound **53**. The only significant response appeared on CN^- addition. The fluorescence band at ~523 nm appeared and the band at 626 nm ($\Phi = 0.15$, ESICT) diminished. The former 523 nm emission

band is unambiguously assigned to the ESIPT emission. The blue shift induced by the addition of CN^- was high with an isoemissive point at 531 nm. After the addition of 20 equiv. of CN^-, the peak at 626 nm was completely quenched. The ratio of emission intensities (I_{523}/I_{626}) exhibited a 75-fold decrease. The detection limit of the probe **53** for CN^- is 2.4 μmol L^{-1}, which is quite close to the maximum level permissible in drinking water (1.9 μmol L^{-1}).

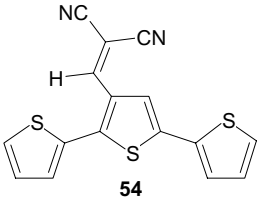
Addition of cyanide ion resulted in reduction of the vinylic proton signal at 8.10 ppm, which disappeared upon the addition of 1 equiv. of cyanide ion. A new signal appeared at 4.25 ppm, corresponding to the β-proton of dicyanovinyl function. Meanwhile, the upfield shifts of two sets of aromatic protons are observed at the *ortho*- and *meta*-positions relative to the ethylene group. The structure of **53**-CN adduct was further confirmed by mass spectrometry analysis. These results are consistent with the assumption that CN^- attacks the β-conjugated position of dicyanovinyl moiety. The molecule of probe **53** is nearly planar, with an angle of 10.1° between two phenyl rings. Such planar conformation provides an efficient π-conjugation and thus favours the efficient ICT transition from the amino group to the dicyanovinyl moiety. The ground-state geometry undergoes an apparent twist upon the addition of CN^- ion. The π-conjugation between the dicyanovinyl and the salicylideneaniline is interrupted resulting in a significant blue shift in the absorption decreasing the ICT character. In the case of probe **53**, the electron density in the HOMO was localized on the salicylideneaniline moiety, while that in the LUMO was mainly localized on the dicyanovinyl group. Consequently, generation of a charge separation can be expected while an electron is promoted from the HOMO to the LUMO. However, the electron distribution in **53**-CN, particularly in the LUMO, was quite different from that in **53**. Because of the interruption of the π-conjugation, the electron population in the LUMO of **53**-CN was confined to the salicylideneaniline moiety, without involving the malononitrile.

Probe **54** has been also suggested for the ICT mechanism operation. When compound **54** is excited at 415 nm, it exhibits two emission bands with maxima at 462 and 589 nm.[219] The major emission band at 589 nm is attributed to the ICT. It is supported by the solvent-polarity dependent shift of the emission band, whereas the absorption bands remained unaltered on changing the solvent polarity. Upon the addition of different anions (Cl^-, Br^-, F^-, AcO^-, ClO_4^-, NO_2^-, N_3^- and SH^-) to the solution of **54**, no considerable change in the emission spectra was observed. Upon addition of the cyanide anion, the emission intensities of the peaks at 462 and 589 nm were gradually increased and decreased, respectively. The ratio of emission intensities (F_{462}/F_{589}) exhibited a 14-fold enhancement. After the addition of 20 equiv. of cyanide anion, the peak at 589 nm was completely quenched. To get more insight into the mechanism of the colorimetric change and ratiometric fluorescence enhancement of **54** in the presence of CN^-, DFT calculations were carried out for compounds **54** and **54**-CN at the B3LYP/6-31G(d) level using a suite of Gaussian 09 programs. In the optimized structure of **54**, the dihedral angle between the dicyano group and the middle thiophene ring of terthiophene is 15°, indicating an effective π-conjugation between the terthiophene and dicyano groups *via* the vinyl bridge. Addition of CN^- to the latter eliminates the conjugation hampering the ICT process in the reaction product **54**-CN.

The high coordinating ability of gallium(III) in complexes with cyclic tetradentate ligands **55** and **56** was employed to construct novel colorimetric probes useful for detection of F^- and CN^- ions (Scheme 40).[206]

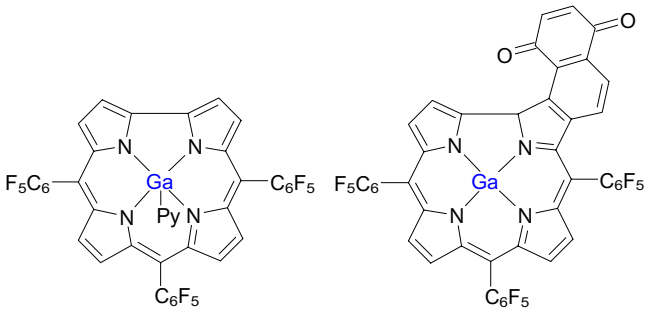
In the porphyrinoid series, corroles have attracted special attention due to convenient methodologies of their synthesis. These macrocycles having one direct pyrrole–pyrrole linkage possess unique spectral properties, which are used in optical and sensing applications. Addition of the cyanide ion to these probes leads to decreasing intensity of the band at 570 nm and increasing intensity of that at 609 nm as well as a red shift in the absorption spectrum. The binding constant of the probe **55** interaction with the cyanide ion was estimated as $\log K = 10.52$ with stoichiometry of one anion per two ligands. This value is much higher than that for the probe **56** ($\log K = 6.89$). The corrole probe **55** is able to quantify *ca.* 1.00 μmol L^{-1} of cyanide. The compound **56** demonstrated somewhat lower sensing characteristics, which was attributed to electronic effects of the fused quinone moiety. In order to confirm the compounds **55** and **56** as molecular probes, several MALDI-TOF-MS titrations with fluoride and cyanide ions were performed. Both probes were found to interact with cyanide ion also in the gas phase.

Structure 54



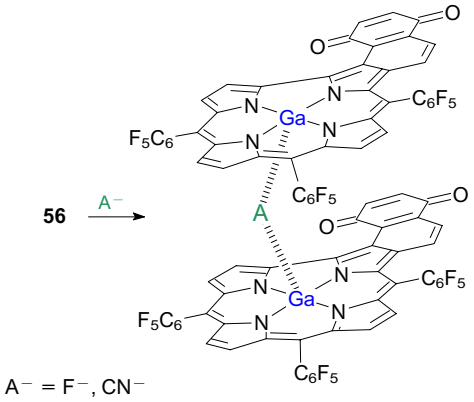
54

Structures 55, 56



55 **56**

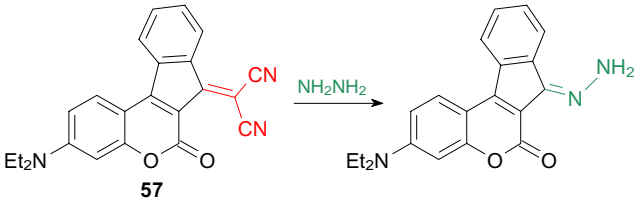
Scheme 40



$A^- = F^-, CN^-$

7-Diethylaminocoumarin and 1-indanone-fused fluorescent dye **57** as a ratiometric probe undergoes rapid covalent bonding with hydrazine (Scheme 41), showing the subsequent blue shifts in the absorption and fluorescence spectra.[220]

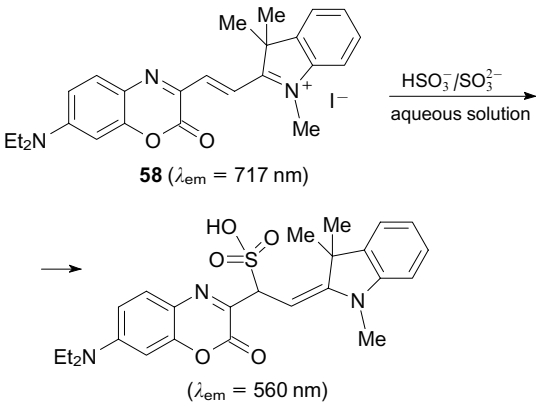
Scheme 41



The probe **57** was proposed as a convenient alternative to traditional coumarins. Condensation of the compound **57** with hydrazine leads to release of malonodinitrile, and formation of the corresponding hydrazone. The latter results in the inhibition of the ICT effect and appearence of remarkable blue shifts. Dye **57** represents a rapid naked-eye probe working at the biological pH (7.4) levels, and is highly selective towards a number of similar contaminants (*e.g.*, functionalized organic amines and hydrazides). Upon treatment with increasing concentrations of hydrazine (0 – 130 μmol L^{-1}), the fluorescence of the probe **57** at 557 nm gradually rose and the final enhancement factor was over 190-fold. The observed fluorescence intensity is proportional to hydrazine concentration of up to 10 μmol L^{-1}. The detection limit of the probe for hydrazine was determined to be 8.6 nmol L^{-1}.

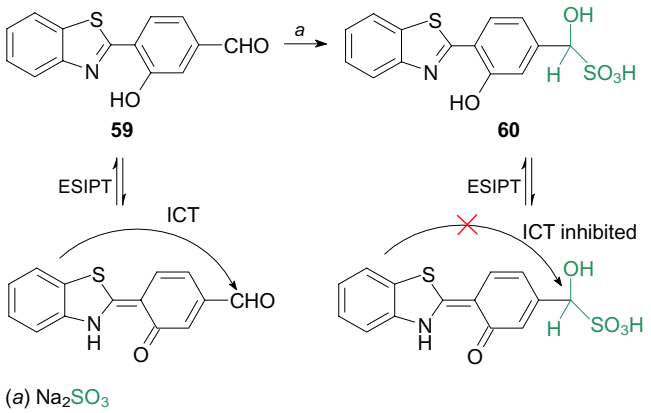
An 1,4-oxazine-based colorimetric sensor **58** was developed for ratiometric fluorescent detection of bisulfite ion (Scheme 42).[317] The compound exhibits the naked-eye colour change in the presence of sulfite ions, while no response is noted for a variety of other inorganic anions, such as halogens, azide and dithionite. The mechanistic and pH-effect studies revealed that the addition of HSO_3^- to the C=C double bond is the main factor responsible for the fluorescence. The detection limit for bisulfite was estimated to be 87 nmol L^{-1}. During the reaction with bisulfite in an aqueous solution, the chemical shifts of vinyl protons in the ^1H NMR spectra were shifted upfield, which may indicate the nucleophilic addition of HSO_3^-. The HR-MS analysis confirms the formation of the probe **58**-SO_3^{2-} adduct. Hindrance of the ICT-effect therein is a key reason for the observed ratiometric properties. The probe **58** was suggested for the efficient bisulfite detection in food, as well as sulfur dioxide in living systems. Among the numerous advantages of this probe, the ease of synthesis, low cost, simple and real-time detection and high resolution should be noted.

Scheme 42



4-(Benzothiazol-2-yl)-3-hydroxybenzaldehyde **59** is of significant research interest as another example of the SO_3^{2-} fluorescent sensor (Scheme 43).[202]

Scheme 43

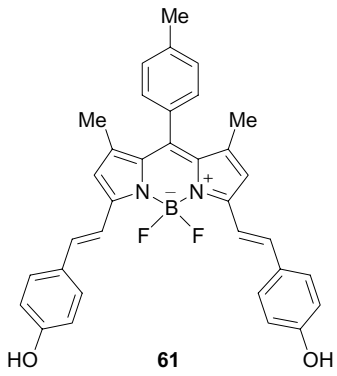


On the basis of absorption and emission studies, the sensing mechanism for probe **59** with SO_3^{2-} is proposed in Scheme 43. The SO_3^{2-} ion attacks the aldehyde function of the probe **59** to form adduct **60**, in which the ICT process is inhibited thus resulting in a significant blue shift in the adduct emission spectra. Unlike other 2-(benzothiazol-2-yl)phenol-based fluorescent probes in which the ESIPT process was inhibited, both probe **59** and the reaction product **60** exhibit an ESIPT process upon excitation because of the presence of the free hydroxy function. Therefore, the favoured large Stokes shift resulting from the ESIPT process was always available for probe **59** both in the absence and in the presence of SO_3^{2-}. The large Stokes shifts exhibited by probe **59** and the formed dye **60**, along with their absorption spectral overlap allowed single wavelength excitation in the fluorescence detection. Compound **59** itself shows yellow emission (λ_{em}^{max} = 563 nm) with a 186 nm Stokes shift. Upon interaction with Na_2SO_3, the simultaneous change of the fluorescence takes place: λ_{em}^{max} = 467, 133 nm Stokes shift. The proposed reaction mechanism is also supported by the NMR spectral data and HR-MS studies. The proton signal at 9.94 ppm (H_a) of the aldehyde group shifts to 5.09 ppm (H_b), which is assigned to the proton at the saturated carbon atom of the formed adduct **60**.

Boron fluoride anionic complex with dipyrrolomethylenes bearing styrene substituents **61** was prepared for the determination of hypochlorite anion.[139]

As expected, the compound without styryl substituents showed absorption and emission bands centred at 497 and 507 nm, respectively, along with green emission, which is typical of BODIPY derivative. For styryl derivative **61** an absorption maximum is shifted to the longer wavelengths at 638 nm, because of the extra π-conjugation of two styryl substituents. Strong magenta emission with maximum at 657 nm is observed. Complex **61** provides good selectivity over H_2O_2 and *tert*-butyl hydroperoxide with almost linear

Structure 61



61

growth of the fluorescence intensity on addition of ClO^-. In aqueous media, the probe demonstrated colorimetric change from blue to purple and orange fluorescence, selectively to hypochlorite, with the detection limit of 0.26 μmol L^{-1}. The proposed oxidation pathway involves epoxidation with a subsequent hydrolytic ring opening and formation of ketone functions, which leads to marked orange emission in the presence of even small amounts of NaClO (Scheme 44).

To gain more information of the reaction between probe **61** and NaOCl, the oxidation products were studied by mass spectrometry. After mixing compound **61** with 5 equivalents of NaOCl for 30 min, the mass spectrum of the resulting mixture has a peak at m/z = 546.25 corresponding to the molecular ion of **61** and the peak at 580.30 that corresponds to the product **62a** of epoxidation followed by ring-opening hydrolysis. Further oxidation of **62a** into β-hydroxy ketone **62b** explains the orange emission of probe upon the addition of NaOCl.

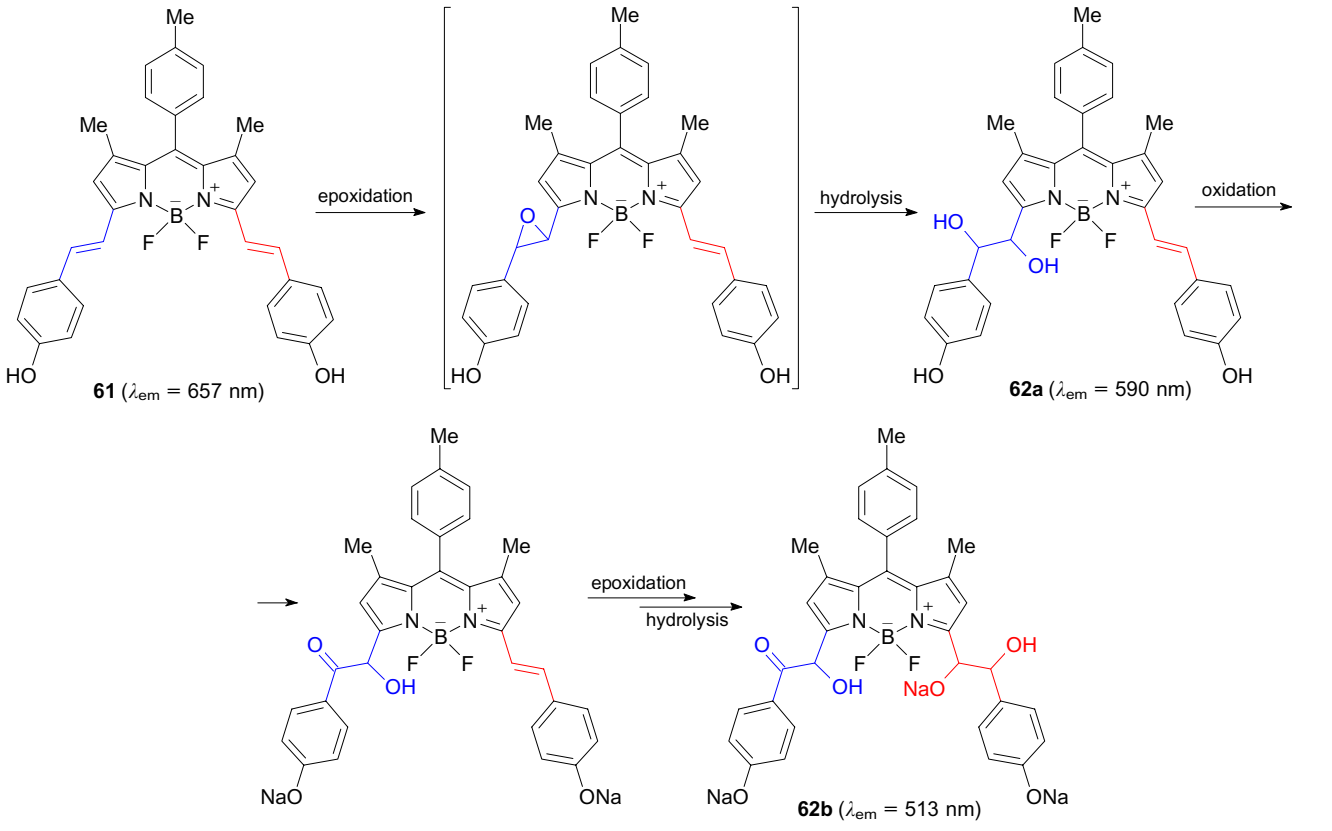
8. Probes for multiple analytes

Supramolecular conjugates constructed using low-molecular-weight structures [356, 357] are of much attention because they have many practical applications.[358, 359] A common way to provide such conjugates with special characteristics is to introduce functional groups into their molecular structure. Many supramolecular conjugates have found application in photovoltaics,[360] field-effect transistors,[361] oil or dye absorbing [362] and various stimuli-responsive materials.[363]

An L-phenylalanine derivative **63** consisting of benzoxazole as the proton-binding site, highly π-conjugated fluorophore with low HOMO energy level and cyano moieties as electron-withdrawing groups, has been synthesized.[271] It proved to be a sensitive probe to several analytes (Fig. 4).

Based on this derivative, materials that exhibit responses to both acid and organic amine vapours were studied. The xerogel film based on the probe **63** possesses high green fluorescence. It was used as a dual chemosensor and is capable to quantify volatile acid and organic amine vapours. The fluorescence of the sensing solution and xerogel film decreased gradually upon addition of trifluoroacetic acid (TFA). The nitrogen atom of benzoxazole moiety is considered as a proton binding site. Upon exposure of the xerogel film to saturated aniline vapour (over 91%), fluorescence quenching was also observed. The quenching effect is due to the PET from the HOMO of the aromatic amine to that of the excited probe **63**. The sensing effect is specified by the short response time and low detection limit. The detection limits of the new chemosensor **63** were found to be 796 ppt and 25 ppb for gaseous aniline and TFA, respectively.

Scheme 44



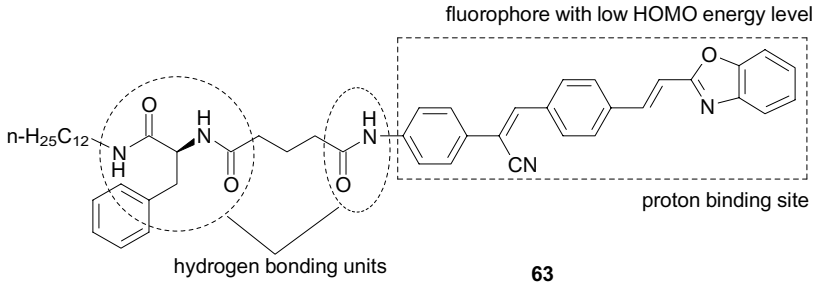
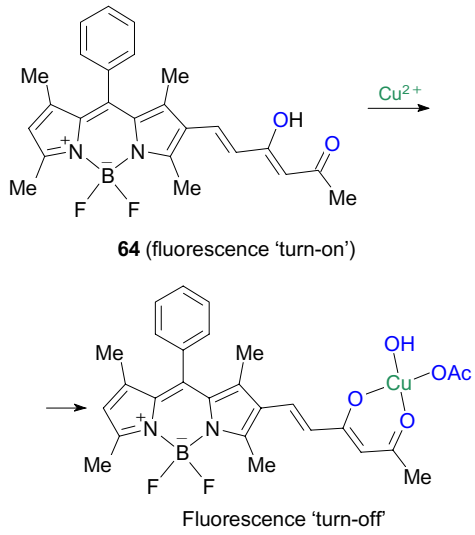


Figure 4. Structure of the probe **63**.

A BODIPY-complex **64** containing an additional acetylacetone side chain was studied as an 'on-off-on' type fluorescent chemosensor.[140] The molecule shows remarkable selectivity for Cu^{2+} ion over many other cations (*e.g.*, Na^+, K^+, Li^+, Ba^{2+}, Mn^{2+}, Ca^{2+}, Ph^{2+}, *etc.*) , due to the specific complexation with the enolate moiety (Scheme 45). The complexation quenches emission of the compound **64** at 570 nm.

Scheme 45



The DFT calculations for the probe **64** and **64**-Cu^{2+} complex were carried out to understand their geometry and optical properties. The geometries were optimized by DFT with B3LYP/6-31G(d) basis set using the Gaussian-09 software program. The HOMO and LUMO of the probe **64** were located over the entire molecule, indicating extensive π-conjugation between the BODIPY and β-diketone units. This accounts for significant red shifts of absorption and emission maxima compared to those of the parent dye. In the complex **64**-Cu^{2+}, the electron density of HOMO-2 is also located on the BODIPY and Cu^{2+}-coordinated β-diketone moieties. However, the LUMO electron density is localized on the Cu^{2+} ion, indicating a strong ligand-to-metal charge transfer process. This explains non-fluorescence nature of **64**-Cu^{2+} complex making the probe **64** a selective sensor for Cu^{2+} ions. The ^{1}H NMR studies revealed considerable changes in the form of the enolic OH proton signal (δ = 15.65 ppm) following the addition of Cu^{2+} ion.

The cupric complex of the probe **64** exhibits recovery of the quenched fluorescence on reaction with S^{2-} anion with high specificity. Formation of cupric sulfide is accompanied by the release of the molecule of **64** with fluorescence at 570 nm, which was additionally proved by its chromatographic isolation and the detailed ^{1}H NMR spectral studies. Thus, the probe **64** turned out to be very useful as a dual chemosensor for detecting both the cupric and sulfide ions. Moreover, it can be repeatedly used for a tandem detection of Cu^{2+} and S^{2-} ions. It is also useful for imaging Cu^{2+} and sensing sulfide ions in living biological substrates. Moreover, the application of the dye **64** in logic gate systems by sequential addition of Cu^{2+} and S^{2-} ions is suggested.

The probe **65** provides one more 'on-off-on' example of response to several analytes. Despite the fact that many metal cations possess similar sizes, they often demonstrate different coordination energies. This can be employed for the selective determination of one ion over another. A supramolecular detector **65** consisting of calix[4]arene bearing pendant benzothiazolyl and phenolic substituents has been investigated for cation- and anion-binding abilities (Scheme 46).[203]

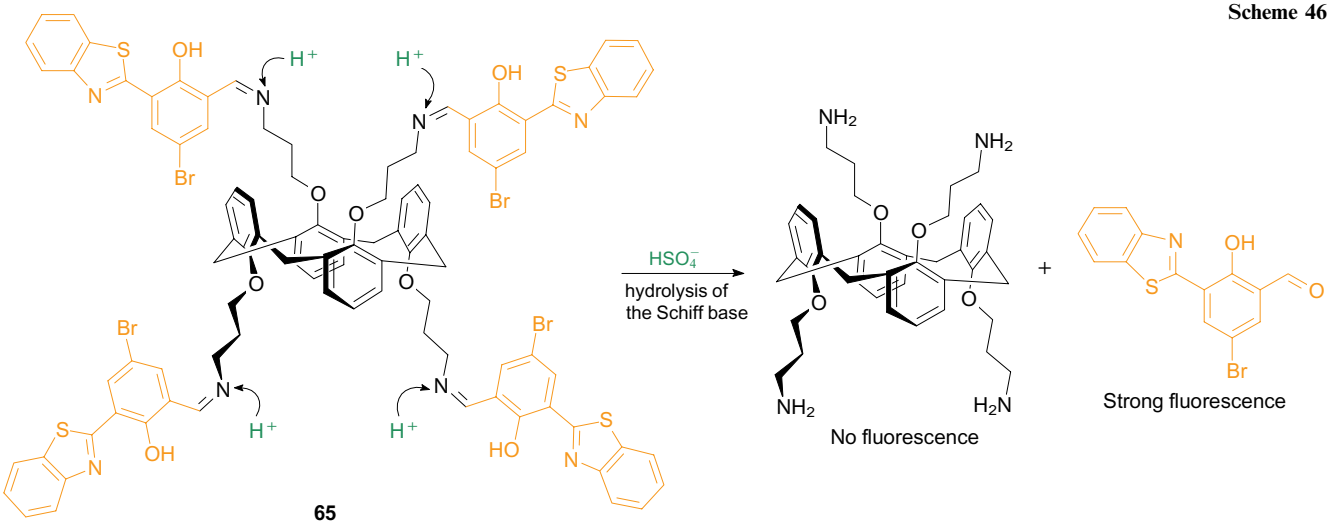
It was found that the conjugate **65** displays high and selective affinity to the Cu^{2+} ion with 'on-off-on' type sensing recognition on further addition of sulfide anions. The probe **65** exhibits the emission maximum at 542 nm being excited at 370 nm. High fluorescence of the probe is completely and selectively quenched by Cu^{2+} ion, indicating a strong complex formation of **65** with this cation. The generated **65**-Cu^{2+} complex is useful for S^{2-} recognition due to the high affinity of sulfide to Cu^{2+} ion. On addition of S^{2-} to **65**-Cu^{2+} solution, a remarkable fluorescence enhancement was observed at 542 nm. Meanwhile, addition of other anions, including F^-, Cl^-, Br^-, I^-, $H_2PO_4^-$, HPO_4^{2-}, NO_2^-, NO_3^-, AcO^-, ClO_4^-, SO_4^{2-}, HSO_4^-, CO_3^{2-}, HCO_3^- and OH^- does not produce any significant fluorescence enhancement. These results demonstrate the L-Cu^{2+} complex to have a high selectivity toward S^{2-} ion.

It is also important to emphasize, that the strong fluorescence was experimentally observed on contact of the probe **65** with HSO_4^- ions with *ca.* 1 μmol L^{-1} sensing limit and 10-fold fluorescence enhancement at 542 nm, which has been attributed to the hydrolysis of the four Shiff base moieties. This was convincingly confirmed by the dynamic ^{1}H NMR spectroscopy, which indicated the appearance and growth of the aldehyde proton signal. On the other hand, compound **65** was very inert towards the acidic phosphate or highly basic fluoride and hydroxide anions. The system is easily reusable and seem to be highly promising.

The probe **66** was found to provide sensory effects to Zn^{2+} and sulfide ions (Scheme 47).[272]

When excited at 340 nm, the probe **66** exhibits a weak fluorescence emission (λ_{max} = 500 nm). Upon addition of the metal ions such as K^+, Na^+, Mg^{2+}, Fe^{2+}, Fe^{3+},

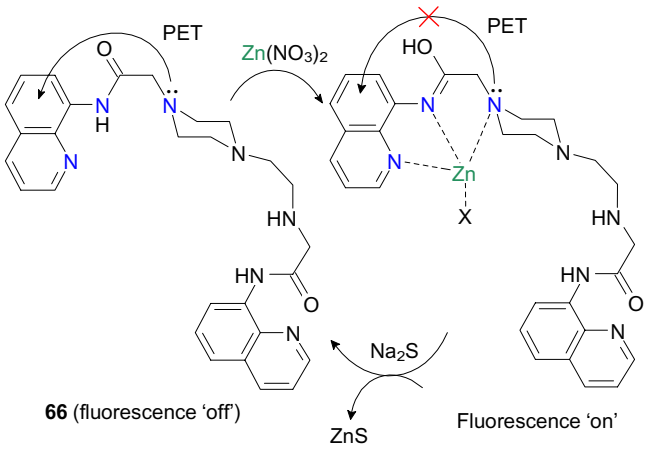
Scheme 46



65

$HSO_4^- + H_2O \longrightarrow SO_4^- + H^+$

Scheme 47

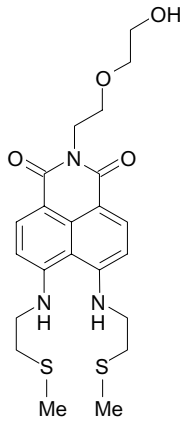


X is a solvent or NO_3^-

Mn^{2+}, Ca^{2+}, Al^{3+}, Ga^{3+}, Cr^{3+}, Co^{2+}, Ga^{3+}, Ni^{2+}, Cu^{2+} and Pb^{2+}, no or slight increase in intensity at 500 nm was observed. However, the probe **66** showed a green fluorescence enhancement in the presence of Zn^{2+} ion. The sensing mechanism of compound **66** towards Zn^{2+} has been proposed on the basis of UV/Vis titration, the Job's plot, ^{1}H NMR titration, theoretical calculations and ESI-mass spectroscopy analysis. In order to understand the sensory reaction mechanism of probe **66** towards Zn^{2+} ion, the DFT calculations by the B3LYP/6-31G(d,p) basis set with the Gaussian 03 program were performed. According to the calculation results, zinc(II) ion turned to be coordinated to 2-, 5- and 6-nitrogen atoms of compound **66**. Time-dependent density functional theory (TD-DFT) calculations were carried out to provide more information about the electronic interactions between ligand **66** and Zn^{2+}. In the case of ligand, the molecular orbital (MO) contribution of the first lowest excited state was mainly determined for HOMO → LUMO + 1 transition (330.61 nm). The transition indicated the PET from the ligand piperazine nitrogen atom to that of the quinoline one with the initial non-radiative process of **66**. For **66**-Zn^{2+} complex, the main MO contribution of the fifth lowest excited state was determined for HOMO-3 → LUMO transition (327.50). This transition is of the $\pi \rightarrow \pi^*$ type and indicates 'turn-on' sensing mechanism by inhibited PET transition from the N atom of the piperazine group to the quinolone one.

Diketo-azaphenalene bearing aza- and thiaethylene glycol side groups **67** was explored as a novel 'on-off-on' type probe for fluoride, cyanide and carbon dioxide.[158]

Structure 67



67

Addition of F^- and CN^- ions led to red shifts in the absorption spectra, which can be explained by the increased ICT due to the strong hydrogen bonding between amino function and anions. Similar enhanced ICT effect was previously reported for naphthalimide derivatives.[364, 365] Addition of cyanide ion provides also a moderate fluorescence quenching effect. These changes were explained on the basis of the considerable hydrogen bonding with the title polyaromatics, with detection limits to fluoride and cyanide ions equal to 1.56×10^{-10} and 2.47×10^{-10} mol L^{-1} respectively. The ^{1}H NMR studies clearly demonstrated the broadening of amine proton signals and differences in the corresponding chemical shifts, which indicated the possibility of complete deprotonation. On further exposure to CO_2 gas, the fluoride complex showed a visible colorimetric change, resulting in an 'on-off-on' type fluorescence. Presumably, the unstable intermediate carbamic acid can transform into bicarbonate anion, with simultaneous release of the highly fluorescent naphthalimide derivative.

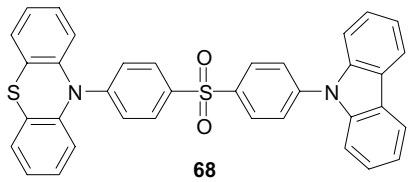
9. Probes sensitive to conformational effects

Changes in the molecular packing of the proper materials dependening on temperature, pressure and aggregation can be utilized to alter their photophysical properties,[273 – 276] since the photofluorescent properties of organic dyes are significantly influenced by their conformations. Such materials are considered as good candidates for sensors. For example, many dyes changing their photofluorescent properties through thermal treatment without melting have been prepared, because temperature change is a well-known way to induce dynamic transition in molecular assembled structures.[274, 277 – 279] A large number of studies also showed the possibility to use conformational stimulations to control the molecular arrangement and thereby the optical response of fluorescent π-conjugated molecules of organic dyes.

The conventional fluorophores, such as fluorescein, rhodamines, cyanines are known to aggregate in water-containing environment resulting in aggregation-caused quenching (ACQ). This effect greatly limits their practical application, for example, in physiological environment.[280 – 283] However, the discovery of the AIE of organic dyes provide new opportunities to overcome the ACQ effect. In contrast to ACQ, organic dyes with AIE effect emit intensely upon aggregation while showing no fluorescence in dilute solutions.[284] Various mechanisms have been studied to elucidate the reasons for the AIE phenomena. Restriction of intramolecular rotations (RIR), J-aggregate formation, conformational planarization, *E*/*Z* isomerization can be mentioned as the most actively discussed mechanisms.[285 – 287] For example, the RIR process inhibits the free vibration of the fluorophore and intramolecular rotations of its fragments, providing an emission increase.[288, 289] Mechano- and aggregation-responsive sensors are reviewed in a number of excellent papers.[8, 10, 290] Therefore, only a few examples of conformation-effected analytes are presented in this text.

Xu *et al.*[291] have developed an asymmetric probe **68**, which could integrate the properties of AIE and mechanofluorescence (MF).

Structure 68



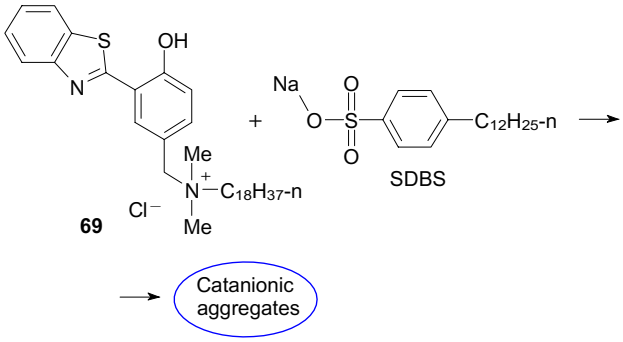
68

A high photofluorescence quantum yield (93.3%) and a long fluorescence lifetime (1.23 ms) have been observed for the powder form of compound **68**. Moreover, when the powder sample of **68** was scratched under pressure, a strong green luminescence appeared even in the daylight. This study proposes a strategy to integrate the features of AIE and MF effects into the same compound, which provides its potential applications in design of sensory materials.

Tang and coworkers [292] developed an AIE-active probe **69** for sensitive detection of an anionic surfactant, sodium dodecylbenzenesulfonate (SDBS) (Scheme 48).

This probe can form highly emissive catanionic aggregates or micelles with SDBS thus restricting the intramolecular motion. Thus, the probe **69** can be used for quantitative determination of SDBS concentration. It effectively avoids the interference of small anions and was used for selective detection of SDBS with a detection limit of 0.051 μmol L^{-1}, which is lower than the standard colorimetric Methylene Blue method (≈0.144 μmol L^{-1}).[293]

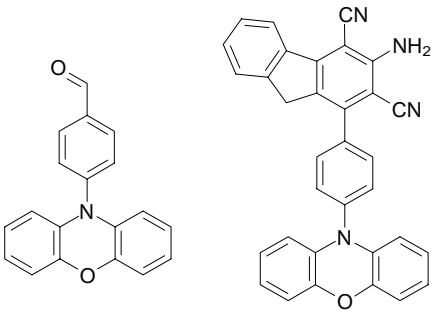
Scheme 48



Two unique compounds **70** and **71** containing phenoxazine moiety emitting light in solids have been synthesized.[259]

Both compounds are nonfluorescent in dilute tetrahydrofuran solutions and display AIE on addition of a large amount of water. When the water fraction reaches a certain amount (75% for **70**, 70% for **71**), both compounds **70**, **71** show crystallization-induced emission. By careful evaporaton of the solutions of **70** and **71** in appropriate solvents, two single crystals were obtained for compound **70** and three single crystals were obtained for compound **71**, showing polymorphism-dependent emission (PDE). By analyzing the X-ray diffraction data, π – π stacking between phenoxazine molecules was found as the main intermolecular contact that is responsible for the emissions of the crystals, while the hydrogen bonding plays a key role in their formation. Moreover, it was also elucidated that the dihedral angle between the planes of phenoxazine and benzene rings is essential for conjugation between electron donor and electron acceptor in one molecule. The larger the angle, the more blue-shifted the emission. It is also worthwhile to note that a loosely packed structure, with larger cell volume and lower cell density, makes it easier for a crystal to change morphology and to show mechanochromic fluorescence under pressure.

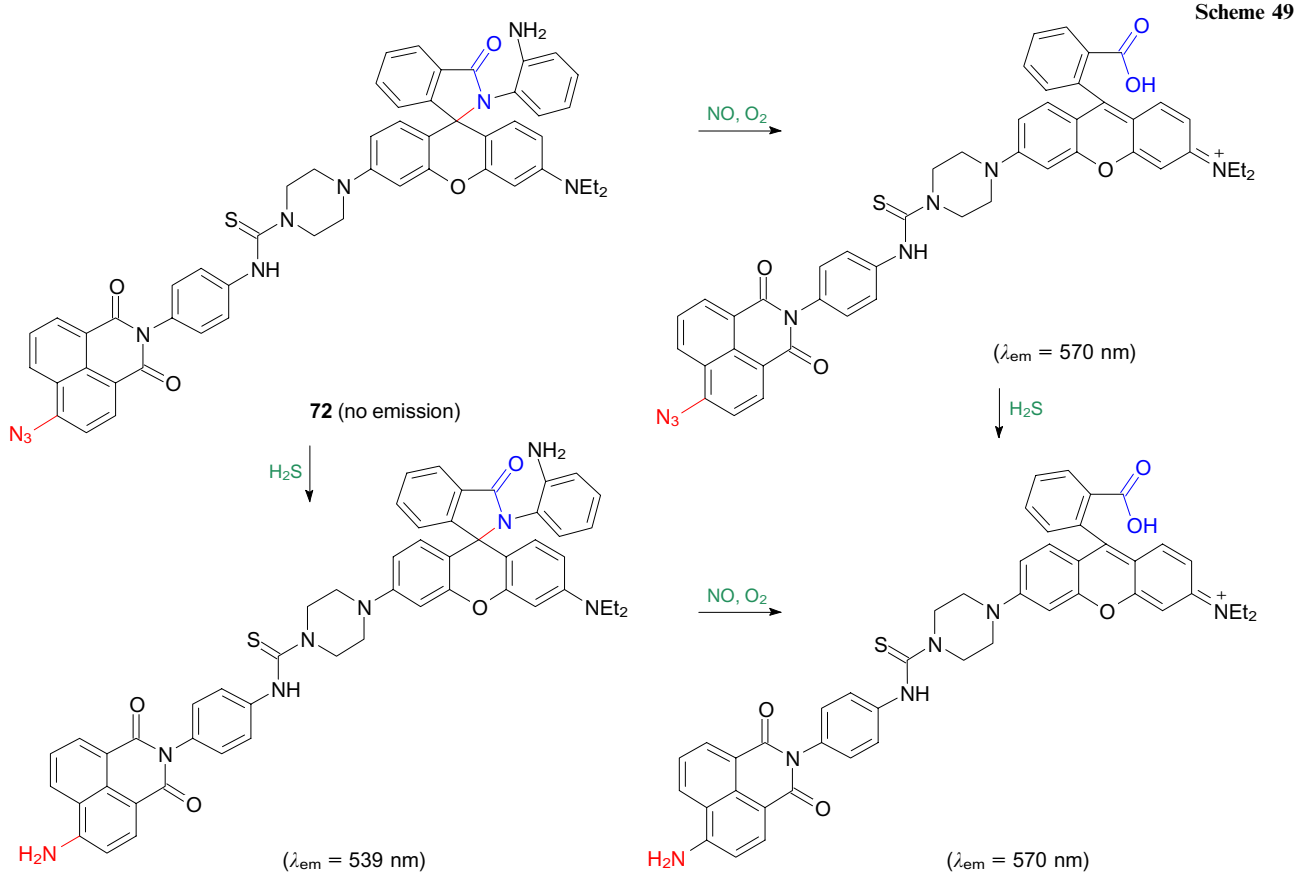
Structures 70, 71



70 **71**

A long chain-linked polyheterocyclic probe **72** comprising naphthalimide structure was synthesized and examined as a potential highly emissive conjugate for detection of hydrogen sulfide and nitric oxide in a logic gate manner (Scheme 49).[294]

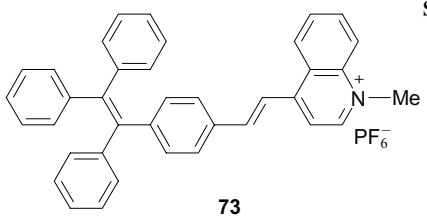
Scheme 49



For this probe, an azide-linked naphthalimide and a modified rhodamine were connected through a rigid piperazine linker that prevents close contact of the two fluorophores and provides an efficient Förster resonance energy transfer (FRET) from excited naphthalimide moiety to rhodamine fragment. The absorption bands of naphthalimide and rhodamine fluorophores are at *ca.* 432 nm and 550 nm, respectively. They are well separated and can be independently excited. As a result, the presence of H_2S can transform the azide group into amine one and thereby turn on naphthalimide fluorescence. Meanwhile, the addition of NO breaks the lactame ring in the rhodamine moiety and leads to its efficient emission. The reverse order of the addition of reactants did not cause any considerable mechanistic changes and led again to the fluorescence at 570 nm. This design can ensure the multiple sensing of NO and H_2S in a logic gate manner. Intracellular dihydrogen sulfide and nitric oxide could also be effectively detected at tens of μmol L^{-1} range, as compound **72** did not exhibit any significant cytotoxicity in murine fibrosarcoma L929 cells.

A cationic polyene-conjugated quinoline fluorescent probe **73** has been designed for sensing of iodide and Hg^{2+} ions in aqueous solutions.[295] The compound **73** possesses AIE.

Structure 73



73

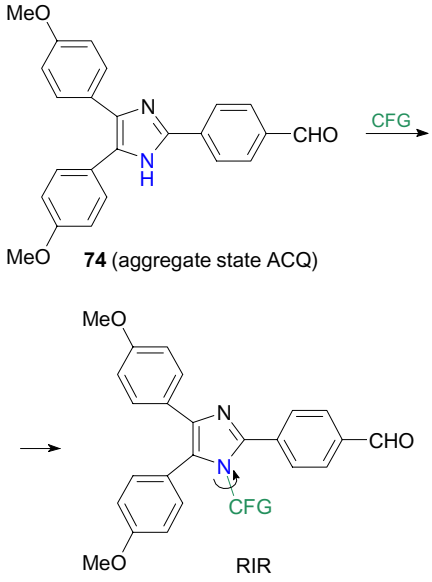
Photoexcitation of a dilute solution of probe **73** gives a very weak emission because of the active intramolecular rotation of the triphenylethene group, which consumes the energy of excitons through the non-radiative relaxation channel. The AIE properties of the probe **73** in DMSO–water mixtures were then checked by varying the amount of water fraction (f_w). As f_w increased from 0% to 80%, the emission spectra of the probe **73** stayed at a low level without any significant change. However, after f_w exceeding 80%, the fluorescence was coming up and the emission intensity at 610 nm rose sharply with increasing water content. At f_w = 99%, the emission reached maximum and showed approximately 13-fold enhancement over that in pure DMSO. Meanwhile, the starting colourless solution turned intense red under the 365 nm wavelength irradiation. The observed phenomenon could be attributed to the formation of molecular aggregates which suppressed the non-radiative relaxation channels. The average diameter of the probe **73** particles in the mixed solution with f_w of 90% and 99% was determined to be 132.5 and 111.4 nm respectively, by dynamic light scattering (DLS), confirming the formation of nanoaggregates. Clearly, the probe **73** is a typical AIE fluorogen with red emission. Careful examination of the crystal packing structure reveals that the distance between two quinolinium planes of adjacent molecules is 5.201 Å, which can hinder the intermolecular π – π stacking interaction and thus avoid the quenching of fluorescence in the condensed phase.

Compound **73** has orange or red fluorescence in the solid state or in H_2O, respectively. Addition of I^- anion resulted in drastic reduction of the emission, with excellent linear dependence on the anion concentration and near-nanomolar sensing limit. The standard method was used to

analyze the concentration of I^- ion in running water samples with the found sensing limit of 0.07 μmol L^{-1} of Hg^{2+}. However, in the presence of Hg^{2+} ion the remarkable recovery of the fluorescence is observed due to the strong affinity between Hg^{2+} and iodide. The detection limit for iodide ion and Hg^{2+} based on these findings is coming to the nanomolar level.

Based on the steric effect of conformational functional group (CFG) on the imidazole-containing probe **74**, various CFGs have been introduced into the imidazole moiety to study the effect of different sterically hindered groups, thus developing a series of AIE-fluorophores.[221] The results show that CFG not only plays a crucial role in the restriction of intramolecular rotation in the aggregate state, but also affects the planarity of molecules. Due to these factors, the probe **74** originally showing the ACQ effect was converted into a fluorophore with the AIE-effect (Scheme 50).

Scheme 50

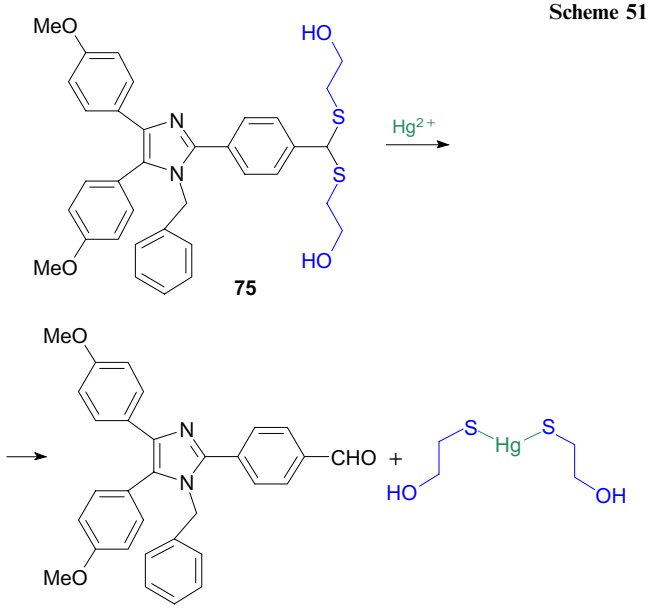


ACQ is aggregation-caused quenching, CFG is conformational function group, RIR is restriction of intramolecular rotations

Thus, a fluorescent molecular probe **75** with excellent AIE property to detect mercury ion has been synthesized (Scheme 51).

The responsive mechanism of the probe **75** was confirmed by ^1H NMR titration experiments and mass spectrometry. The probe **75** exhibits favourable water solubility, high selectivity and sensitivity, good linearity and superior stability over a wide pH range (4 – 9). The fluorescence intensity of the probe **75** rose and the maximum fluorescent emission wavelength was red-shifted from 475 to 495 nm after adding Hg^{2+} ion in concentrations from 1 μmol L^{-1} to 10 μmol L^{-1}. Furthermore, in the range of 1 – 10 μmol L^{-1}, the fluorescence intensity at 495 nm was in a good linear relationship with the concentration of mercury ion. The lowest detection limit of the probe **75** for Hg^{2+} was calculated to be 0.036 μmol L^{-1}. Furthermore, the probe **75** was applied to detect mercury ion in real water samples and imaging of mercury ion in living cells. Owing to its favourable biocompatibility, non-invasive and on-site

Scheme 51



imaging, compound **75** has great potential in detection of mercury ions in environmental and biological samples.

10. Conclusion

Fluorescence makes it possible to create numerous modern sensory systems and technologies. Most of fluorescent probes are based on the use of organic dyes, fused π-conjugated arenes and heteroarenes. Due to the 'push-pull' polarized π-electron systems and various functional groups in their molecules, fluorescent dyes provide diverse mechanisms of both fluorescence increase and fluorescence quenching.

The data presented in this review allow us to note a number of trends in design of novel sensory molecules and materials. One trend is the construction of new latent forms of known laser dyes. The obvious advantage of this trend is that the spectral responses of the new sensory structures in this case are based on the obviously high fluorescent characteristics of such dyes. The latent forms of a series of rhodamines, fluoresceins and coumarins have been synthesized and used successfully in the related sensory applications. The new effective sensors for metal cations were mentioned in Section 5. For analytes of nucleophilic nature, the most effective sensors are cyanine dyes and their analogues, which have highly polarized electronic structures capable of very rapid and irreversible reactions with nucleophiles, such as in Michael's reactions. Among such sensors, one can note ratiometric probes, which were able to detect cyanide ions at concentrations an order of magnitude lower than the maximum permissible concentration.

Another promising trend in developing new sensory systems is the synthesis and application of hybrid structures in which the possibilities of intramolecular distribution of electron densities are combined with the effects of intermolecular interactions. The advantage of this trend is based on that the spectral response capabilities of the molecular sensor can be transformed due to extremely diverse intermolecular contacts that become possible within the corresponding hybrid materials. The prospects for creating sensors of this type are illustrated by the aggregation-dependent structures of Section 9.

There is no doubt that a study of chemical and photophysical mechanisms of sensory effects in much detail will also contribute to a successful design of novel specific probes for modern sensory technologies.

The review was prepared with the financial support of the Russian Science Foundation (grant No. 17-13-01302).

References

1. J.R.Lakowicz. In *Principles of Fluorescence Spectroscopy*. (3rd Ed.). (Springer, 2006). P. 623
2. Y.Yang, Q.Zhao, W.Feng, F.Li. *Chem. Rev.*, **113**, 192 (2013)
3. B.Daly, J.Ling, A.P.De Silva. *Chem. Soc. Rev.*, **44**, 4203 (2015)
4. K. Chen, Q. Shu, M. Schmittel. *Chem. Soc. Rev.*, **44**, 136 (2015)
5. H.S.Wang. *TrAC — Trends Anal. Chem.*, **85**, 181 (2016)
6. J.J.Zhang, F.F.Cheng, J.J.Li, J.J.Zhu, Y.Lu. *Nano Today*, **11**, 309 (2016)
7. Y.Fu, W.Xu, Q.He, J.Cheng. *Sci. China Chem.*, **59**, 3 (2016)
8. Y.Sagara, S.Yamane, M.Mitani, C.Weder, T.Kato. *Adv. Mater.*, **28**, 1073 (2016)
9. D.Wu, A.C.Sedgwick, T.Gunnlaugsson, E.U.Akkaya, J.Yoon, T.D.James. *Chem. Soc. Rev.*, **46**, 7105 (2017)
10. M.Gao, B.Z.Tang. *ACS Sensors*, **2**, 1382 (2017)
11. N.Kwon, Y.Hu, J.Yoon. *ACS Omega*, **3**, 13731 (2018)
12. K.Singh, A.M.Rotaru, A.A.Beharry. *ACS Chem. Biol.*, **13**, 1785 (2018)
13. Z.Yang, J.Cao, Y.He, J.H.Yang, T.Kim, X.Peng, J.S.Kim. *Chem. Soc. Rev.*, **43**, 4563 (2014)
14. A.C.Sedgwick, L.Wu, H.H.Han, S.D.Bull, X.P.He, T.D.James, J.L.Sessler, B.Z.Tang, H.Tian, J.Yoon. *Chem. Soc. Rev.*, **47**, 8842 (2018)
15. R.Balamurugan, J. H.Liu, B.T.Liu. *Coord. Chem. Rev.*, **376**, 196 (2018)
16. J.Zhang, X.Chai, X.P.He, H.J.Kim, J.Yoon, H.Tian. *Chem. Soc. Rev.*, **48**, 683 (2019)
17. M.Shamsipure, A.Barati, Z.Nematifar. *J. Photochem. Photobiol. C Photochem. Rev.*, **39**, 76 (2019)
18. N.De Acha, C.Elosúa, J.Corres, F.Arregui. *Sensors*, **19**, 599 (2019)
19. J.Han, J.Zhang, M.Gao, H.Hao, X.Xu. *Dyes Pigm.*, **162**, 412 (2019)
20. S.Pal, N.Chatterjee, P.K.Bharadwaj. *RSC Adv.*, **4**, 26585 (2014)
21. J.Yao, M.Yang, Y.Duan. *Chem. Rev.*, **114**, 6130 (2014)
22. P.A.Panchenko, O.A.Fedorova, Y.V.Fedorov. *Russ. Chem. Rev.*, **83**, 155 (2014)
23. X.Li, X.Gao, W.Shi, H.Ma. *Chem. Rev.*, **114**, 590 (2014)
24. K.P.Carter, A.M.Young, A.E.Palmer. *Chem. Rev.*, **114**, 4564 (2014)
25. Y.You, W.Nam. *Chem. Sci.*, **5**, 4123 (2014)
26. A.Granzhan, H.Ihmels, M.Tian. *ARKIVOC*, **6**, 494 (2015)
27. X.Chen, T.Pradhan, F.Wang, J.S.Kim, J.Yoon. *Chem. Rev.*, **112**, 1910 (2012)
28. H.Zheng, X.-Q.Zhan, Q.-N.Bian, X.-J.Zhang. *Chem. Commun.*, **49**, 429 (2013)
29. N.Boens, V.Leen, W.Dehaen. *Chem. Soc. Rev.*, **41**, 1130 (2012)
30. Y.Song, Z.Chen, H.Li. *Curr. Org. Chem.*, **16**, 2690 (2012)
31. C.M.L.Carvalho, E.-H.Chew, S.I.Hashemy, J.Lu, A.H.Holmgren. *J. Biol. Chem.*, **283**, 11913 (2008)
32. X.Lu, Z.Guo, M.Feng, W.Zhu. *ACS Appl. Mater. Interf.*, **4**, 3657 (2012)
33. E.M.Nolan, S.J.Lippard. *J. Am. Chem. Soc.*, **129**, 5910 (2007)
34. S.Saha, P.Mahato, G.U.Reddy, E.Suresh, A.Chakrabarty, M.Baidya, S.K.Ghosh, A.Das. *Inorg. Chem.*, **51**, 336 (2012)
35. S.-Y.Ding, M.Dong, Y.-W.Wang, Y.-T.Chen, H.-Z.Wang, C.-Y.Su, W.Wang. *J. Am. Chem. Soc.*, **138**, 3031 (2016)
36. M.Suresh, A.Ghosh, A.Das. *Chem. Commun.*, 3906 (2008)
37. S.Ou, Z.Lin, C.Duan, H.Zhang, Z.Bai. *Chem. Commun.*, 4392 (2006)
38. W.Liu, L.Xu, H.Zhang, J.You, X.Zhang, R.Sheng, H.Li, S.Wu, P.Wang. *Org. Biomol. Chem.*, **7**, 660 (2009)
39. N.Dave, M.Y.Chan, P.-J.J.Huang, B.D.Smith, J.Liu. *J. Am. Chem. Soc.*, **132**, 12668 (2010)
40. N.Kumar, I.Leray, A.Depauw. *Coord. Chem. Rev.*, **310**, 1 (2016)
41. M.Akamatsu, H.Komatsu, T.Mori, E.Adams, R.Shin, H.Sakai, M.Abe, J.P.Hill, K.Ariga. *ACS Appl. Mater. Interf.*, **6**, 8208 (2014)
42. V.Kumar, A.Kumar, U.Diwan, M.K.Singh, K.K.Upadhyay. *Bull. Chem. Soc. Jpn.*, **89**, 754 (2016)
43. B.Lozano-Torres, S.El Sayed, A.M.Costero, S.Gil, M.Parra, R.Martínez-Máñez, F.Sancenón. *Bull. Chem. Soc. Jpn.*, **89**, 498 (2016)
44. S.Y.Moon, N.R.Cha, Y.H.Kim, S.-K.Chang. *J. Org. Chem.*, **69**, 181 (2004)
45. H.Lee, S.S.Lee. *Org. Lett.*, **11**, 1393 (2009)
46. Z.Q.Hu, C.S.Lin, X.M.Wang, L.Ding, C.L.Cui, S.F.Liu, H.Y.Lu. *Chem. Commun.*, **46**, 3765 (2010)
47. L.Marbella, B.Serli-Mitasev, P.Basu. *Angew. Chem., Int. Ed.*, **48**, 3996 (2009)
48. J.Li, Y.Lu. *J. Am. Chem. Soc.*, **122**, 10466 (2000)
49. A.K.Jain, V.K.Gupta, L.P.Singh, J.R.Raisoni. *Electrochim. Acta*, **51**, 2547 (2006)
50. Y.Xiao, A.A.Rowe, K.W.Plaxco. *J. Am. Chem. Soc.*, **129**, 262 (2007)
51. P.S.Hariharan, S.P.Anthony. *Anal. Chim. Acta*, **848**, 74 (2014)
52. D.Dhananjay, K.Gurpreet, R.Anan, G.Loganathan, C.Prateeti, A.Jaydeep, P.Jorge, D.Dharumadurai, R.C.Angshuman, A.A.Mohammad, K.Niranjan, B.Bhaskar. *Eur. J. Inorg. Chem.*, **2014**, 3350 (2014)
53. B.Lukowiak, B.Vandewalle, R.Riachy, J.Kerr-Conte, V.Gmyr, S.Belaich, J.Lefebvre, F.Pattou. *J. Histochem. Cytochem.*, **49**, 519 (2001)
54. J.Osredka, N.Sustar. *J. Clinic. Toxicol.*, 3 (2011)
55. M.Saleem, K.H.Lee. *RSC Adv.*, **5**, 72150 (2015)
56. J.W.Lee, J.D.Helmann. *Nature (London)*, **440**, 363 (2006)
57. J.P.Summer, R.Kopelman. *Analyst*, **130**, 528 (2005)
58. N.C.N.Andrewa. *Engl. J. Med.*, **341**, 1986 (1999)
59. D.Galaris, V.Skiada, A.Barbouti. *Cancer Lett.*, **266**, 21 (2008)
60. E.D.Weinberg. *Eur. J. Cancer Prev.*, **5**, 19 (1996)
61. G.Alez. *Webster's Digital Services*, 1, (2012)
62. Z.Yang, M.She, B.Yin, J.Cui, Y.Zhang, W.Sun, J.Li, Z.Shi. *J. Org. Chem.*, **77**, 1143 (2012)
63. M.Zhang, H.Tan, Z.Xie, L.Zhang, X.Jing, Z.Sun. *ACS Appl. Mater. Interf.*, **5**, 1078 (2013)
64. J.D.Haas, T.Brownlie. *J. Nutr.*, **131**, 676S (2001)
65. E.Gaggelli, H.Kozlowski, D.Valensin, G.Valensin. *Chem. Rev.*, **106**, 1995 (2006)
66. E.L.Que, D.W.Domaille, C.J.Chang. *Chem. Rev.*, **108**, 1517 (2008)
67. P.Verwilst, K.Sunwoo, J.S.Kim. *Chem. Commun.*, **51**, 5556 (2015)
68. D.Strausak, J.F.B.Mercer, H.H.Dieter, W.Stremmel, G.Multhaup. *Brain Res. Bull.*, **55**, 175 (2001)
69. J.S. Valentine, P.J.Hart. *Proc. Natl. Acad. Sci. USA*, **100**, 3617 (2003)
70. K.J.Barnham, C.L.Masters, A.I.Bush. *Nat. Rev. Drug. Discov.*, **3**, 205 (2004)
71. R.Kramer. *Angew. Chem., Int. Ed.*, **37**, 772 (1998)
72. M.F.Yardim, T.Budinova, E.Ekinci, N.Petrov, M.Razvigorova, V.Minkova. *Chemosphere*, **52**, 835 (2003)
73. L.Jiao, J.Li, S.Zhang, C.Wei, E.Hao, M.G.H.Vicente. *New J. Chem.*, **33**, 1888 (2009)
74. C.Kokkinos, A.Economou, I.Raptis, T.Speliotis. *Anal. Chim. Acta*, **622**, 111 (2008)
75. A.A.Nemec, G.D.Leikauf, B.R.Pitt, K.Wasserloos, J.A.Barchowsky, A.M.J.Respir. *Cell. Mol. Biol.*, **41**, 69 (2009)

76. M.Costa, T.L.Davidson, H.Chen, Q.Ke, P.Zhang, Y.Yan, C.Huang, T.Kluz. *Mutat. Res.*, **592**, 79 (2005)
77. D.Zendelovska, G.Pavlovska, K.Cundeva, T.Stafilov. *Talanta*, **54**, 139 (2001)
78. M.A.Bezerra, W.N.L. dos Santos, V.A.Lemos, M.Korn, S.L.C.Ferreira. *J. Hazard. Mater.*, **148**, 334 (2007)
79. E.A.Takara, S.D.Pasini-Cabello, S.Cerutti, J.A.Gasquez, L.D.J.Martinez. *J. Pharm. Biomed. Anal.*, **39**, 735 (2005)
80. T.Stafilov. *Spectrochim. Acta B: Atomic Spect.*, **55**, 893 (2000)
81. Y.Jiang, W.Kong, Y.Shen, B.Wang. *Tetrahedron*, **71**, 5584 (2015)
82. L.Bian, X.Ji, W.Hu, J.Agric. *Food Chem.*, **62**, 4870 (2014)
83. L.A.Schurig-Briccio, R.B.Gennis. *J. Bacteriol.*, **194**, 4107 (2012)
84. J.F.Zhang, Y.Zhou, J.Yoon, J.S.Kim. *Chem. Soc. Rev.*, **40**, 3416 (2011)
85. A.Habib, M.Tabata. *J. Inorg. Biochem.*, **98**, 1696 (2004)
86. C.M.Goodman, C.D.McCusker, T.Yilmaz, V.M.Rotello. *Bioconjugate Chem.*, **15**, 897 (2004)
87. E.Nyarko, T.Hara, D.J.Grab, A.Habib, Y.Kim, O.Nikolskaia, T.Fukuma, M.Tabata. *Chem. Biol. Interact.*, **148**, 19 (2004)
88. X.Chen, Y.Zhou, X.Peng, J.Yoon. *Chem. Soc. Rev.*, **39**, 2120 (2010)
89. Y.Zhou, J.Yoon. *Chem. Soc. Rev.*, **41**, 51 (2012)
90. M.E.Jun, B.Roy, K.H.Ahn. *Chem. Commun.*, **47**, 7583 (2011)
91. S.Y.Zhang, C.-N.Ong, H.-M.Shen. *Cancer Lett.*, **208**, 143 (2004)
92. A.Pastore, F.Piemonte, M.Locatelli, A.Lo Russo, L.M.Gaeta, G.Tozzi, G.Federici. *Clin. Chem.*, **47**, 1467 (2001)
93. D.M.Townsend, K.D.Tew, H.Tapiero. *Biomed. Pharmacother.*, **57**, 145 (2003)
94. *Cyanide Toxicity*. (Atlanta, GA: U.S. Department of Health and Human Services, 1991)
95. *Cyanide in Biology*. (London: Academic Press, 1981)
96. *Guidelines for Drinking-Water Quality*. (Geneva: World Health Organization, 2008)
97. D.T.Thompson. In *Cyanide: Social, Industrial, and Economic Aspects*. (Eds C.Young, L.Tidwell, C.Anderson). (Warrendale: The Minerals, Metals and Materials Society, 2001). P. 582.
98. L.Ma, Y.X.Xu, K.N.Wang, C.J.Zhou, D.X.Cao, Y.Y.Shan, Q.Q.Wu. *Inorg. Chem. Commun.*, **58**, 24 (2015)
99. P.A.Gale, C.Caltagirone. *Chem. Soc. Rev.*, **44**, 4212 (2015)
100. X.Z.Song, S.Y.Song, S.N.Zhao, Z.M.Hao, M.Zhu, X.Meng, L.L.Wu, H.J.Zhang. *Adv. Funct. Mater.*, **24**, 4034 (2014)
101. R.M.Duke, E.B.Veale, F.M.Pfeffer, P.E.Krugeret, T.Gunnlaugsson. *Chem. Soc. Rev.*, **39**, 3936 (2010)
102. P.A.Gale. *Chem. Soc. Rev.*, **39**, 3746 (2010)
103. Y.P.Zhang, D.D.Li, Y.Li, J.H.Yu. *Chem. Sci.*, **5**, 2710 (2014)
104. S.N.Zhao, L.L.Wu, J.Feng, S.Y.Song, H.J.Zhang. *Inorg. Chem. Front.*, **3**, 376 (2016)
105. J.Du, X.Y.Wang, M.Jia, T.J.Li, J.F.Mao, Z.J.Guo. *Inorg. Chem. Commun.*, **11**, 999 (2008)
106. D.W.Zhang, X.Z.Jiang, Z.Y.Dong, H.Q.Yang, A.Martinez, G.H.Gao. *Tetrahedron*, **69**, 10457 (2013)
107. H.B.Kim, Y.F.Liu, D.Y.Nam, Y.N.Li, S.N.Park, J.Y.Yoon, M.H.Hyun. *Dyes Pigm.*, **106**, 20 (2014)
108. J.Y.Yoon, S.K.Kim, N.J.Singh, K.S.Kim. *Chem. Soc. Rev.*, **35**, 355 (2006)
109. M.An, B.Y.Kim, H.Seo, A.Helal, H.S.Kim. *Spectrochim. Acta A: Mol. Biomol. Spect.*, **169**, 87 (2016)
110. P.A.Gale. *Chem. Commun.*, **47**, 82 (2011)
111. A.Gomes, E.Fernandes, J.L.Lima. *J. Biochem. Biophys. Methods*, **65**, 45 (2005)
112. B.Wang, D.Chen, S.Kambam, F.Wang, Y.Wang, W.Zhang, J.Yin, H.Chen, X.Chen. *Dyes Pigm.*, **120**, 22 (2015)
113. J.Kim, Y.Kim. *Analyst*, **139**, 2986 (2014)
114. D.I.Pattison, M.J.Davie. *Biochemistry*, **45**, 8152 (2006)
115. Q.Xu, K.Lee, S.Lee, K.M.Lee, W.J.Lee, J.Yoon. *J. Am. Chem. Soc.*, **135**, 9944 (2013)
116. C.Sparacino-Watkins, J.F.Stolz, P.Basu. *Chem. Soc. Rev.*, **43**, 676 (2014)
117. N.Xiao, C.Yu. *Anal. Chem.*, **82**, 3659 (2010)
118. Z.Lin, Z.Xue, H.Chen, J.-M.Lin. *Anal. Chem.*, **83**, 8245 (2011)
119. Q.Xie, W.He, S.Yu, X.-Y.Chen, X.Zhang, Y.Shen. *Anal. Methods*, **6**, 7716 (2014)
120. J.Zhang, C.Yang, X.Wang, X.Yang. *Analyst*, **137**, 3286 (2012)
121. J.Han, C.Zhang, F.Liu, B.Liu, M.Han, W.Zou, L.Yang, Z.Zhang. *Analyst*, **139**, 3032 (2014)
122. B.Unnikrishnan, S.-C.Wei, W.-J.Chiu, J.Cang, P.-H.Hsu, C.-C.Huang. *Analyst*, **139**, 2221 (2014)
123. S.Garrod, M.E.Bollard, A.W.Nicholls, S.C.Connor, J.Connelly, J.K.Nicholson, E.Holmes. *Chem. Res. Toxicol.*, **18**, 115 (2005)
124. C.Reilly, S.Aust. *Chem. Res. Toxicol.*, **10**, 328 (1997)
125. M.D.J.Kerai, J.A.Timbrell. *Toxicology*, **120**, 221 (1997)
126. S.Goswami, S.Das, K.Aich, B.Pakhira, S.Panja, S.K.Mukherjee, S.Sarkar. *Org. Lett.*, **15**, 5412 (2013)
127. S.D.Zelnick, D.R.Mattie, P.C.Stepaniak. *Aviat. Space Environ. Med.*, **74**, 1285 (2003)
128. A.Loudet, K.Burgess. *Chem. Rev.*, **107**, 4891 (2007)
129. Y.Chen, D.Qi, L.Zhao, W.Cao, C.Huang, J.Jiang. *Chem. – Eur. J.*, **19**, 7342 (2013)
130. M.L.Giuffrida, E.Rizzarelli, G.A.Tomaselli, C.Satriano, G.T.Sfrazzetto. *Chem. Commun.*, **50**, 9835 (2014)
131. N.Boens, W.Qin, M.Baruah, W.M. De Borggraeve, A.Filarowski, N.Smisdom, M.Ameloot, L.Crovetto, E.M.Talavera, J.M.Alvarez-Pez. *Chem. – Eur. J.*, **17**, 10924 (2011)
132. S.Madhu, D.K.Sharma, S.K.Basu, S.Jadhav, A.Chowdhury, M.Ravikanth. *Inorg. Chem.*, **52**, 11136 (2013)
133. X.Kong, F.Su, L.Zhang, J.Yaron, F.Lee, Z.Shi, Y.Tian, D.R.Meldrum. *Angew. Chem., Int. Ed.*, **54**, 12053 (2015)
134. M.Isik, T.Ozdemir, I.S.Turan, S.Kolemen, E.U.Akkaya. *Org. Lett.*, **15**, 216 (2013)
135. J.Zhang, F.Pan, Y.Jin, N.Wang, J.He, W.Zhang, W.Zhao. *Dyes Pigm.*, **155**, 276 (2018)
136. X.Xue, H.Fang, H.Chen, C.Zhang, C.Zhu, Y.Bai, W.He, Z.Guo. *Dyes Pigm.*, **130**, 116 (2016)
137. S.O.Tümay, E.Okutan, I.F.Sengul, E.Özcan, H.Kandemir, T.Doruk, M.Çetin, B.Çoşut. *Polyhedron*, **117**, 161 (2016)
138. L.-Y.Niu, Y.-S.Guan, Y.-Z.Chen, L.-Z.Wu, C.-H.Tung, Q.-Z.Yang. *J. Am. Chem. Soc.*, **134**, 18928 (2012)
139. S.Jantra, P.Butta, P.Jithavech, P.Rojsitthisak, T.Palaga, P.Rashatasakhon, M.Sukwattanasinitt, S.Wacharasindhu. *Dyes Pigm.*, **162**, 189 (2019)
140. A.B.More, S.Mula, S.Thakare, S.Chakraborty, A.K.Ray, N.Sekar, S.Chattopadhyay. *J. Lumin*, **190**, 476 (2017)
141. J.Callan, A.P. de Silva, D.Magri. *Tetrahedron*, **61**, 8551 (2005)
142. J.Gan, K.Chen, C.P.Chang, H.Tian. *Dyes Pigm.*, **57**, 21 (2003)
143. A.P.de Silva, A.Goligher, H.Gunaratne, T.Rice. *ARKIVOC*, **7**, 229 (2003)
144. E.Martin, R.Weigand, A.Pardo. *J. Lumin.*, **68**, 157 (1996)
145. V.Gruzinskii, A.Kukhto, G.Shakkah. *J. Appl. Spectrosc.*, **65**, 463 (1998)
146. Z.F.Tao, X.Qian. *Dyes Pigm.*, **43**, 139 (1999)
147. W.Stewart. *J. Am. Chem. Soc.*, **103**, 7615 (1981)
148. W.Zhu, M.Hu, R.Yao, H.Tian. *J. Photochem. Photobiol., A: Chem.*, **154**, 169 (2003)
149. H.Facoetti, P.Robin, P. Le Barny, M.Schott, C.M.Bouche, P.Berdague. *Synth. Met.*, **81**, 191 (1996)
150. W.Zhu, N.Minami, S.Kazaoui, Y.Kim. *J. Mater. Chem.*, **13**, 2196 (2003)
151. I.Grabchev, I.Moneva, V.Bojinov, S.Guittonneau. *J. Mater. Chem.*, **10**, 1291 (2000)
152. F.Cosnard, V.Wintgens. *Tetrahedron Lett.*, **39**, 2751 (1998)
153. V.B.Bojinov, N.I.Georgiev, N.V.Marinova. *Sens. Actuators B: Chem.*, **148**, 6 (2010)
154. P.Chinapang, V.Ruangpornvisuti, M.Sukwattanasinitt, P.Rashatasakhon. *Dyes Pigm.*, **112**, 236 (2015)

155. P.-X.Liu, H.Chen, N.Xu, H.-N.Wang, X.Meng, Z.-Y.Zhou, Z.-M.Su. *Inorg. Chem. Commun.*, **79**, 60 (2017)
156. Z.Zhang, S.Lu, C.Sha, D.Xu. *Sens. Actuators B: Chem.*, **208**, 258 (2015)
157. Y.Fu, P.Li, J.-X.Kang, X.-Y.Liu, G.-Y.Li, F.Ye. *J. Lumin.*, **178**, 156 (2016)
158. M.Lee, S.Jo, D.Lee, Z.Xu, J.Yoon. *Dyes Pigm.*, **120**, 288 (2015)
159. X.D.Li, M.S.Zhan. *Chin. Chem. Lett.*, **22**, 1111 (2011)
160. A.Y.G.Fuh, Y.D.Chen, C.K.Liu, K.T.Cheng. *Dyes Pigm.*, **92**, 949 (2012)
161. S.T.Ha, K.L.Foo, R.T.Subramaniam, M.M.Ito, S.T.Ong. *Chin. Chem. Lett.*, **22**, 1191 (2011)
162. W.Lee, S.B.Yuk, J.Choi, D.H.Jung, S.H.Choi, J.Park, J.P.Kim. *Dyes Pigm.*, **92**, 942 (2012)
163. S.Menati, A.Azadbakht, R.Azadbakht, A.Taeb, A.Kakanejadifard. *Dyes Pigm.*, **98**, 499 (2013)
164. P.Zhang, B.B.Shi, T.B.Wei, Y.M.Zhang, Q.Lin, H.Yao, X.M.You. *Dyes Pigm.*, **99**, 857 (2013)
165. M.M.Ibrahim, H.M.Ali, M.A.Abdullah, P.Hassandarvish. *Molecules*, **17**, 12449 (2012)
166. Y.Z.Xie, G.G.Shan, P.Li, Z.Y.Zhou, Z.M.Su. *Dyes Pigm.*, **96**, 467 (2013)
167. R.A.Ahmadi, S.Amani. *Molecules*, **17**, 6434 (2012)
168. T.Tao, F.Xu, X.C.Chen, Q.Q.Liu, W.Huang, X.Z.You. *Dyes Pigm.*, **92**, 916 (2012)
169. A.Zabulica, M.Balan, D.Belei, M.Sava, B.C.Simionescu, L.Marin. *Dyes Pigm.*, **96**, 686 (2013)
170. G.Ceyhan, M.Tümer, M.Köse, V.McKee, S.Akar. *J. Lumin.*, **132**, 2917 (2012)
171. S.M.Seyedi, R.Sandaroos, G.H.Zohuri. *Chin. Chem. Lett.*, **21**, 1303 (2010)
172. L.Yin, X.Jia, X.S.Li. *Chin. Chem. Lett.*, **21**, 774 (2010)
173. Y.L.Yang, N.N.Wan, W.P.Wang, Z.F.Xie, J.D.Wang. *Chin. Chem. Lett.*, **22**, 1071 (2011)
174. J.Zhao, S.Ji, Y.Chen, H.Guo, P.Yang. *Phys. Chem. Chem. Phys.*, **14**, 8803 (2012)
175. B.K.Paul, N.Guchhait. *J. Lumin.*, **132**, 2194 (2012)
176. M.A.Satam, R.K.Raut, R.D.Telore, N.Sekar. *Dyes Pigm.*, **97**, 32 (2013)
177. K.Y.Chen, Y.M.Cheng, C.H.Lai, C.C.Hsu, M.L.Ho, G.H.Lee, P.T.Chou. *J. Am. Chem. Soc.*, **129**, 4534 (2007)
178. A.K.Mahapatra, K.Maiti, P.Sahoo, P.K.Nandi. *J. Lumin.*, **143**, 349 (2013)
179. S.Park, J.E.Kwon, S.H.Kim, J.Seo, K.Chung, S.Y.Park, D.J.Jang, B.M.Medina, J.Gierschner, S.Y.Park. *J. Am. Chem. Soc.*, **131**, 14043 (2009)
180. S.Xu, Y.Shao, F.Wu, G.Liu, L.Liu, J.Peng, Y.Sun. *J. Lumin.*, **136**, 291 (2013)
181. M.A.Satam, R.K.Raut, N.Sekar. *Dyes Pigm.*, **96**, 92 (2013)
182. S.Prabhu, S.Saravanamoorthy, M.Ashok, S.Velmathi. *J. Lumin.*, **132**, 979 (2012)
183. H.Xu, Y.Yue, H.Wang, I.Chen, Y.Hao, B.Xu. *J. Lumin.*, **132**, 919 (2012)
184. Z.Q.Guo, W.Q.Chen, X.M.Duan. *Dyes Pigm.*, **92**, 619 (2011)
185. Y.Li, D.Wang, L.Wang, Z.Li, Q.Cui, H.Zhang, H.Yang. *J. Lumin.*, **132**, 1010 (2012)
186. V.S.Patil, V.S.Padalkar, A.B.Tathe, N.Sekar. *Dyes Pigm.*, **98**, 507 (2013)
187. Y.Ito, K.Amimoto, T.Kawato. *Dyes Pigm.*, **89**, 319 (2011)
188. C.K.Lim, J.Seo, S.Kim, I.C.Kwon, C.H.Ahn, S.Y.Park. *Dyes Pigm.*, **90**, 284 (2011)
189. Y.J.Zhang, X.P.He, M.Hu, Z.Li, X.X.Shi, G.R.Chen. *Dyes Pigm.*, **88**, 391 (2011)
190. S.Goswami, S.Maity, A.K.Das, A.C.Maity, T.K.Mandal, S.Samanta. *Tetrahedron Lett.*, **54**, 5232 (2013)
191. T.Li, Z.Yang, Y.Li, Z.Liu, G.Qi, B.Wang. *Dyes Pigm.*, **88**, 103 (2011)
192. Q.Huang, X.F.Yang, H.Li. *Dyes Pigm.*, **99**, 871 (2013)
193. K.C.Tang, M.J.Chang, T.Y.Lin, H.A.Pan, T.C.Fang, K.Y.Chen, W.Y.Hung, Y.H.Hsu, P.T.Chou. *J. Am. Chem. Soc.*, **133**, 17738 (2011)
194. W.T.Chuang, C.C.Hsieh, C.H.Lai, C.H.Lai, C.W.Shih, K.Y.Chen, W.Y.Hung, Y.H.Hsu, P.T.Chou. *J. Org. Chem.*, **76**, 8189 (2011)
195. S.K.Fang, H.Y.Tsai, J.W.Hu, K.Y.Chen. *Int. J. Photoenergy*, **2014**, ID 124753 (2014)
196. Y.-J.Dong, X.-L.Li, Y.Zhang, W.-K.Dong. *Supramol. Chem.*, **29**, 518 (2017)
197. H.Zhang, T.Sun, Q.Ruan, J.-L.Zhao, L.Mu, X.Zeng, Z.Jin, S.Su, Q.Luo, Y.Yan, C.Redshaw. *Dyes Pigm.*, **162**, 257 (2019)
198. M.Patil, S.Bothra, S.K.Sahoo, H.A.Rather, R.Vasita, R.Bendre, A.Kuwar. *Sens. Actuators B: Chem.*, **270**, 200 (2018)
199. M.Dhanushkodi, G.G.V.Kumar, B.K.Balachandar, S.Sarveswari, S.Gandhi, J.Rajesh. *Dyes Pigm.*, **173**, 107897 (2020)
200. C.Chang, F.Wang, J.Qiang, Z.Zhang, Y.Chen, W.Zhang, Y.Wang, X.Chen. *Sens. Actuators B: Chem.*, **243**, 22 (2017)
201. W.-C.Lin, S.-K.Fang, J.-W.Hu, H.-Y.Tsai, K.-Y.Chen. *Anal. Chem.*, **86**, 4648 (2014)
202. X.Liu, Q.Yang, W.Chen, L.Mo, S.Chen, J.Kang, X.Song. *Org. Biomol. Chem.*, **13**, 8663 (2015)
203. S.Erdemir, B.Tabakci, M.Tabakci. *Sens. Actuators B: Chem.*, **228**, 109 (2016)
204. Y.Ding, Y.Tang, W.Zhu, Y.Xie. *Chem. Soc. Rev.*, **44**, 1101 (2015)
205. N.M.M.Moura, C.Núñez, M.A.F.Faustino, J.A.S.Cavaleiro, M.G.P.M.S.Neves, J.L.Capelo, C.Lodeiro. *J. Mater. Chem. C*, **2**, 4772 (2014)
206. C.I.M.Santos, E.Oliveira, J.F.B.Barata, M.A.F.Faustino, J.A.S.Cavaleiro, M.G.P.M.S.Neves, C.Lodeiro. *J. Mater. Chem.*, **22**, 13811 (2012)
207. T.Liu, A.D.Chien, L.Jiwei, G.Zhang, C.L.Fraser. *J. Mater. Chem.*, **21**, 8401 (2011)
208. E.M.Nolan, S.J.Lippard. *Chem. Rev.*, **108**, 3443 (2008)
209. G.M.Fischer, C.Jungst, M.Isomaki-Krondahl, D.Gauss, H.M.Moller, E.Daltrozzo, A.Zumbusch. *Chem. Commun.*, **46**, 5289 (2010)
210. X.Chen, X.Zhang, G.Zhang. *Chem. Commun.*, **51**, 161 (2015)
211. N.Kaur, S.Kumar. *Tetrahedron*, **67**, 9233 (2011)
212. R.I.Khan, A.Ramu, K.Pitchumani. *Sens. Actuators B: Chem.*, **266**, 429 (2018)
213. C.Duan, J.-F.Zhang, Y.Hu, L.Zeng, D.Su, G.-M.Bao. *Dyes Pigm.*, **162**, 459 (2019)
214. Q.Zhang, J.Zhang, H.Zuo, C.Wang, Y.Shen. *Tetrahedron*, **72**, 1244 (2016)
215. H.J.Kim, K.C.Ko, J.H.Lee, J.Y.Lee, J.S.Kim. *Chem. Commun.*, **47**, 2886 (2011)
216. K.-Y.Chen, W.-C.Lin. *Dyes Pigm.*, **123**, 1 (2015)
217. S.Wang, X.Fei, J.Guo, Q.Yang, Y.Li, Y.Song. *Talanta*, **148**, 229 (2016)
218. J.Chao, Z.Li, Y.Zhang, F.Huo, C.Yin, H.Tong, Y.Liu. *Sens. Actuators B: Chem.*, **228**, 192 (2016)
219. P.B.Pati, S.S.Zade. *RSC Adv.*, **3**, 13457 (2013)
220. Y.Liu, D.Ren, J.Zhang, H.Li, X.-F.Yang. *Dyes Pigm.*, **162**, 112 (2019)
221. S.Huang, T.Gao, A.Bi, X.Cao, B.Feng, M.Liu, T.Du, X.Feng, W.Zeng. *Dyes Pigm.*, **172**, 107830 (2020)
222. H.-S.Lv, S.-Y.Huang, Y.Xu. X.Dai, X.-Y.Miao, B.-X.Zhao. *Bioorg. Med. Chem. Lett.*, **24**, 535 (2014)
223. S.L.Shen, X.-P.Chen, X.-F.Zhang, J.-Y.Miao, B.-X.Zhao. *J. Mater. Chem. B*, **3**, 319 (2015)
224. S.-K.Ko, Y.-K.Yang, J.Tae, I.Shin. *J. Am. Chem. Soc.*, **128**, 14150 (2006)
225. M.Suresh, A.Shrivastav, S.Mishra, E.Suresh, A.Das. *Org. Lett.*, **10**, 3013 (2008)
226. Y.Zhao, Y.Sun, X.Lv, Y.Liu, M.Chen, W.Guo. *Org. Biomol. Chem.*, **8**, 4143 (2010)
227. Y.Zhou, X.-Y.You, Y.Fang, J.-Y.Li, K.Liu, C.Yao. *Org. Biomol. Chem.*, **8**, 4819 (2010)
228. J.Ni, B.Li, L.Zhang, H.Zhao, H.Jiang. *Sens. Actuators B: Chem.*, **215**, 174 (2015)

229. Y.Jiao, L.Zhang, P.Zhou. *Talanta*, **15**, 14 (2016)
230. D.Lee, K.M.K.Swamy, J.Hong, S.Lee, J.Yoon. *Sens. Actuators B: Chem.*, **266**, 416 (2018)
231. N.Nath, B.Godat, C.Zimprich, S.J.Dwight, C.Corona, M.McDougall, M.Urh. *J. Immunol. Methods*, **431**, 11 (2016)
232. E.Walker, A.Dvornikov, K.Coblentz, P.Rentzepis. *Appl. Opt.*, **47**, 4133 (2008)
233. V.F.Traven, I.V.Ivanov, S.M.Dolotov, O.I.Kobeleva, T.M.Valova, V.A.Barachevsky. *J. Photochem. Photobiol. A: Chem.*, **295**, 34 (2014)
234. V.F.Traven, D.A.Cheptsov, M.V.Bulanova, N.P.Solovjova, T.A.Chibisova, S.M.Dolotov, I.V.Ivanov. *Photochem. Photobiol.*, **94**, 659 (2018)
235. V.F.Traven, D.A.Cheptsov, G.V.Vershinina, N.P.Solovjeva, T.A.Chibisova, S.M.Dolotov, I.V.Ivanov. *J. Photochem. Photobiol. A: Chem.*, **351**, 8 (2018)
236. Patent RU 2478116 (2013)
237. Y.Jiao, L.Zhang, P.Zhou. *Talanta*, **150**, 14 (2016)
238. J.Kuchlyan, S.Basak, D.Dutta, A.K.Das, D.Mal, N.Sarkar. *Chem. Phys. Lett.*, **673**, 84 (2017)
239. K.Wechakorn, K.Suksen, P.Piyachaturawat, P.Kongsaeree. *Sens. Actuators B: Chem.*, **228**, 270 (2016)
240. J.Zhao, Q.Gao, F.Zhang, W.Sun, Y.Bai. *J. Lumin.*, **180**, 278 (2016)
241. Q.Chen, Z.Fang. *Spectrochim. Acta A: Mol. Biomol. Spect.*, **193**, 226 (2018)
242. J.X.Yin, X.Ma, G.H.Wei, D.B.Wei, Y.G.Du. *Sens. Actuators B: Chem.*, **177**, 213 (2013)
243. N.K.Singhal, B.Ramanujam, V.Mariappanadar, C.P.Rao. *Org. Lett.*, **8**, 3525 (2006)
244. S.Areti, J.K.Khedkar, S.Bandaru, R.Teotia, J.Bellare, C.P.Rao. *Anal. Chim. Acta*, **873**, 80 (2015)
245. L.X.Li, Z.J.Fang. *Spectrosc. Lett.*, **48**, 578 (2015)
246. X.M.Gu, Z.J.Fang. *Spectrochim. Acta A: Mol. Biomol. Spect.*, **173**, 495 (2016)
247. F.Ge, H.Ye, H.Zhang, B.X.Zhao. *Dyes Pigm.*, **99**, 661 (2013)
248. H.J.Kim, J.E.Park, M.G.Choi, S.Ahn, S.K.Chang. *Dyes Pigm.*, **84**, 54 (2010)
249. X.F.Yang, Y.Li, Q.Bai. *Anal. Chim. Acta*, **584**, 95 (2007)
250. Y.Feng, Z.Kuai, Y.Song, J.Guo, Q.Yang, Y.Shan, Y.Li. *Talanta*, **170**, 103 (2017)
251. J.Li, Y.Zeng, Q.Hu, X.Yu, J.Guo, Z.Pan. *Dalt. Trans.*, **41**, 3623 (2012)
252. V.C.Ezeh, T.C.Harrop. *Inorg. Chem.*, **52**, 2323 (2013)
253. R.Sheng, J.Ma, P.Wang, W.Liu, J.Wu, H.Li, X.Zhuang, H.Zhang, S.Wu. *Biosens. Bioelectron.*, **26**, 949 (2010)
254. V.F.Traven, D.A.Cheptsov, N.P.Solovjova, T.A.Chibisova, I.I.Voronov, S.M.Dolotov, I.V.Ivanov. *Dyes Pigm.*, **146**, 159 (2017)
255. Patent RU 2643951 (2018)
256. K.-P.Wang, Y.Lei, J.-P.Chen, Z.-H.Ge, W.Liu, Q.Zhang, S.Chen, Z.-Q.Hu. *Dyes Pigm.*, **151**, 233 (2018)
257. X.Zhou, Y.Zeng, C.Liyan, X.Wu, J.Yoon. *Angew. Chem.*, **128**, 4807 (2016)
258. M.Akiba, A.S.Dvornikov, P.M.Rentzepis. *J. Photochem. Photobiol. A: Chem.*, **190**, 69 (2007)
259. Y.Chen, Z.Peng, Y.Tao, Z.Wang, P.Lu, Y.Wang. *Dyes Pigm.*, **161**, 44 (2019)
260. A.Rose, Z.Zhu, C.F.Madigan, T.M.Swager, V.Bulovic. *Nature (London)*, **434**, 876 (2005)
261. Y.Salinas, R.Martinez-Manez, M.D.Marcos, F.Sancenon, A.M.Costero, M.Parra, S.Gil. *Chem. Soc. Rev.*, **41**, 1261 (2012)
262. N.Venkatramaiah, S.Kumar, S.Patil. *Chem. – Eur. J.*, **18**, 14745 (2012)
263. S.S.Nagarkar, B.Joarder, A.K.Chaudhari, S.Mukherjee, S.K.Ghosh. *Angew. Chem., Int. Ed.*, **52**, 2881 (2013)
264. X.Huang, X.Gu, G.Zhang, D.Zhang. *Chem. Commun.*, **48**, 12195 (2012)
265. V.Bhalla, S.Pramanik, M.Kumar. *Chem. Commun.*, **49**, 895 (2013)
266. N.Dey, S.K.Samanta, S.Bhattacharya. *ACS Appl. Mater. Interf.*, **5**, 8394 (2013)
267. K.K.Kartha, A.Sandeep, V.C.Nair, M.Takeuchi, A.Ajayaghosh. *Phys. Chem. Chem. Phys.*, **16**, 18896 (2014)
268. S.W.Thomas, G.D.Jolyand, T.M.Swager. *Chem. Rev.*, **107**, 1339 (2007)
269. K.K.Kartha, S.S.Babu, S.Srinivasan, A.Ajayaghosh. *J. Am. Chem. Soc.*, **134**, 4834 (2012)
270. H.Su, R.Liu, M.Shu, M.Tang, J.Wang, H.Zhu. *Dyes Pigm.*, **162**, 52 (2019)
271. P.Xue, B.Yao, P.Wang, P.Gong, Z.Zhang, R.Lu. *Chem. – Eur. J.*, **21**, 17508 (2015)
272. J.M.Jung, J.H.Kang, J.Han, H.Lee, M.H.Lim, K.-T.Kim, C.Kim. *Sens. Actuators B: Chem.*, **267**, 58 (2018)
273. Y.Sagara, T.Kato. *Nat. Chem.*, **1**, 605 (2009)
274. T.Mutai, H.Satou, K.Araki. *Nat. Mater.*, **4**, 685 (2005)
275. S.Yamane, K.Tanabe, Y.Sagara, T.Kato. *Top. Curr. Chem.*, **318**, 395 (2012)
276. T.Kato, Y.Shoji, M.Yoshio, S.Yamane, T.Yasuda. *J. Synth. Org. Chem. Jpn.*, **68**, 1169 (2010)
277. S.Yamane, Y.Sagara, T.Kato. *Chem. Commun.*, **24**, 3597 (2009)
278. Y.Zhao, H.Gao, Y.Fan, T.Zhou, Z.Su, Y.Liu, Y.Wang. *Adv. Mater.*, **21**, 3165 (2009)
279. J.Lott, C.Ryan, B.Valle, J.R.Johnson, D.A.Schiraldi, J.Shan, K.D.Singer, C.Weder. *Adv. Mater.*, **23**, 2425 (2011)
280. M.J.Xue, H.Wang, J.Chen, J.Ren, S.Chen, H.Yang, R.Zeng, Y.Long, P.Zhang. *Sens. Actuators B: Chem.*, **282**, 1 (2019)
281. G.Y.Jiang, G.J.Zeng, W.P.Zhu, Y.Li, X.Dong, G.Zhang, X.Fan, J.Wang, Y.Wu, B.Z.Tang. *Chem. Commun.*, **53**, 4505 (2017)
282. G.X.Feng, B.Liu. *Acc. Chem. Res.*, **51**, 1404 (2018)
283. M.Gao, H.F.Su, S.W.Li, Y.Lin, X.Ling, A.Qin, B.Z.Tang. *Chem. Commun.*, **53**, 921 (2017)
284. H.Gao, X.Zhao, S.J.Chen. *Molecules*, **23**, 419 (2018)
285. P.Gopikrishna, N.Meher, P.K.Iyer. *ACS Appl. Mater. Interf.*, **10**, 12081 (2018)
286. J.Mei, Y.H.Huang, H.Tian. *ACS Appl. Mater. Interf.*, **10**, 12217 (2018)
287. Y.X.Zhang, Y.F.Wang, J.J.Wang, X.J.Liang. *Mater. Horiz.*, **5**, 799 (2018)
288. J.Shi, Y.Li, Q.Q.Li, Z.Li. *ACS Appl. Mater. Interf.*, **10**, 12278 (2018)
289. J.Y.Hu, R.Liu, S.L.Zhai, Y.Wu, H.Zhang, H.Cheng, H.Zhu. *J. Mater. Chem. C*, **5**, 11781 (2017)
290. J.Mei, N.L.C.Leung, R.T.K.Kwok, J.W.Y.Lam, B.Z.Tang. *Chem. Rev.*, **115**, 11718 (2015)
291. S.Xu, T.Liu, Y.Mu, Y.-F.Wang, Z.Chi, C.-C.Lo, S.Liu, Y.Zhang, A.Lien, J.Xu. *Angew. Chem., Int. Ed.*, **54**, 874 (2015)
292. M.Gao, Lu.Wang, J.Chen, S.Li, G.Lu, Li.Wang, Y.Wang, L.Ren, A.Qin, B.Z.Tang. *Chem. – Eur. J.*, **22**, 5107 (2016)
293. *Standard Methods for the Examination of Waters and Wastewaters*. (19th Ed.). (Baltimore, Maryland: American Public Health Association, 1995). P. 5540
294. P.Zhang, J.Li, B.Li, J.Xu, F.Zeng, J.Lv, S.Wu. *Chem. Commun.*, **51**, 4414 (2015)
295. R.X.Zhang, P.F.Li, W.J.Zhang, N.Li, N.Zhao. *J. Mater. Chem. C*, **4**, 10479 (2016)
296. B.Valeur, M.N.Berberan-Santos. In *Molecular Fluorescence. Principles and Applications*. (Weinheim: Wiley-VCH, 2001)
297. W.-K.Dong, S.F.Akogun, Y.Zhang, Y.-X.Sun, X.-Y.Dong. *Sens. Actuators B: Chem.*, **238**, 723 (2017)
298. P.E.Hansen, F.S.Kamounah, D.T.Gryko. *Molecules*, **18**, 4544 (2013)
299. P.G.Umape, V.S.Patil, V.S.Padalkar, K.R.Phatangare, V.D.Gupta, A.B.Thate, N.Sekar. *Dyes Pigm.*, **99**, 291 (2013)
300. L.Sobczyk, M.Obrzud, A.Filarowski. *Molecules*, **18**, 4467 (2013)
301. L.Racané, Z.Mihalić, H.Cerić, J.Popović, V.Tralić-Kulenović. *Dyes Pigm.*, **96**, 672 (2013)

302. C.Li, W.Yang, H.Liu, M.Li, W.Zhou, J.Xie. *Molecules*, **18**, 15737 (2013)
303. X.L.Zhong, F.Gao, Q.Wang, H.R.Li, S.T.Zhang. *Chin. Chem. Lett.*, **21**, 1195 (2010)
304. L.Xie, Y.Chen, W.Wu, H.Guo, J.Zhao, X.Yu. *Dyes Pigm.*, **92**, 1361 (2012)
305. P.T.Chou, S.C.Pu, Y.M.Cheng, W.S.Yu, Y.C.Yu, F.T.Hung, W.P.Hu. *J. Phys. Chem. A*, **109**, 3777 (2005)
306. T.C.Fang, H.Y.Tsai, M.H.Luo, C.W.Chang, K.Y.Chen. *Chin. Chem. Lett.*, **24**, 145 (2013)
307. K.Y.Chen, H.Y.Tsai. *Int. J. Mol. Sci.*, **15**, 18706 (2014)
308. Z.Li, L.-J.Li, T.Sun, L.Liu, Z.Xie. *Dyes Pigm.*, **128**, 165 (2016)
309. H.J.Kim, C.H.Heo, H.M.Kim. *J. Am. Chem. Soc.*, **135**, 17969 (2014)
310. X.Zhu, Q.Lin, Y.M.Zhang, T.B.Wei. *Sens. Actuators B: Chem.*, **219**, 38 (2015)
311. K.Tayade, S.K.Sahoo, R.Patil, N.Singh, S.Attarde, A.Kuwar. *Spectrochim. Acta A: Mol. Biomol. Spect.*, **126**, 312 (2014)
312. A.P. De Silva, D.B.Fox, H.J.M.Huxley, T.S.Moody. *Coord. Chem. Rev.*, **205**, 41 (2000)
313. A.Ganguly, B.K.Paul, S.Ghosh, S.Kar, N.Guchhait. *Analyst*, **138**, 6532 (2013)
314. X.W.Tian, Z.Li, Y.X.Pang, D.Y.Li, X.B.Yang. *J. Agric. Food Chem.*, **65**, 9553 (2017)
315. W.Chen, W.Shi, Z.Li, H.M.Ma, Y.Liu, J.H.Zhang, Q.J.Liu. *Anal. Chim. Acta*, **708**, 84 (2011)
316. J.C.Xu, Y.Zhang, L.T.Zeng, J.B.Liu, J.M.Kinsella, R.L.Sheng. *Talanta*, **160**, 645 (2016)
317. M.X.Li, W.Y.Feng, H.Y.Zhang, G.Q.Feng. *Sens. Actuators B: Chem.*, **243**, 51 (2017)
318. Q.Zhang, Y.Zhang, S.S.Ding, H.Y.Zhang, G.Q.Feng. *Sens. Actuators B: Chem.*, **211**, 377 (2015)
319. D.Li, Y.D.Ma, H.Z.Duan, W.Deng, D.W.Li. *Biosens. Bioelectron.*, **99**, 389 (2018)
320. W.Sun, J.L.Fan, C.Hu, J.F.Cao, H.Zhang, X.Q.Xiong, J.Y.Wang, S.Cui, S.G.Sun, X.J.Peng. *Chem. Commun.*, **49**, 3890 (2013)
321. M.Li, X.M.Wu, Y.Wang, Y.S.Li, W.H.Zhu, T.D.James. *Chem. Commun.*, **50**, 1751 (2014)
322. Z.Q.Guo, W.H.Zhu, H.Tian. *Chem. Commun.*, **48**, 6073 (2012)
323. J.F.Wang, B.Li, W.Y.Zhao, X.F.Zhang, X.Luo, M.E.Corkins, S.L.Cole, C.Wang, Y.Xiao, X.M.Bi, Y.Pang, C.A.McElroy, A.J.Bird, Y.Z.Dong. *ACS Sens.*, **1**, 882 (2016)
324. X.H.Cheng, R.L.Tang, H.Z.Jia, J.Feng, J.G.Qin, Z.Li. *ACS Appl. Mater. Interf.*, **4**, 4387 (2012)
325. L.Yang, X.Li, J.B.Yang, Y.Qu, J.L.Hua. *ACS Appl. Mater. Interf.*, **5**, 1317 (2013)
326. Y.D.Lin, Y.S.Peng, W.T.Su, C.H.Tu, C.H.Sun, T.J.Chow. *Tetrahedron*, **68**, 2523 (2012)
327. S.S.Sun, A.J.Lees. *Chem. Commun.*, 1687 (2000)
328. H.Miyaji, J.L.Sessler. *Angew. Chem.*, **113**, 154 (2001)
329. K.Kumia, D.E.Giles, P.M.May, P.Singh, G.T.Hefter. *Talanta*, **43**, 2045 (1996)
330. H.N.Kim, M.H.Lee, H.J.Kim, J.S.Kim, J.Yoon. *Chem. Soc. Rev.*, **37**, 1465 (2008)
331. H.S.Jung, K.C.Ko, J.H.Lee, S.H.Kim, S.Bhuniya, J.Y.Lee, Y.Kim, S.J.Kim, J.S.Kim. *Inorg. Chem.*, **49**, 8552 (2010)
332. Y.H.Lee, M.H.Lee, J.F.Zhang, J.S.Kim. *J. Org. Chem.*, **75**, 7159 (2010)
333. D.T.Quang, J.S.Kim. *Chem. Rev.*, **110**, 6280 (2010)
334. D.G.Cho, J.L.Sessler. *Chem. Soc. Rev.*, **38**, 1647 (2009)
335. K.S.Lee, H.J.Kim, G.H.Kim, I.Shin, J.I.Hong. *Org. Lett.*, **10**, 49 (2008)
336. Z.Ekmekci, M.D.Yilmaz, E.U.Akkaya. *Org. Lett.*, **10**, 461 (2008)
337. H.B.Yu, Q.Zhao, Z.X.Jiang, J.G.Qin, Z.Li. *Sens. Actuators B: Chem.*, **148**, 110 (2010)
338. T.Zhang, T.Y.Wang, Z.J.Fang. *RSC Adv.*, **6**, 18357 (2016)
339. X.M.Gu, Q.Chen, Z.J.Fang. *Dyes Pigm.*, **139**, 334 (2017)
340. R.M.Rapoport, F.Murad. *Circ. Res.*, **52**, 352 (1983)
341. M.Y.Chae, A.W.Czarnik. *J. Am. Chem. Soc.*, **114**, 9704 (1992)
342. M.H.Lee, S.W.Lee, S.H.Kim, C.Kang, J.S.Kim. *Org. Lett.*, **11**, 2101 (2009)
343. A.S.A.Youssef. *Phosphorus Sulfur Silicon Relat. Elem.*, **177**, 173 (2002)
344. K.-D.Ahn, J.-H.Lee, I.Cho, K.H.Park, J.-H.Kang, D.K.Han, J.-M.Kim. *J. Photopolymer Sci. Technol.*, **13**, 493 (2000)
345. C.W.Lee, Z.Yuan, K.D.Ahn, S.H.Lee. *Chem. Mater.*, **14**, 4572 (2002)
346. I.D.Tevis, W.W.Tsai, L.C.Palmer, T.Aytun, S.I.Stupp. *ACS Nano*, **6**, 2032 (2012)
347. G.M.Peters, J.T.Davis. *Chem. Soc. Rev.*, **45**, 3188 (2016)
348. K.J.Skilling, F.Citossi, T.D.Bradshaw, M.Ashford, B.Kellam, M.Marlow. *Soft Matter*, **10**, 237 (2014)
349. N.Cheng, Q.Z.Hu, Y.X.Guo, Y.Wang, L.Yu. *ACS Appl. Mater. Interf.*, **7**, 10258 (2015)
350. Y.Hisamatsu, S.Banerjee, M.B.Avinash, T.Govindaraju, C.Schmuck. *Angew. Chem., Int. Ed.*, **52**, 12550 (2013)
351. M.M.F.Choi, S.Shuang. *Analyst*, **125**, 301 (2000)
352. P.Gong, J.B.Sun, P.C.Xue, C.Qian, Z.Q.Zhang, J.B.Sun, R.Lu. *Dyes Pigm.*, **118**, 27 (2015)
353. G.H.Hong, J.B.Sun, C.Qian, P.C.Xue, P.Gong, Z.Q.Zhang, R.Lu. *J. Mater. Chem. C*, **3**, 2371 (2015)
354. J.Zhang, S.Zhu, L.Valenzano, F.T.Luo, H.Liu. *RSC Adv.*, **3**, 68 (2013)
355. L.G.Nandi, C.R.Nicoleti, I.C.Bellettini, V.G.Machado. *Anal. Chem.*, **86**, 4653 (2014)
356. S.S.Babu, V.K.Praveen, A.Ajayaghosh. *Chem. Rev.*, **114**, 1973 (2014)
357. V.K.Praveen, C.Ranjith, E.Bandini, A.Ajayaghosh, N.Armaroli. *Chem. Soc. Rev.*, **43**, 4222 (2014)
358. F.Aparicio, B.Nieto-Ortega, F.Nájera, F.J.Ramírez, J.T.L.Navarrete, J.Casado, L.Sánchez. *Angew. Chem., Int. Ed.*, **53**, 1373 (2014)
359. W.Miao, D.Yang, M.Liu. *Chem. Eur. J.*, **21**, 7562 (2015)
360. P.Xue, P.Wang, B.Yao, J.Sun, P.Gong, Z.Zhang, C.Qian, R.Lu. *ACS Appl. Mater. Interf.*, **6**, 21426 (2014)
361. D.A.Stone, A.S.Tayi, J.E.Goldberger, L.C.Palmera, S.I.Stupp. *Chem. Commun.*, **47**, 5702 (2011)
362. P.Bairi, B.Roy, A.K.Nandi. *J. Mater. Chem.*, **21**, 11747 (2011)
363. S.Sarkar, S.Dutta, S.Chakrabarti, P.Bairi, T.Pal. *ACS Appl. Mater. Interf.*, **6**, 6308 (2014)
364. Z.Xu, K.-H.Baek, H.N.Kim, J.Cui, X.Qian, D.R.Spring, I.Shin, J.Yoon. *J. Am. Chem. Soc.*, **132**, 601 (2010)
365. Z.Xu, S.J.Han, C.Lee, J.Yoon, D.R.Spring. *Chem. Commun.*, **46**, 1679 (2010)